

**MICROGEL BIOCONJUGATES FOR TARGETED DELIVERY TO
CANCER CELLS**

A Thesis
Presented to
The Academic Faculty

by

William H. Blackburn

In Partial Fulfillment
of the Requirements for the Degree
Doctor of Philosophy in the
School of Chemistry and Biochemistry

Georgia Institute of Technology
December 2008

COPYRIGHT 2008 BY WILLIAM H. BLACKBURN

MICROGEL BIOCONJUGATES FOR TARGETED DELIVERY TO CANCER CELLS

Approved by:

Dr. Andrew Lyon, Advisor
School of Chemistry and Biochemistry
Georgia Institute of Technology

Dr. Bridgette Barry
School of Chemistry and Biochemistry
Georgia Institute of Technology

Dr. Christoph J. Fahrni
School of Chemistry and Biochemistry
Georgia Institute of Technology

Dr. Nicholas V. Hud
School of Chemistry and Biochemistry
Georgia Institute of Technology

Dr. Joseph M. Le Doux
Wallace H. Coulter Department of
Biomedical Engineering
Georgia Institute of Technology

Date Approved: August 14, 2008

ACKNOWLEDGEMENTS

I would like to thank my advisor Prof. Andrew Lyon for giving me the opportunity to work on projects that kept me excited. His guidance has helped me throughout my time at Georgia Tech. While things did not always go smoothly for me, he gave me the chance to show that I deserved this degree. He also let me initiate a collaboration, which has led to the majority of my work. I became a scientist during my time at Georgia Tech, and this is thanks to Andrew.

I also have to thank my wife, Ali, for supporting me, both emotionally and financially while I earned my PhD. She helped me through the times where motivation was lacking, and she often revived my confidence. Her love and support means the world to me.

I wish to thank my parents and sister for their encouragement throughout my entire life. Their support has allowed me to get to this point, and I will always lean on them for guidance.

I would also like to thank our collaborators in Prof. John McDonald's lab, especially Dr. Erin Dickerson for all of her help with my projects. With her help, I was able to get hands on experience with biological techniques.

I would like to thank Prof. Rob Dickson and Sungmoon Choi for all their help in our bioimaging project, especially in providing silver nanoclusters.

Finally, I would like to thank both former and current members of the Lyon group. I have learned from all of them, as they taught me new techniques and critiqued my work. Whether it was learning how to do a synthesis, or just talking about the Braves, they provided me with a valuable experience that I will not soon forget.

TABLE OF CONTENTS

	Page
ACKNOWLEDGEMENTS	iii
LIST OF TABLES	ix
LIST OF FIGURES	x
LIST OF SYMBOLS AND ABBREVIATIONS	xiii
SUMMARY	xvi
<u>CHAPTER</u>	
1 Introduction to Hydrogels and Their Use as Biomaterials	1
1.1 Introduction	1
1.1.1 Definition of Hydrogels	2
1.1.2 Classification of Hydrogels	3
1.1.2.1 Macro gels	3
1.1.2.1.1 Physically Cross-linked Hydrogels	4
1.1.2.1.2 Chemically Cross-linked Hydrogels	5
1.1.2.2 Microgels and Nanogels	6
1.1.3 Stimuli-sensitive Polymers	6
1.1.4 Swelling Properties of Hydrogels	10
1.1.5 Microgels and Nanogels	11
1.2 Synthesis of Hydrogel Nanoparticles	15
1.2.1 Emulsion and Precipitation Polymerization	15
1.2.2 Core/Shell Structure Materials	19
1.2.3 Post Polymerization Modification of Hydrogels	22
1.3 Bioconjugated Hydrogel Particles in Nanotechnology	24

1.3.1 Drug/Gene Delivery	25
1.3.2 Encapsulation and Microreactors	35
1.3.3 Analytical Applications	38
1.3.4 Biomaterials	43
1.4 Conclusions and Outlook	48
1.5 References	50
2 The Use of AFFF-MALLS to Characterize Microgel Particle Size	64
2.1 Introduction	64
2.1.1 Uses of AFFF-MALLS	67
2.1.2 Microgels	72
2.2 Experimental Section	73
2.2.1 Materials	73
2.2.2 Microgel Core Synthesis	73
2.2.3 Microgel Shell Synthesis	74
2.2.4 Core Degradation	74
2.2.5 Particle Characterization	74
2.2.5.1 Static Light Scattering	75
2.2.5.2 Photon Correlation Spectroscopy	75
2.3 Results and Discussion	76
2.4 Conclusions	81
2.5 References	82
3 Size Controlled Synthesis of Monodispersed, Core/Shell Nanogels	85
3.1 Introduction	85
3.2 Experimental Section	88
3.2.1 Nanogel Core Synthesis	88

3.2.2. Nanogel Shell Synthesis	89
3.2.3 Particle Characterization	90
3.2.3.1 Static Light Scattering	90
3.2.3.2 Fluorimetry	91
3.3 Results and Discussion	92
3.4 Conclusions	102
3.5 References	103
4 Targeted Nanogel Delivery of siRNA to Cancer Cells	107
4.1 Introduction	107
4.2 Experimental Section	109
4.2.1 Materials	109
4.2.2 Nanogel Core Synthesis	110
4.2.3 Nanogel Shell Synthesis	110
4.2.4 YSA Synthesis	111
4.2.5 Peptide Conjugation	111
4.2.6 siGLO Encapsulation	112
4.2.7 Particle Characterization	112
4.2.7.1 Static Light Scattering	112
4.2.7.2 Absorbance Measurements	112
4.2.7.3 Fluorimetry	113
4.2.8 Cell Culture	113
4.2.9 Particle/transfection experiments	114
4.2.9.1 siGLO-encapsulated particle transfection	114
4.2.9.2 Ephrin Competition Assay	114
4.2.9.3 Scrambled Peptide Targeting	115

4.2.10 Confocal Microscopy	115
4.3 Results and Discussion	115
4.4 Conclusions	122
4.5 References	123
5 Chemotherapeutic Potential of Protein Knockdown By Nanogel Delivery of siRNA	128
5.1 Introduction	128
5.2 Experimental Section	131
5.2.1 Materials	131
5.2.2 Nanogel Core Synthesis	132
5.2.3 Nanogel Shell Synthesis	132
5.2.4 Peptide Conjugation	132
5.2.5 siRNA Encapsulation	132
5.2.6 Particle Characterization	133
5.2.6.1 Absorbance Measurements	133
5.2.7 Cell Culture	133
5.2.8 Particle/transfection Experiments	133
5.2.8.1 Commercial Agent Transfection	133
5.2.8.2 siGLO-encapsulated Particle Transfection	134
5.2.8.3 EGFR-siRNA-encapsulated Particle Transfection	134
5.2.9 Toxicity Studies	135
5.2.9.1 Trypan Blue Exclusion Assay	135
5.2.9.2 Tox 8 Assay	136
5.2.10 Confocal Microscopy	137
5.2.11 Western Blot Analysis	137
5.3 Results and Discussion	138

5.4 Conclusions	146
5.5 References	147
6 Ag-Encapsulated Nanogels for <i>In Vivo</i> Imaging	150
6.1 Introduction	150
6.2 Experimental Section	153
6.2.1 Materials	153
6.2.2 Nanogel Core Synthesis	153
6.2.3 Nanogel Shell Synthesis	154
6.2.4 Peptide Conjugation	154
6.2.5 Ag Nanodot Encapsulation	154
6.2.6 Static Light Scattering	154
6.2.7 Fluorescence Microscopy	155
6.2.8 Targeting to Matrigel™ Plug	155
6.3 Results and Discussion	156
6.4 Conclusions	163
6.5 References	165
7 Future Outlook	169
VITA	172

LIST OF TABLES

	Page
Table 2.1: Native and degraded core nanogel radii and peak intensity values	80
Table 3.1: Parameters for pNIPAm core particle syntheses	92
Table 3.2: Parameters for pNIPMAm core particle syntheses	96
Table 5.1: Absorbance measurements of supernatant from siGLO-loaded nanogels	139

LIST OF FIGURES

	Page
Figure 1.1: Structuring of water around pNIPAm hydrogel networks as the temperature increases above the LCST of 31 ° C.	9
Figure 1.2: Free-radical precipitation polymerization- a growing oligoradical chain reaches a critical length and collapses on itself, creating a precursor particle, to which monomer adds until used up, forming microgels.	17
Figure 2.1: Differential weight fraction plot for pNIPAm- <i>co</i> -DHEA/pNIPAm core/shell particles, as determined by AFFF-MALLS.	77
Figure 2.2: Scheme of DHEA cleavage by sodium periodate.	78
Figure 2.3: Picture of vials containing pNIPAm- <i>co</i> -DHEA core/pNIPAm shell microgels. Vial 1 contains native microgels. Vial 2 contains core-degraded microgels.	79
Figure 3.1: Overlay of radius data as sample elutes to detector and is shown as voltage (a,c,e) for pNIPAm- <i>co</i> -AAc core particles, and corresponding differential weight fraction plots, as determined by AFFF-MALLS (b,d,f). Synthetic parameters for (a,b) are shown in Table 3.1, row 1; (c,d) are shown in Table 3.1, row 2; (e,f) are shown in Table 3.1, row 3.	93
Figure 3.2: Differential weight fraction plot for pNIPAm- <i>co</i> -AFA core particles, as determined by AFFF-MALLS. Synthetic parameters are shown in Table 3.1, row 4.	94
Figure 3.3: Differential weight fraction plots for pNIPAm- <i>co</i> -AFA core particles, as determined by AFFF-MALLS. Synthetic parameters are shown in Table 3.1, row 5.	95
Figure 3.4: Particle sizes determined for the pNIPMAm core particle syntheses. Error bars do not indicate a standard deviation, but rather the total width of the differential weight fractions for each synthesis.	97
Figure 3.5: Change in size of pNIPAm core particles versus pNIPAm core/shell particles. Error bars indicate the total width of the differential weight fractions.	98
Figure 3.6: Change in size of pNIPMAm core particles versus pNIPMAm core/shell particles. Error bars indicate the total width of the differential weight fractions.	99

- Figure 3.7: Temperature-dependent turbidity measurements for (a) pNIPAm core/shell particles and (b) pNIPMAm core/shell particles. 100
- Figure 3.8: Absorbance of free folic acid (red), and pNIPAm core/shell particles before (black) and after (blue) folic acid conjugation. 101
- Figure 4.1: Confocal microscopy images of Hey cells following exposure to siGLO-loaded/YSA-conjugated nanogels. (A) shows the green (AFA) channel and (B) shows the red (siGLO) channel. (C) is an overlay of these channels. (D) shows the green channel and (E) shows red channel following exposure of Hey cells to unloaded YSA-conjugated nanogels. (F) is an overlay of these images. 117
- Figure 4.2: Confocal microscopy images of BG-1 cells following exposure to siGLO-loaded/YSA-conjugated nanogels. (A) shows the green (AFA) channel and (B) shows the red (siGLO) channel. (C) is an overlay of these channels. 118
- Figure 4.3: Confocal microscopy images of Hey cells following exposure to non-targeting pNIPMAm nanogels. (A) shows the green (AFA) channel and (B) shows the red (siGLO) channel. (C) is an overlay of these channels. 119
- Figure 4.4: Confocal microscopy images of Hey cells following exposure to siGLO-loaded/YSA-conjugated nanogels after 1 h ephrin incubation. (A) shows the green (AFA) channel and (B) shows the red (siGLO) channel. (C) is an overlay of these channels. (D) shows the green channel and (E) shows red channel following exposure of Hey cells to siGLO-loaded/YSA-conjugated nanogels (no ephrin). (F) is an overlay of these images. 121
- Figure 5.1: The knockdown of EGFR by nanogel-delivered siRNA at 24, 48, 72, 96, and 120 h incubation times. Controls shown are unloaded YSA-conjugated particles and pNIPMAm particles, as well as untreated cells. Untreated cells were set at 100% activity. 141
- Figure 5.2: Immunoblot showing EGFR knockdown by various concentrations of siRNA delivered via nanogels. “YSA” designates unloaded YSA-conjugated nanogels, while the control is untreated cells. The β -actin levels show equal protein loading among each well. 142
- Figure 5.3: Tox 8 assay on siRNA-loaded nanogel delivery to Hey cells. The fluorescence indicates cell activity. Concentrations denote siRNA delivered by nanogels. Controls are unloaded YSA-conjugated nanogels, unloaded pNIPMAm nanogels, and untreated cells. 144
- Figure 5.4: Cytotoxic effects of taxol with (red) and without (black) siRNA delivery by nanogels. 145

- Figure 6.1: Fluorescence microscopy image of Ag nanodot encapsulated nanogels at day 1. Panel A shows the green channel (AFA). Panel B shows the red channel (Ag nanodots). 158
- Figure 6.2: Fluorescence microscopy image of Ag nanodot encapsulated nanogels at day 5. Panel A shows the green channel (AFA). Panel B shows the red channel (Ag nanodots). 160
- Figure 6.3: Fluorescence microscopy image of Matrigel™ plug. Panel A shows dual fluorescence in vessels. Panel B shows the red channel. 162
- Figure 6.4: Dual fluorescence microscopy image of vessels in Matrigel™ plug. 163

LIST OF ABBREVIATIONS

NIPAm	N-isopropylacrylamide
NIPMAm	N-isopropylmethacrylamide
PEG	poly(ethylene glycol)
UCST	upper critical solution temperature
LCST	lower critical solution temperature
VPTT	volume phase transition temperature
NMR	nuclear magnetic resonance
SANS	small angle neutron scattering
DSC	differential scanning calorimetry
MAA	methacrylic acid
SFEP	surfactant free emulsion polymerization
BIS	<i>N, N'</i> -methylenebisacrylamide
APS	ammonium persulfate
KPS	potassium persulfate
TBA	N-tert-butylacrylamide
DLS	Dynamic light scattering
DNA	deoxyribonucleic acid
PEO	poly(ethylene oxide)
PLGA	poly(lactic acid-co-glycolic acid)
BSA	bovine serum albumin
RNA	ribonucleic acid
MIP	molecularly imprinted polymer
CaM	calmodulin

MRI	magnetic resonance imaging
ECM	extracellular matrix
AFFF	asymmetric field flow fractionation
CHDF	capillary hydrodynamic chromatography
TEM	transmission electron microscopy
MALLS	multi-angle laser light scattering
PCS	photon correlation spectroscopy
R_z	radius of gyration
R_h	hydrodynamic radius
R	Rayleigh ratio
M_w	molar mass
A_2	second virial coefficient
$P(\Theta)$	angular dependence of scattered light
Δn	change in refractive index
Δc	change in concentration
PBS	phosphate buffered saline
VLP	virus-like particles
CSQ	calsequestrin
DHEA	<i>N, N'</i> -(1, 2- dihydroxyethylene bisacrylamide)
SDS	sodium dodecyl sulfate
NaIO_4	sodium periodate
AAc	acrylic acid
EPR	enhanced permeability and retention
RES	reticuloendothelial system
EDC	1-ethyl-3-methyl-(3-dimethylaminopropyl) carbodiimide

AFA	4-acrylamidofluorescein
DMSO	dimethylsulfoxide
EphA2	erythropoietin-producing hepatocellular receptor
siGLO	siGLO Red Transfection Indicator
YSA	YSAYPDSVPMMS peptide
NHS	N-hydroxysuccinimide
siRNA	small interfering RNA
HUVEC	human umbilical vein endothelial cells
RNAi	RNA interference
dsRNA	double stranded RNA
RISC	RNA Induced Silencing Complex
EGFR	epidermal growth factor receptor
PET	positron emission tomography
FMT	fluorescence-mediated tomography
Ag nanodots	silver nanoclusters

SUMMARY

This thesis focuses on the use of hydrogel nanoparticles as cancer cell targeting delivery vehicles. Chapter 1 gives a detailed background of hydrogels and their many uses. Chapter 2 describes the use of AFFF-MALLS to investigate the characteristics of microgels. Chapter 3 details nanogel synthesis and their bioconjugation. The nanogels were designed to be ideal drug delivery vehicles, in terms of size and targeting capability. These particles are the focus of the remaining chapters.

Chapter 4 details the encapsulation and delivery of siRNA to ovarian cancer cells. High siRNA loading levels are seen in the particles, as well as effective transport into the cells. Protein silencing by the nanogel delivered siRNA is then described in Chapter 5. The protein silencing leads to apparent increased cancer cell toxicity after subsequent chemotherapy delivery. Successful *in vitro* targeting led to *in vivo* delivery of nanogels, described in Chapter 6. The nanogels were used to deliver silver nanoclusters to Matrigel™ plugs in mice. Chapter 7 lists the future experiments that should be done on the projects listed in the previous chapters.

CHAPTER 1

INTRODUCTION TO HYDROGELS AND THEIR USE AS BIOMATERIALS

*Adapted from Singh, Neetu; Blackburn, William H.; and Lyon, L. Andrew.
“Bioconjugation of Soft Nanomaterials”, Biomedical Nanostructures, John Wiley &
Sons, Inc, 2008, 61-91.*

1.1 Introduction

The last decade of research in the physical sciences has seen a dramatic increase in the study of nanoscale materials, and in their application to problems in biotechnology. The intriguing optical, electrical, magnetic, and mechanical properties of many nanostructures can be exploited for sensing, imaging, and therapeutics. However, much of the work has focused on “hard” materials such as carbon nanostructures, magnetic materials, metals, and semiconductors, since these are the materials that display the most profound and advantageous nanoscale phenomena. Despite the continued interest in these established areas of nanoscience, new classes of soft nanomaterials are being developed from more traditional polymeric constructs. Specifically, nanostructured hydrogels and their conjugates with biomolecular entities are emerging as a promising group of materials for multiple biotech applications. This chapter will present some of the recent advances in the marriage between bioconjugated, nanoscale, water-swelling networks and the biosciences.

The relevance of “nano” to a soft material can be very different from that of an optically, magnetically, or electrically active material, since most hydrogels are mainly interesting from a structural or physicochemical standpoint. Therefore, the goal of this chapter is simply to explore current research in polymeric hydrogel particles, where the nanoscale dimensions of the hydrogel have particular relevance to the length scales of the biological system under study. The focus on polymer particles is important, as these discrete structures bridge the gap between more traditional areas of nanoscience and the world of soft matter. The focus on hydrogels arises from the growing need to understand how hydrophilic polymers can impact emerging areas of biotechnology.

1.1.1 Definition of Hydrogels

As a classification of materials, gels escape a rigid definition as they combine the properties of solids and fluids. They have structural integrity and do not flow when removed from their container. However, for molecules that are significantly smaller than the gel pore size, the transport of material through a gel is similar to mass transport in a homogeneous fluid. Hydrogels, as the name implies, are gels that swell in aqueous media. They are composed of a hydrophilic polymer component that is cross-linked into a network by either covalent or non-covalent interactions.^[1-3] Cross-linking provides dimensional stability, while the high solvent content gives rise to the fluid-like transport properties. The particular physical properties associated with these materials make hydrogels ideal candidates for a number of applications. Perhaps their most widespread use is in superabsorbent materials, which simply absorb and entrap water as in baby diapers. However, to make an impact in areas such as in vivo diagnostics, drug/gene

delivery, chemical separations, or chemical and biological sensors, many groups have pushed towards the synthesis of more complex polymer architectures that often contain one or more biomolecular components. In this chapter, we will focus on a wide variety of approaches towards bioconjugated, hydrogel nanomaterials. For example, tremendous progress has been made in the assembly of amphiphilic block co-polymers into dimensionally stable micellar particles. We will also address the use of stimuli-sensitive polymers in such materials, as these polymers offer new routes to hydrogels that can sense and respond to local environmental conditions, thereby interfacing with biology in an active fashion.

1.1.2 Classification of Hydrogels

Hydrogels can be classified in many ways but in this chapter, they will be dealt with in terms of gel formation. Based on the type of gels there are two classes of hydrogels. The following sections will describe macrogels and microgels, with the main focus of this chapter being on microgels.

1.1.2.1 Macrogels

The most typical form of a hydrogel is in a macroscopic form.^[4-6] These “bulk” gels can be anywhere from millimeters in dimension or larger. Macrogels can be further classified based on the types of cross-links that connect the gels. Based on the type of cross-links there are two classes of hydrogels.^[7] For more detailed information on non-crystalline polymer networks, the reader is referred to the excellent review by Dušek and Prins.^[8]

1.1.2.1.1 Physically Cross-Linked Hydrogels

Hydrogels containing non-covalent cross-links fall under this definition. Such networks give rise to reversible or degradable materials that undergo a transition from the three-dimensionally stable network to a polymer solution upon changing the solution conditions (e.g. temperature, ionic strength, pH, solvent identity). These types of hydrogels have been used to encapsulate proteins,^[9] cells^[10] or drugs^[11] and then release them by dissolution of the hydrogel structure. One or more types of non-covalent interactions can hold these hydrogels together. These forces are often hydrophobic, hydrogen bonding, or ionic associations.

An example of an ion-sensitive gel is alginate, which is a polysaccharide composed of mannuronic acid and gluconic acid. The polymer chains can be cross-linked by divalent calcium ions,^[7, 12] after which hydrogel can be dissolved by using a chelating agent such as EDTA. Alginate hydrogels have been used for encapsulating proteins and also as a matrix for the encapsulation of cells, often allowing for growth and proliferation of the cells within the encapsulating gel. Another example of cross-linking by ionic interactions is that of dextran, which lacks charged regions, but forms hydrogels in the presence of potassium ions; six oxygen atoms of glucose units on three adjacent polymer chains act to chelate potassium, thereby forming a network.^[13]

Blends and interpenetrating networks between two dissimilar polymers can also form non-covalent cross-links. For example, poly(acrylic acid) and poly(methacrylic acid) form hydrogen bonds with poly(ethylene glycol). The hydrogen bond is formed between the oxygen of the poly(ethylene glycol) and carboxylic group of the poly acids. The hydrogen bonds are formed only when the acid groups are protonated, hence

hydrogel formation is pH triggered.^[14, 15] Oligonucleotides have also been used in the formation of hydrogels. Nagahara et al. coupled water soluble poly(*N,N*-dimethylacrylamide-*co-N*-acryloylsuccinimide) to a single stranded DNA.^[16] At room temperature and in presence of complementary DNA, hydrogels are formed, which then dissolve at temperatures above the DNA melting point.

1.1.2.1.2 Chemically Cross-Linked Hydrogels

Chemically cross-linked gels are usually formed by polymerizing monomers in the presence of cross-linking agents.^[7] Poly(2-hydroxyethyl methacrylate) is a well studied hydrogel-forming polymer. It is typically synthesized by polymerizing 2-hydroxy methacrylate with ethylene glycol dimethacrylate as a cross-linker. Various physical properties, such as the swelling capacity of the hydrogels are controlled by the amount of cross-linker used.^[7] Hydrogels can also be formed by cross-linking of the various functional groups present on the polymer backbone. Polymers containing hydroxyl, amine or hydrazide groups can be cross-linked by using glutaraldehyde, which forms covalent bonds with each of the above-mentioned functionalities.^[7, 17, 18]

Enzymes have been used in the formation of cross-linked hydrogels. In one interesting example, Sperinde et al. employed tetrahydroxy PEG functionalized with glutaminyl groups. This polymer forms hydrogels in the presence of an enzyme transglutaminase and poly(lysine-*co*-phenylalanine), where the enzyme catalyses the reaction between the γ -carboxamide group of the PEG-glutaminyl polymer and ϵ -amine group of the lysine to form an amide bond.^[19, 20]

1.1.2.2 Microgels and Nanogels

The subject of this chapter is largely related to entities smaller than macrogels, which are typically called microgels.^[21, 22] Microgels are colloiddally stable hydrogels whose size can vary from tens of nanometers to micrometers. Perhaps the earliest report of microgel synthesis was by Staudinger in 1935,^[23] but interest in such materials for biotechnology applications has only flourished recently. For recent reviews on the subject of colloidal hydrogels, the reader is referred to excellent compilations of Pelton^[24] and Vincent.^[25]

1.1.3 Stimuli-Sensitive Polymers

A large body of research has recently been devoted to the study of gels that respond to their environment; such materials offer the possibility to design tunable or triggered devices. These stimuli-responsive gels are often called “smart” materials, as a result of their responsivity.^[26, 27] However, such a moniker is unwarranted, as the gel behavior can be simply described as a polymer phase transition or phase separation. There is no more “intelligence” in these materials than that of a melting ice cube. Nonetheless, there is a broad range of stimuli available, as hydrogels can be made responsive to temperature,^[5] pH,^[22, 28] ionic strength,^[29-31] light,^[32-36] electric field^[37] and biomolecules.^[38-42] The responsive behavior of the hydrogels is inherited from the type of the polymer used in making the gel and/or any modifications made post-polymerization.

The use of stimuli-sensitive polymers in fabricating hydrogels has led to many interesting applications, including those using bioconjugated materials; in this section we will discuss some fundamentals of stimuli-responsive materials to lay the groundwork for

later discussions. One of the most widely studied stimuli-sensitive polymers is poly(*N*-isopropylacrylamide) (pNIPAm) formed from the monomer *N*-isopropylacrylamide. Since a great deal of work done in our group has been based on pNIPAm, and also to facilitate the understanding of some of the later parts of this dissertation, it is appropriate to provide a brief background on this polymer. For an in depth understanding the reader is referred a comprehensive review by Schild.^[43] One of the earliest studies on the solution properties of pNIPAm was carried out by Heskins et al.,^[44] where they observed that the phase transition of pNIPAm is endothermic and entropy driven. Due to this striking thermal behavior in aqueous media, pNIPAm has been widely used to make responsive hydrogels. As with most olefin-based monomers, pNIPAm has been synthesized by a variety of techniques: redox initiation, free radical initiation, ionic initiation and also using radiation.^[43] Various functional groups have also been added to the polymer via co-polymerization and post-polymerization modification, thereby making multiresponsive and multifunctional polymers. Another polymer with similar behaviors is poly(*N*-isopropylmethacrylamide) (pNIPMAm). Further discussion of this polymer will follow in this chapter.

The behavior of any polymer in a solvent is related to the balance between solvent-solvent, solvent-polymer, and polymer-polymer interactions. For stimuli-sensitive polymers, the polymer solvation can be “switched” by enforcing one of these interactions or by weakening another. For the case of pNIPAm in water, the polymer hydrogen bonds to water via the amide side chains. However, the isopropyl group on the sidechain induces hydrophobic structuring of the water. This structured water leads to entropically-driven polymer-polymer interactions via the hydrophobic effect.^[43] Under

the conditions where pNIPAm has a random coil structure, the solvent-polymer interactions are stronger than the polymer-polymer interactions. At higher temperatures the hydrogen bonds with the water molecules break and there is an entropically-favored release of bound and structured water, leading to the formation of a globular polymer conformation. In this case the polymer-polymer hydrophobic interactions become stronger than the polymer-solvent interactions, and the polymer phase separates. Figure 1.1 illustrates this concept schematically. The temperature at which this phase separation occurs is called the lower critical solution temperature (LCST). It is this behavior that makes pNIPAm very attractive candidates for the fabrication of stimuli-responsive hydrogels. It is worthwhile noting, however, that one must consider more than simply hydrophilic and hydrophobic sidechain contributions to polymer solvation when describing LCST behavior. For example, the polymer formed from *N*-isopropylmethacrylamide,^[45-50] which differs from NIPAm by only a single methyl group, has a higher LCST in water, which suggests that it is more hydrophilic despite a greater organic content. Apparently, this “increased hydrophilicity” does not arise from an increase in polymer polarity, but instead comes from a decrease in chain flexibility. This changes the entropic contribution to the free energy of mixing, and thus increases the LCST. The majority of work presented in this thesis is based on pNIPMAm nanogels.

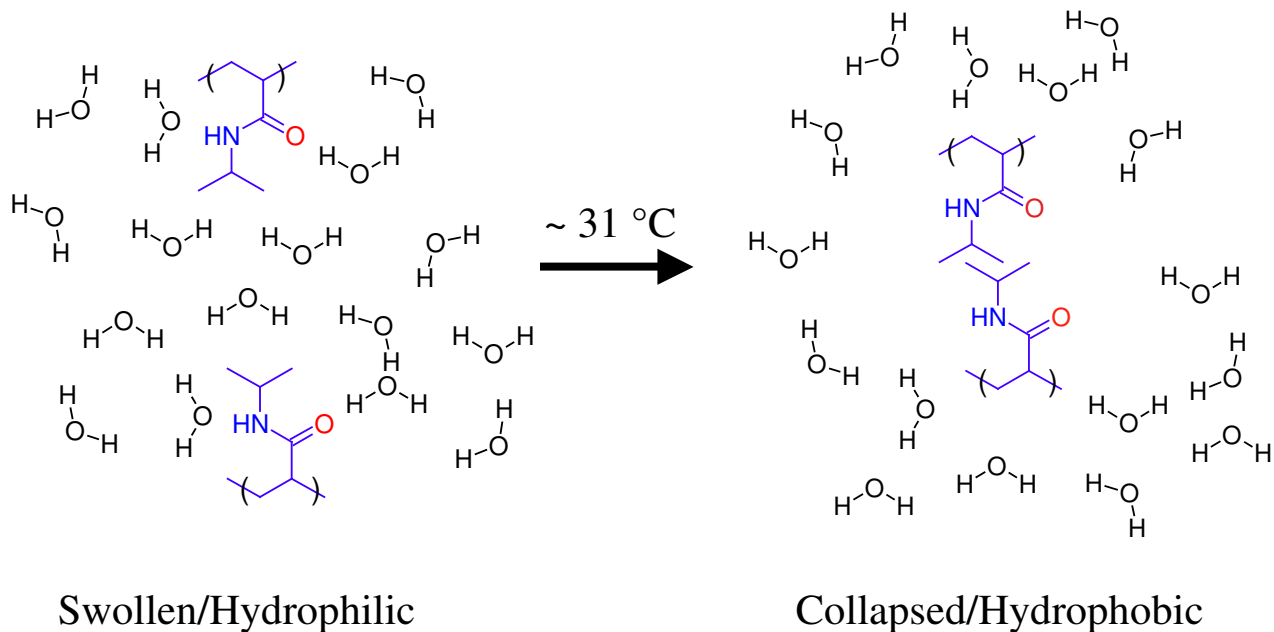


Figure 1.1. Structuring of water around pNIPAm hydrogel networks as the temperature increases above the LCST of 31 °C.

The LCST behavior of pNIPAm has been studied by a variety of techniques including UV-VIS, differential scanning calorimetry, light scattering, viscometry and fluorescence spectroscopy.^[51-59] Wu et al. have extensively studied the phase transition of pNIPAm, where they observed that the transition is not first order *i.e.* the polymer does not directly go from a random coil state to a globular state, but there are other intermediate thermodynamically stable conformations.^[54, 56, 60] There are other classes of thermoresponsive polymers that show an upper critical solution temperature (UCST). In

this case the polymer is phase separated at low temperatures due to inter- or intramolecular interactions, while at high temperatures these interactions break and dissolve or swell the polymer. Most often these interactions are hydrogen bonding or electrostatic. In one example Laschewsky and co-workers have synthesized a block copolymer of pNIPAm and 3-[*N*-(3-methacrylamidopropyl)*N,N*-dimethyl]ammonio propane sulfonate (SPP), which exhibits both LCST and UCST behavior.^[61] The pNIPAm segment provides temperature sensitivity *via* the mechanism described above. On the other hand, SPP is a polyampholytic polymer, which at low temperatures displays strong electrostatic interactions between the oppositely charged regions of the polymers, while these interactions are broken at high temperatures.

1.1.4 Swelling Properties of Hydrogels

The nature of hydrogels is dependent on the type of the monomers used to synthesize them. In case of hydrogels synthesized from pNIPAm, the thermoresponsivity of the parent polymer is inherited by gels made from it. These hydrogels exhibit volume phase transition temperature (VPTT)^[62] at around the LCST of pNIPAm. At temperatures higher than VPTT the hydrogel goes from a swollen (hydrophilic) state to a deswollen (relatively hydrophobic) state. The VPTT of the gels is dependent on several factors including cross-link density, hydrophobic-hydrophilic balance, ionic strength, and solvent composition. Correspondingly, hydrogels fabricated from titratable ionic monomers show pH dependent swelling. The most common ionic monomers used are acrylic acid and methacrylic acid. When the $\text{pH} > \text{pK}_a$ of the acid comonomer, the gel swells due to Coulombic repulsion between the charged monomer units and more favorable solvation

of the deprotonated monomer by the solvent. The equilibrium gel swelling volume is a balance between the osmotic pressure of the polymer network, which is governed by polymer-solvent interactions, and the elasticity of the network.^[8]

In classic and groundbreaking work, the group of the late Toyochi Tanaka showed that ionic thermoresponsive gels, when heated, display a discontinuous transition, while nonionic gels undergo a continuous transition. They have also shown that the shrinking rate of the gel is inversely proportional to the square of the smallest dimension of the gel.^[6, 37, 63-65] Taking advantage of the diffusion length scale, Yan and Hoffman have shown that polymerizing pNIPAm gels at temperatures higher than the LCST of the polymer results in gels having large pore size, which in turn have faster swelling rates.^[66]

This swelling behavior of hydrogels has made them useful in some interesting applications. Thermosensitive pNIPAm gels have been used to control the activity of enzymes. Park and Hoffman demonstrated that by immobilizing an enzyme in the gel, the diffusion of the substrate to the enzyme could be controlled by changing the pore size of the gel, which in turn depends on the temperature of the system. In this way they were able to switch the enzyme on or off by controlling the temperature.^[67] Kim and Healy have synthesized pNIPAm gels with peptide cross-links. These gels can be used as an extracellular matrix mimic, where the peptide can be cleaved by a metalloproteinase, which subsequently leads to gel erosion.^[68]

1.1.5 Microgels and Nanogels

Colloidally stable particles made from hydrogels, also referred to as micro- or nanogels, have similar properties as their macrogel counterparts *i.e.* a pNIPAm microgel,

like the bulk gel, will also undergo a VPTT near the LCST of the parent polymer.^[25, 69] In addition to these properties, microgels have other characteristics of colloidal dispersions such as zeta potentials,^[25, 70, 71] and can also form ordered phases when prepared as a highly monodispersed sol.^[72-75]

Some very important studies have focused on the differences between macro- and microgels with respect to their phase behavior. For example, Wu et al. have shown that the VPTT of the microgels is slightly higher than the LCST of pNIPAm, and also that the transition region is less sharp than that of bulk gels.^[76] The reason for this continuous transition is due to a greater heterogeneity in the subchain lengths of the microgels as compared to traditionally prepared macrogels. When the microgels are subjected to $T > VPTT$, the regions of the particle with longer subchain lengths collapse at a lower temperature than the regions with shorter subchains. Thus one can think of the observed phase transition for a microgel as being the summation of the phase transitions of the different sub-networks in the particle. The Lyon group has also observed this behavior in core/shell structured microgels using fluorescent probes to interrogate cross-linker gradients.^[77]

Understanding the structure of hydrogel nanoparticles is important from the viewpoint of explaining their detailed phase transition behavior, mass transport through the network, and colloidal stability. Light scattering is one of the most common techniques used for structural analysis of hydrogel nanoparticles. Both dynamic and static light scattering have been used extensively and remain the standard techniques for particle characterization.^[25, 76, 78-80] However, other techniques have allowed for even greater insight into the structure of microgels. Guillermo et al. used NMR to determine

the cross-linker distribution in pNIPAm microgel particles and confirmed that these particles have a heterogeneous structure, wherein the periphery of the microgel is more loosely cross-linked than the interior.^[81] Similar studies were carried out by Saunders, where Small Angle Neutron Scattering (SANS) was used to investigate the structural details of pNIPAm microgels synthesized by surfactant free polymerization.^[82] This study again revealed that the microgels prepared by precipitation polymerization have a heterogeneous structure, where in that case it was determined that a thin layer of loosely cross-linked chains was present at the particle periphery. Woodward et al. used Differential Scanning Calorimetry (DSC) to determine the influence of cross-linking density on the phase transition of the particles. They observed an overall decrease in phase transition enthalpy with increase in cross-linker density.^[83] In addition to DSC they also used pulsed gradient spin echo (PGSE) NMR to study the mobility of the solvent in the particle as a function of cross-linker density and observed that the diffusion of solvent is reduced with the increase in the cross-linker density, hence making the particles more rigid at high cross-linker density. Senff et al. have used rheometry to understand the phase behavior of microgels and to determine the effective “softness” of microgel particles.^[73, 84, 85] This group has also carried out studies aimed at determining the internal structure of microgels.^[86, 87] Again, it was determined that the cross-link density is highest at the center of the particle and decreases gradually to the surface. They also found that the internal structure of the microgels depends on the manner in which they are synthesized. A semibatch reaction (reactants are added gradually over a certain time period) gives more homogeneous morphology than a simple batch reaction (all the reactants are added at the start). This effect is attributed to the faster reactivity of the

cross-linker, which gets incorporated at a faster rate during the early stages of a batch reaction. Similar behavior has also been reported by Pelton.^[69, 88]

Chemical functionalization of microgels not only facilitates control over the volume phase transition but also allows post-polymerization modifications and provides handles to trigger response to external stimuli like pH, ionic strength or light. However to achieve efficient design of functional microgels based on chemical modification, it is important to understand how the functional groups are distributed in the polymer network. A recent report by Hoare and Pelton gives an insight into this aspect. The researchers describe two different methods of obtaining controllable distribution of the functional groups in the system.^[89] As the first method, acrylic acid groups were incorporated in acrylamide/NIPAm microgels by hydrolyzing the acrylamide blocks. The second method involved direct copolymerization of methacrylic acid (MAA) with NIPAm. The distribution of the acid functional groups obtained by the two methods had different topochemical distributions. Another factor that influenced the distribution is the temperature of AM hydrolysis i.e. above or below the LCST of the microgel. Based on potentiometric and conductometric titrations as well as electrophoretic mobility evaluations of the microgels, it was found that at a temperature below the LCST, most of the carboxyl groups were located throughout the microgel, whereas at a temperature above the LCST, a high percentage of carboxyl groups was found to be located at or near the surface of the microgels. In case of *p*MAA-*co*-*p*NIPAm microgels, there exists a core-shell kind of a structure with MAA mostly forming the shell. This difference in the distribution of the carboxyl groups in the microgels produced by the two different comonomers is because of the difference in the polymerization kinetics due to different

reactivity ratio of the monomers. The copolymer of acrylamide and NIPAm is expected to have random incorporation of the monomers resulting in acrylamide and hence carboxyl groups on hydrolysis, throughout the bulk of the microgel. On the other hand, the reactivity ratios of MAA and NIPAm suggest that there is greater affinity for the homopolymerization of NIPAm, which is followed by MAA monomer polymerization resulting in the core-shell- like structure.

1.2. Synthesis of Hydrogel Nanoparticles

Hydrogel nanoparticles have been synthesized by numerous approaches. In this section we will discuss some of the commonly used methods, where the synthetic technique being employed is typically dictated by the desired application or the type of study to be carried out. The synthetic method is of particular importance when one considers bioconjugation of the resultant material, as the location, density, and identity of the chemoligation sites on the microgel will dictate the function and utility of the bioconjugate.

1.2.1. Emulsion and Precipitation Polymerization

Surfactant Free Emulsion Polymerization (SFEP), or precipitation polymerization, is the most common technique to synthesize thermosensitive hydrogel particles. Although pNIPAm microgel synthesis by this method was not reported in the literature until 1986, the technique was apparently first utilized by Philip Chibante in 1978.^[69, 90] If carried out carefully, this method can afford particles with very narrow size distribution. In this method all the monomers, NIPAm and the cross-linker (typically *N,N'*-

methylenebisacrylamide (BIS)), are dissolved in water. The solution is purged with N₂ and heated to a temperature far above the pNIPAm LCST (usually ~70 °C), followed by addition of a thermally decomposed free-radical initiator such as ammonium persulfate (APS) or potassium persulfate (KPS).

Microgels synthesized by this method are formed by homogenous nucleation. There are two reasons for carrying out the polymerization at high temperature. One relates to the formation of sulfate radicals, which initiate the polymerization. Secondly, after initiation the NIPAm monomer is attacked by the sulfate radical, followed by radical propagation and chain growth. Once the chain reaches a critical length, it collapses upon itself producing precursor particles. The chain collapses because the polymerization temperature is higher than the LCST of the polymer, hence the name precipitation polymerization. The precursor particles grow by aggregation with the other precursor particles, being captured by existing particles, by capturing growing oligoradicals, and by monomer addition. The charge imparted by the initiator stabilizes the microgels once they have reached a critical size. Figure 1.2 shows the proposed mode of particle growth that occurs during precipitation polymerization. This method is extremely versatile from the standpoint of particle size control. For example, to synthesize smaller microgels, the precursor particles must be stabilized earlier in the reaction. Since there is not enough charge available from initiator fragments to stabilize small precursor particles, an ionic surfactant can be added to impart colloidal stability earlier in the reaction. Similarly, larger particles can be obtained by decreasing the surfactant concentration. Precipitation polymerization can also be used to incorporate comonomers in the microgel. The Lyon group and others have copolymerized ionic monomers with pNIPAm to create pH

responsive microgels.^[22, 31, 91-95] Our group has also copolymerized a hydrophobic comonomer *N-tert*-butylacrylamide (TBA) into pH/temperature responsive microgels; these particles exhibit phase transitions at lower temperatures due to the increase in hydrophobicity of the gel while retaining a pH tunable VPTT.^[95] Similarly, other functionalities can also be copolymerized in these particles by this method.

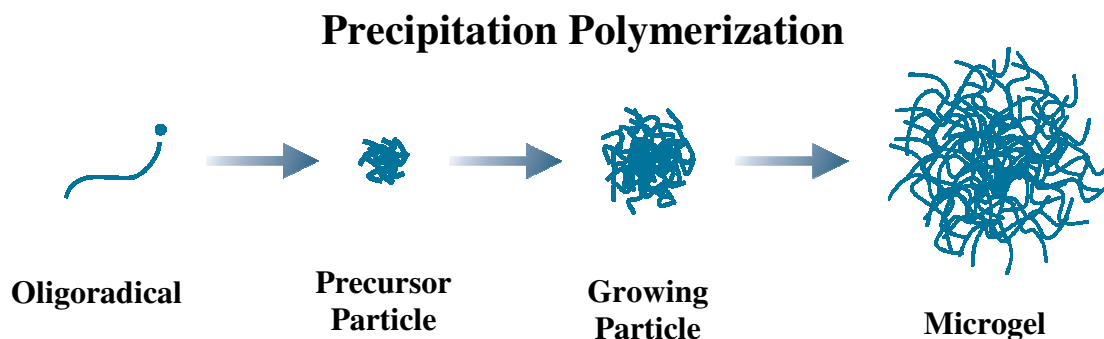


Figure 1.2. Free-radical precipitation polymerization- a growing oligoradical chain reaches a critical length and collapses on itself, creating a precursor particle, to which monomer adds until used up, forming microgels.

The presence of a cross-linker is critical in preventing the dissolution of the polymer particle as it is cooled below the LCST. However, Gao and Friskin have reported that it is possible to make pNIPAm microgels by precipitation polymerization without using a cross-linker.^[96, 97] They attributed this effect to “self cross-linking” of pNIPAm chains by a chain transfer reaction occurring at either or both of two possible sites: the hydrogen atom attached to the *tert*-C on the pendant isopropyl group and the hydrogen atom on the *tert*-C of the main chain backbone. These results indicate that in precipitation polymerization the cross-link density might be higher than one expects on the basis of the cross-linker concentration used in the reaction.

Precipitation polymerization has a few drawbacks. First, the method is useful only for materials that are stable at high temperatures and hence cannot be used to incorporate biological macromolecules. Also the method is best for materials that are hydrophobic so that they can attach to the collapsed precursor particle easily. Hence, if a hydrophilic comonomer is to be copolymerized, only a certain wt % can be incorporated. Beyond that wt % the growing oligomer will be too hydrophilic to undergo efficient chain collapse, thereby resulting in polydisperse microgel dispersions, or the complete lack of particle formation. To overcome these hurdles many researchers have used inverse microemulsion polymerization. In this method an aqueous solution of all the monomers is added to an appropriate amount of oil and surfactant and is stirred to form thermodynamically stable microemulsions. Polymerization can be initiated by having the initiator in the aqueous or in the oil phase. This method has been used to synthesize hydrogel particles with high wt % of ionic monomers; Neyret and Vincent used microemulsion polymerization to prepare zwitterionic pNIPAm microgels.^[98] In this case

they used a UV-activated photoinitiator dissolved in the organic phase. McAllister et al. used the same technique to synthesize a highly cationically charged hydrogel. These particles were able to bind to DNA and can potentially be used in gene delivery.^[99] One other method for preparing microgels, which is similar to microemulsion polymerization, utilizes lipids to form liposomes inside which the particle is formed. Kazakov et al. have demonstrated that liposomes can form a “nanoreactor” inside which microgels can be polymerized.^[100]

1.2.2. Core/Shell Structured Materials

Core/shell hydrogel particles can broadly be divided in two classes: one where the core is made from non-hydrogel material and the shell is made from hydrogel and the second being where both the core and the shell are made of a hydrogel-like material. In the first class of materials the core is usually made of solid material such as polystyrene, silica or gold nanoparticles. Dingenouts et al. synthesized a polystyrene core with small amount of NIPAm as a co-monomer by SFEP.^[101] The polystyrene-*co*-pNIPAm particles were stabilized by the sulfate groups from the initiator. These cores were then used as seeds for polymerizing a cross-linked shell of pNIPAm. For the shell synthesis the reaction was carried out at 80 °C, which provided a core particle with a deswollen pNIPAm-rich periphery, onto which pNIPAm polymerizing in solution aggregated by a precipitation polymerization mechanism. Xiao et al. synthesized similar particles where pNIPAm chains which were grafted on the polystyrene core resulting in a “hairy” particle.^[102]

In another example, Zha et al. have used silica particles prepared by the Stöber method^[103] as a core material.^[104] Vinyl groups were introduced to the surface of the particles via a silane coupling reaction. These particles were then used as seeds for precipitation polymerization of pNIPAm, which resulted in the formation of silica-core/pNIPAm-shell particles. This approach further allowed for the synthesis of hollow pNIPAm capsules by dissolution of the silica with HF. Similarly, Kim and Lee have synthesized gold-core/pNIPAm-shell particles by SFEP. The size of the gold nanoparticles was ~60 nm, which were stabilized by citrate. These gold nanoparticles were then reacted with oleic acid, which helps in attaching the pNIPAm hydrogel shell to the gold core during SFEP.^[105]

The second type of core/shell materials is the one that has hydrogel in both the core and the shell. Our group first reported the synthesis of this type of hydrogel particles by two-stage precipitation polymerization.^[22] In this method a polymer shell of the same or different structure or functionality of the core, is added onto preformed core particles thereby allowing control over the radial distribution of the functional groups in the particle. In a typical synthesis, preformed pNIPAm or pNIPMAm core particles are heated to ~70 °C, followed by addition and initiation of the shell monomer solution. The reaction is carried out for ~4 h and then the mixture is cooled and filtered. This method gives core/shell particles with no increase in polydispersity, as all oligomers formed in solution precipitate on pre-formed core particles. To prevent heteronucleation there are several important parameters that should be controlled, including the concentration of the core, initiator, surfactant and the shell monomer. The mechanism by which this reaction takes place is somewhat similar to that for the core microgels. Since the reaction

temperature is well above the VPTT of the core particles, the particles are in a collapsed state. The collapsed particles are hydrophobic and hence they tend to capture the growing oligomers, which results in the formation of the shell.

Core/shell particles prepared in this fashion can exhibit very interesting properties.^[21,45,46,77,106-110] Since the shell can be synthesized using different comonomers than the core, the particles can show multiple phase transition behavior with temperature.^[22, 45, 46] Furthermore, depending upon the cross-linker density of the shell, compression or “shrink-wrapping” of the core can be observed due to a cross-link gradient in the shell.^[106, 107, 109, 110] The Lyon group has also used this synthetic method to make hollow hydrogel capsules.^[111] To accomplish this, the core is fabricated with a degradable cross-linker and the shell with a non-degradable one. The degradable cross-linker that we have used contains a vicinal diol, which can be degraded by stoichiometric addition of periodate. After core degradation, the particles were cleaned extensively by centrifugation, after which DLS and fluorescence were used to confirm the hollow structure.

Berndt and Richtering have also synthesized core/shell particles having two different polymers in the core and the shell.^[45] In their demonstration, the core was made of pNIPAm and the shell consisted of poly(*N*-isopropylmethacrylamide) (pNIPMAm), which has a LCST of 45 °C. They studied the thermoresponsivity of these particles and found, in a similar fashion to previous work from our group, that the particles had two transitions corresponding to the LCSTs of the two polymers. In a recent study the researchers investigated the effect of shell thickness and cross-linking density on the structure of the doubly-temperature sensitive core-shell microgel networks using Small

Angle Neutron Scattering (SANS) techniques.^[112, 113] It was observed that variation of cross-linking density in the shell mainly affects the dimensions of the shell without affecting the core. However, increase in the shell to core mass ratio, leads to increased expansion of the core with a broader core-shell interface between the LCSTs, thus indicating the elastic force exerted on the core by expanding shell. Studies at a temperature below the LCST of the core suggested that the core of the core-shell particle was unable to swell to the same extent as a core in the absence of a shell, thus indicating that the expanded shell prohibits the swelling of the core. In another report, the same research group observed that an increased shell thickness shifts the core transition towards higher temperatures while the collapse of the core can shift the transition of a thin shell to lower temperatures.^[114] An additional thermal transition is also observed in these core-shell microgels, which was attributed to the formation of additional hydrogen bonds near the core-shell interface resulting from the overcompensation of the thermodynamic forces during the core transitions by the elastic forces in the shell.

1.2.3 Post Polymerization Modification of Hydrogels

For certain applications not all of the desired hydrogel functionalities can be added during the polymerization step. There are several reasons for this: the desired functionalities may not be stable during the polymerization step or the molecules are simply not polymerizable. This is especially true for most biomolecular structures from which hybrid gels would be prepared. To allow further functionalization of hydrogels, most often a small amount of comonomer with acidic or basic functionality is copolymerized during the polymerization step. These functional groups are then used for

attachment of molecules that could not be directly incorporated by polymerization. This particular class of syntheses encompasses a large variety of particles, of which only a few will be mentioned in this chapter.

The group of Haruma Kawaguchi has used post polymerization modifications extensively for making particles with variety of functions.^[115] For example, to synthesize a tetra-functional particle, they first synthesized standard microgels using acrylamide, BIS, methacrylic acid and *p*-nitrophenyl acrylate as the co-monomers. The thus introduced ester side chain can be hydrolyzed to give acidic particles, or after hydrolysis can be reacted with ethylene diamine to give amphoteric particles. The acid groups were also coupled with a long chain alkyl amine to form hydrophobic particles. Finally the acid groups were coupled to an IgG to form bio-functionalized microgels. This particular report illustrates the tremendous versatility in microgel structure and function that is offered by post polymerization modification.

Another interesting system involved the synthesis of pNIPAm chains bearing terminal carboxyl groups, which were then grafted to microgels. The carboxy termini were then used to attach the enzyme trypsin, resulting into a particle having two different kinds of pNIPAm chains on the surface: one with trypsin and the other without it. Surprisingly, it was found that the two chains had different transition temperatures. The free chains collapsed at a lower temperature than the trypsin conjugated chains, thereby exposing the enzyme for substrate binding. Hence by this simple construct they were able to control the enzyme activity by controlling the temperature.^[116]

In a report by Delair, et al, the immobilization of DNA on microgels by post polymerization modification was described. Microgels composed of pNIPAm with an

amine comonomer were synthesized. Single stranded DNA with an amine group at the 5' end was reacted with 1,4-phenylene diisocyanate in 1:2 ratio so that one of the isocyanates was coupled to the DNA, while the other one remained free. After purification, the DNA was coupled to the pNIPAm microgels by reacting the free isocyanate with the amines on the surface of the particles. The DNA particles were then used for detection of viral DNA and also for formation of two dimensional arrays on planar substrates.^[117]

Post polymerization modification can not only be used for coupling biomolecules but also for grafting synthetic polymer chains. Hu et al. synthesized pNIPAm microgels and grafted pNIPAm chains on these particles by RAFT.^[118] They then used these particles to study thermal behavior of the grafted polymer. In another example Hu and Wu grafted poly(ethylene oxide) (PEO) chains on the microgel particles. The hydrophilic PEO chains were observed to stretch from the particle surface as the particles size decreased with the increase in temperature.^[119]

1.3. Bioconjugated Hydrogel Particles in Nanotechnology

The synthetic methods described in the previous sections have enabled the field to advance towards the application of hydrogel nano- and microparticles in more complex biotech and nanotech applications. In this section, we will describe some of these applications, highlighting systems where the ability to create synthetically and topologically complex hydrogels has led to successful incorporation into advanced nanosystems.

1.3.1. Drug/Gene Delivery

Recently, significant efforts have been put into devising colloidal drug carriers. It has been hypothesized that an actively targeted particulate drug carrier will increase the therapeutic efficacy of a drug by delivering that drug to the diseased site, while also reducing systemic side-effects of the drug. An ideal drug carrier should be able to target and deliver only to the diseased sites, it should not induce immune response, and it should be degradable and produce non-toxic degradation products.^[120]

The particulate carriers that have been most widely studied are liposomes and polymer nanoparticles. Liposomal drug carriers have been studied extensively, with a few liposomal formulations currently being available in the market, while many others are in the development “pipe-line”. One important drawback of liposomes is payload leakage. Since the boundary of the liposomes is a simple lipid bilayer, performance can be hampered by passive diffusion of drugs across that boundary.^[121] Among polymer particles, the most widely studied are poly(lactic acid-*co*-glycolic acid) (PLGA) particles.^[122] The popularity of this material largely stems from its degradation into non-toxic byproducts, which can be removed from the body via the renal system. However, this construct suffers from numerous drawbacks, as it is a very hydrophobic, immunogenic polymer with acidic degradation products. The increase in acidity associated with polymer degradation can induce non-specific inflammatory responses, which can be very detrimental in targeted delivery applications. Non-viral gene delivery systems have been proposed as a safer alternative to viral vectors, since they will induce host immune response to a lesser extent than viral vectors. Several cationic polymers such as polyethyleneimine, polyamidoamine and polylysine, have been used for non-viral

gene delivery, but they all lack the biocompatibility needed for in vivo use.^[123] Conversely, hydrogel nanoparticles represent a potentially useful class of materials in drug/gene carrier systems, but have been studied much less extensively. Here we report a few examples of recent efforts involving nanoparticulate hydrogel delivery vehicles.

In an effort to employ naturally-occurring polymers as delivery vehicles, Wang and Wu used agarose gel particles for protein delivery.^[124] A model protein ovalbumin was encapsulated in ~500-nm diameter, spherical agarose gel particles. Following protein loading, it was demonstrated that the particles released ovalbumin in a temperature dependent fashion, where the rate of protein release was higher at elevated temperatures. This was due to the larger swelling volume of agarose at higher temperature, which facilitates mass transport. Another example of protein delivery was reported by Li et al.,^[125] who demonstrated the use of poly(vinyl alcohol) hydrogel nanoparticles for this application. These particles were prepared by an emulsion technique without incorporating any cross-linker. The model protein bovine serum albumin (BSA) was incorporated during the particle formation. As with the previous example, the rate of release of BSA increased with temperature. The authors attribute this behavior to the decrease in the number of cross-links at higher temperature in the polymer network, thereby making the gel network more “open” for the transport of BSA. Using this methodology, the authors were able to demonstrate release of BSA over ~30 h. Biodegradable hydrogel nanoparticles have been prepared by Kim et al. using glycidyl methacrylate dextran as the major co-monomer and dimethacrylate poly(ethylene glycol) as a covalent cross-linker.^[126] In this case, the particles were prepared by free radical polymerization and a hydrophobic drug, clonazepam, was then loaded in the particles. It

was found that the release rate was dependent on the pH as well as the concentration of the enzyme dextranase, which degraded the dextran and eroded the particles. Na and Bae have used self assembled hydrogel particles of pullulan acetate and sulfonamide conjugates to study the release of the drug adriamycin.^[127] In this case the pullulans had pH responsive polymer incorporated in the structure, which caused the particles to shrink and aggregate at pH < 7. The shrinking of the particles in turn caused the expulsion of the drug into the surrounding medium.

Peppas and co-workers have used hydrogels as a delivery vehicle to carry insulin.^[128] Poly(methacrylic acid) and poly(ethylene glycol) were used to synthesize the hydrogels by UV-initiated free radical polymerization. Insulin was then conjugated to the protein transferrin, and this complex was loaded into the hydrogels. The insulin-transferrin conjugate is used as it has been shown to cross the intestinal epithelium. By loading the insulin-transferrin complex into the hydrogels, Peppas and co-workers feel this can be used as an oral delivery system for insulin, as it provided increased stability against proteolytic degradation. Insulin was conjugated to transferrin by reacting it with dimethylmaleic anhydride (DMMA). The transferrin was conjugated with succinimidyl 3-(2-pyridyldithio)propionate (SDSP). The DMMA and SDSP were then reacted to form the insulin-transferrin conjugate, which were then loaded into the hydrogels. A 22-fold increase in transport of insulin across Caco-2 cell monolayers was seen with conjugate-loaded hydrogels versus insulin alone.

An interesting example of controlled release of a drug from a microgel comes from the group of David Needham.^[129] They used ~6.5 μm diameter methacrylic acid microgels as a matrix for drug encapsulation and release. While these particles are by no

means in the nanoscale-range, they illustrate an interesting concept that could be extended to the nanoscale. Under conditions where the particles are deprotonated and hence swollen due to Coulombic repulsion between the negatively charged regions, the particles could be loaded with the anti-cancer drug doxorubicin. Upon reducing the pH of the medium below the acid pKa, the particles condensed. To prevent leakage of the drug from the polymer, the particles were then coated with a lipid bilayer. These lipid coated particles were then suspended in a medium of $\text{pH} > \text{pKa}$. Surprisingly, no gel swelling was observed and hence no drug was observed to leak from the construct. In order to release the drug, a series of voltage pulses were applied to electromechanically disrupt the bilayer and cause the swelling of the particle. Thus, the authors illustrated that the drug could be protected and then be released on demand using a subtle stimulus. A similar example was published by Jeffrey Moore's lab. Again, in this example the polymer constructs are not at nanoscale level but nonetheless provide an interesting concept.^[130] A pH sensitive gel was photopolymerized in a cylindrical shape. The gel was fabricated from 2-hydroxyethyl methacrylate, acrylic acid and ethyleneglycol dimethacrylate. Palmitoyl chloride was then covalently bound to the surface of the gel. This modification of the gel created an ion barrier that enabled the pH sensitive gel to remain in a condensed state even in high pH media. This barrier was disrupted by a surfactant, which caused the gel to swell. The ability of the fatty acid layer to maintain a sharp chemical potential gradient is analogous to the function of a cell membrane and shows the promise of creating highly non-equilibrium systems from well-designed nanomaterials.

While the previous examples were simple demonstrations of ex vivo controlled release from hydrogel particles, others have applied nanoparticulate hydrogels to in vivo delivery. For example, Hsiue et al. have used pNIPAm nanoparticles for ocular delivery.^[131] Two formulations were used, where one was composed of a solution of linear pNIPAm, while the other was mixture of linear pNIPAm and pNIPAm particles. The drug release and cytotoxicity studies were carried out on rabbits. The drug epinephrine, which reduces intraocular pressure, was then delivered from each of the two formulations. It was observed that the intraocular pressure was decreased for ~24 h when the linear pNIPAm system was used, while the mixed system extended the therapeutic effect to ~32 h. Systems such as these are therefore potentially interesting for the clinical treatment of glaucoma.

As mentioned above, an ideal drug carrier should not induce an immune response in the host. This is commonly achieved by making the surface of the particle hydrophilic, which can prevent opsonization (i.e. adhesion enhanced phagocytosis) by macrophages.^[132] For example, Gaur et al. synthesized cross-linked polyvinylpyrrolidone hydrogel nanoparticles (~100 nm diameter).^[133] The surface of these particles was then made hydrophilic by attaching poloxamers and poloxamines, which are examples of polyethylene glycol/polypropylene glycol block copolymers. In vivo studies in mice indicated that less than 1% of the dose was retained by the macrophages in the liver, and even after 8 h of injection ~5-10% of these particles were still circulating in the vasculature. This enhanced circulation time, and the lack of liver accumulation, could enable the use of such particles in drug delivery. They also reported that increase in size and hydrophobicity increased their uptake by reticulo-endothelial system, suggesting that

both factors may play a role in the ability of the body's defense mechanisms to recognize the particles as foreign invaders.

Targeting is an important property for a drug carrier, as one can potentially enhance the uptake and retention of the nano-carrier at the site of disease via active targeting. The Lyon group has synthesized a folic acid labeled pNIPAm core/shell microgel that can target cancer cells.^[134] Folic acid is a well-known ligand for targeting cancer cells because most tumors overexpress folate receptors. In this demonstration, pNIPAm core/shell hydrogel particles were synthesized, where the pNIPAm core was fluorescently labeled and the pNIPAm shell contained a small amount of a co-monomer containing a primary amine. We then covalently coupled folic acid to the amine-containing hydrogel shell in order to surface localize the targeting ligand. When these particles were incubated with cancer cells that were overexpressing the folate receptor, the hydrogel nanoparticles were taken up by receptor mediated endocytosis. It was also observed that the particles exhibited thermal cytotoxicity above the phase transition temperature. The exact reason for this effect is not known but is suspected to be intracellular aggregation and protein adsorption on deswollen, hydrophobic pNIPAm particles. Since these particles apparently retain their thermoresponsivity in the cytosol, it was hypothesized that they could enable thermally-triggered delivery of chemotherapeutic payloads, thereby enabling both active targeting and triggered delivery in one vehicle.

In another example of active targeting, Choi et al. used pNIPAm microgels for targeting liver cells.^[135] They used pNIPAm-*co*-acrylic acid microgels that were tagged with fluorescein, while the targeting moiety in this case was galactose, which is a ligand

for asialoglycoproteins. It was observed that galactosylated microgels were internalized in the cells via this ligand-receptor interaction. Furthermore, since these particles are thermoresponsive, they studied temperature dependent uptake of these particles. The uptake efficiency increased with the increase in temperature, which they suggested was due to enhanced uptake efficiency for smaller particles, although the increase in particle hydrophobicity could also enhance uptake. The Wooley group has investigated SCKs with targeting ligands like folic acid, integrins and peptides.^[136-138] They have also demonstrated that nanoparticles coupled with a short peptide belonging to protein transduction domain of HIV exhibited targeting ability to CHO and HeLa cell lines.

Kumacheva and co-workers describe another hydrogel design to be used for cancer targeting.^[139] In this work, pNIPAm-co-AAc hydrogel particles averaging 150 nm in diameter were synthesized. Hydrogel particles were conjugated with transferrin by carbodiimide coupling. The transferrin was used to target the particles to HeLa cells, as transferrin receptors are present on the surface of HeLa cells, thereby enabling receptor-mediated endocytosis. These hydrogels were loaded with Rhodamine 6G (R6G) and later with doxorubicin to study uptake and delivery. The transferrin-conjugated particles delivered 100 times more R6G to cells than bare microgels, and cell mortality was greatly enhanced over bare, doxorubicin-loaded microgels ($72.6\% \pm 5.0\%$ vs. $33.8\% \pm 2.8\%$).

The polysaccharide chitosan and its derivatives, on account of their biocompatibility, biodegradability, nontoxicity and mucoadhesive property, are very attractive precursors for synthesizing delivery vehicles. Kumacheva and coworkers recently developed chitosan-based microgels which release the cancer drug methotrexate disodium, MTX triggered by a pH change.^[140] The microgel synthesis strategy was

designed to yield a particle of well-defined size, with a surface which could be bioconjugated with cell receptor-specific ligands and ability to deliver the drug in response to a pH stimulus. The synthesis involved grafting of (2-hydroxyl) propyl-3-trimethylammonium to the chitosan to form the derivative *N*-[(2-hydroxyl-3-trimethylammonium) propyl]chitosan chloride (HTCC). The quaternary ammonium side chains were cross-linked by ionic association to negatively charged tripropylphosphate (TPP) to form microgels. The microgels were stable at physiological pH and showed swelling in the range of $3 < \text{pH} < 6$ due to increased electrostatic repulsion in the polymer network arising mostly from the high degree of protonation of the primary and secondary amino groups of HTCC. The protonation of TPP at pH 2.5 (pK_a values of TPP = 2.3 and 6.3), resulted in the decrease of the degree of cross-linking resulting in tremendous increase in the microgel size (from diameter 180nm to ~1100nm). Since the microgel was positively charged at pH 7.4 they were able to easily load a negatively charged drug MTX through electrostatic interactions. The loaded drug was released (pH 7.4) about 66% in a single day, while 30% remained trapped beyond 5 days. At pH 5.0, about 93% of the loaded drug was released after 1 day and about 95% after 3 days. Receptor-mediated intracellular uptake, which triggers drug-releasing cellular pH changes, was facilitated by conjugation of transferrin to the surface of the microgels using carbodiimide coupling chemistry. The MTX-loaded, transferrin-conjugated microgels were conjugated with negatively charged luminescent CdSe/ZnS quantum dots to allow imaging of the cellular entry of the particles. The transferrin-conjugated MTX-loaded microgels showed 4.8 and 2.8-fold increase in cell mortality when compared to pure and non-bioconjugated MTX-loaded microgels respectively.

Synthetic/viral composite systems have also been explored. For example, Jana et al. prepared polyvinylpyrrolidone nanoparticles and encapsulated them in a reconstituted Sendai viral envelope containing only the fusion proteins.^[141] These particles were incubated with human hepatoblastoma cell lines, which resulted in internalization of the polymer particles, as confirmed by fluorescence. Na et al. have used self assembled polysaccharide (curdlan) particles for targeting.^[142] Curdlan was hydrophobically modified with a carboxylated sulfonylurea derivative. The targeting ligand was lactobionic acid, which targets HepG2 cells. As expected, the degree of non-targeted uptake was significantly diminished relative to that for particles targeted to HepG2 cells.

Many groups have used cationic polymers such as chitosan for gene delivery. Chitosan is a natural cationic polysaccharide consisting of D-glucosamine and *N*-acetyl-D-glucosamine. This polymer has been shown to be biocompatible, non-immunogenic and degradable, thereby making it potentially suitable as a delivery vehicle. In the presence of polyanions, chitosan can form hydrogel nanoparticles by complex coacervation. For example, chitosan-DNA nanoparticles have been widely studied for their application in gene delivery. Mao et al. have synthesized chitosan-DNA nanoparticles and studied the transfection efficiency.^[123] Targeting agents, like transferrin, have also been conjugated to these particles to increase the internalization, while drugs like chloroquine have been encapsulated within these particles to investigate controlled release. Mitra et al. have used chitosan to encapsulate doxorubicin, a highly toxic chemotherapeutic drug.^[143] For encapsulation they first conjugated doxorubicin with dextran. This drug-dextran conjugate readily formed particles when mixed with chitosan. In vivo studies then showed that the chitosan-drug conjugate circulated in the

blood longer than the drug alone and also that the conjugate decreased the size of tumor to a larger extent than the free drug.

In a very recent example of using soft polymeric nanoparticles bioconjugates for targeted drug delivery *in vivo*, Langer and coworkers used a nanoparticle construct of biocompatible and biodegradable poly(D,L-lactic-*co*-glycolic acid)-*block*-poly(ethylene glycol) (PLGA-PEG).^[144] PLGA-*b*-PEG copolymers having terminal carboxyl groups were precipitated into nanoparticles in presence of the cancer therapy agent docetaxel, resulting in the encapsulation of the drug within the nanoparticles. With an aim to target the particles specifically to cancer cells, the terminal carboxyl groups on the nanoparticles surface were conjugated to RNA oligonucleotide aptamers (specific to PSMA proteins expressed on the surface of LNCaP prostate epithelial cancer cell) by carbodiimide coupling chemistry. Animal studies showed that the aptamer bioconjugate nanoparticle results in complete shrinkage of the tumor after a single intratumoral injection of maximal tolerated dose for i.v. administered docetaxel. The nanoparticle synthesis involves FDA approved materials and the technique thus holds promise for clinical trials of the effectiveness of polymeric nanoparticles bioconjugates in cancer therapy. Additional advantages for clinical studies include small size, facile synthesis, relative stability and immunogenic nature of the targeting agents.

Hubbell and coworkers synthesized nanoparticles by emulsion polymerization and evaluated their performance as circulating carriers.^[145] Particles were composed of cross-linked poly(propylene sulfide) and Pluronic F-127 was used as a surfactant, which becomes entangled in the network. This creates a PEGylated outer surface on the nanoparticles. Two particle sizes were synthesized; 40 nm and 100 nm in diameter. The

nanoparticles were injected into the tail vein of mice, and the smaller size particles have a blood half-life of 6 h versus a half-life of 2.9 h for the larger particles. Longer circulation of nanoparticles can lead to potential as drug carriers.

Zhang and Mirsa have synthesized a functionalized Fe_3O_4 conjugated with doxorubicin, encapsulated it in a thermosensitive polymer and studied drug release from the particles. The magnetic Fe_3O_4 nanoparticles were functionalized with methyl-3-mercaptopropionate, and the doxorubicin was then conjugated through a hydrazinolysis reaction. The outer polymer was synthesized in several steps, including free radical copolymerization and hydrazinolysis reactions. The magnetic nanoparticles were then mixed with the polymer and 1, 6-diaminohexane at a ratio of 2:3:1 in DMSO to encapsulate the drug-conjugated nanoparticles. The release of the drug from the particles was then studied. At 37 °C, the release of the drug is at a high rate for 5 h, then a sustained release is seen over 48 h. Acidic conditions also lead to favorable drug release, making these particles potential sustained-release drug carriers.^[146]

1.3.2. Encapsulation and Microreactors

The large internal free volume and hydrophilicity of hydrogels makes them useful in encapsulation of various species such as DNA, RNA, small molecules, and proteins. When encapsulated, the hydrogel network can protect these species or release them in a controlled manner, as discussed previously. In this section we will discuss the encapsulating property of microgels for applications other than drug delivery.

It has been observed that mass transport rates of small molecules in hydrogels depend on the pore size, where larger pore sizes make it easier for the molecules to

diffuse in the gel. In case of thermoresponsive microgels, a temperature dependent diffusion is observed. At $T < VPTT$ higher diffusion rates are observed than at $T > VPTT$, due to a decrease in pore size of the polymer network at higher temperatures. Also, the charge on the polymer network is an important parameter, where it is easier to encapsulate molecules that are oppositely charged with respect to the polymer. In addition to this, a hydrophobic polymer network will enhance the encapsulation of a hydrophobic moiety.

Akiyoshi et al. have used cholesterol bearing pullulans to encapsulate various proteins and peptides, e.g. insulin in which case they observed the conformational stability of the macromolecule using circular dichroism (CD) spectroscopy.^[147, 148] No spontaneous release of insulin was observed from the nanoparticle, suggesting a very strong complexation in the macromolecular assembly. They observed that free insulin aggregated when subjected to heating but the encapsulated protein resisted such aggregation. They further studied the insulin stability against α -chymotrypsin activity, which degrades insulin. The pullulan-insulin complex resisted degradation to a much larger extent than the free insulin. Hence this system can potentially be used for protection of the species of interest. Similarly, they have used pullulans as molecular chaperones for an enzyme.^[149] Carbonic anhydrase B is an enzyme that denatures and aggregates at high temperature. The authors complexed the enzyme with the pullulans in the enzyme's denatured state. The complex was cooled and the enzyme was released from the particles. They observed that the enzyme refolded in its native state and again became active.

Developing strategies for controlling the permeability of hollow nanoparticles can allow their use as nanoreactors. Advancement in this respect has been achieved by Meier and coworkers, who synthesized nanoreactors based on ABA-triblock copolymer micelles.^[150] For designing of the nanoreactors, the researchers used amphiphilic triblock polymers and assembled a natural membrane channel protein, porin OmpF in situ with the micellar assembly of the triblock polymer, yielding porin-containing nanoparticles. The membrane protein serves as a channel for permeation of small hydrophilic molecules through the hydrophobic region of the polymeric micelles. An enzyme β -lactamase was also encapsulated in the inside of the porin-containing micellar nanoparticles. The micelles were made stable by cross-linking the underlying triblock copolymers by photopolymerizing the reactive end groups of the blocks. To verify enzyme activity, the researchers studied the hydrolysis of the antibiotic ampicillin by the encapsulated enzyme by monitoring the hydrolysis product formed (ampicillinoic acid) that subsequently diffused out of the nanoreactors. They observed that the enzyme retained its activity even while encapsulated in the micelle. No reaction was observed without the porin channels because of the inability of the ampicillin to enter the hydrophilic interior (where the enzyme was located) of the micelle through the thick hydrophobic shell. However the hydrolysis rate due to the encapsulated enzyme was lower than that due to a free enzyme. This is due to the limited diffusion of the ampicillin and the ampicillinoic acid due to the low number of narrow porin channels in the shell. Based on a similar scheme, Gelder and coworkers formed a similar nanoreactor encapsulating a prodrug-activating enzyme and demonstrated that the nanoreactors could efficiently hydrolyze the prodrug.^[151]

1.3.3. Analytical Applications

Given the ability to synthesize a variety of responsive hydrogel structures, chemical and biological sensing applications remains an intriguing application. One of the earliest types of hydrogel nanoparticle employed in “sensing” was a pH responsive particle. The simplest method of fabrication involves the use of pH responsive moiety, such as a weak acid, which can be copolymerized into the polymer network. At low pH, the acid groups are protonated and the particles will be in a somewhat condensed form, while at a higher pH where the acid groups are deprotonated, the particles adopt a swollen structure due to Coulombic repulsion among the negatively charged regions and a change in the free energy of mixing with water. Similarly, charged microgels are responsive to ionic strength, where an oppositely charged ion neutralizes the charge and causes the gel to shrink. Similar approaches have enabled the fabrication of cross-linked block co-polymer micelles with pH responsivity. While this approach appears to be a generalizable motif by which one can imagine designing hydrogel nanoparticles that “sense” their surroundings, very little else has been done on creating hydrogel nanoparticles for real chemical sensing applications. However, a few examples are beginning to emerge. For example, we have demonstrated that hydrogel microstructures can be rendered sensitive to protein binding provided the interaction is multivalent and therefore results in an increase in the microgel cross-link density.^[42] This approach has been extended to reversible biosensors based on antibody:antigen displacement or competitive binding. In this example, we have first incubated antigen-presenting microgels with antibodies, which then bind to the microgel surface. These microgels also possess a photoaffinity labels (benzophenone) which can then be photoactivated, thereby

photo-coupling the antibodies to the microgels. The antibody-antigen based cross-links can then be reversibly switched by exposure to free antigen, which displaces the cross-link and swells the particle. This approach has been coupled to a microlensing technology that allows for rapid, label free readout of the sensor response.^[152]

In addition to these applications, microgels have been used for the separation of proteins from complex media. Kawaguchi et al. reported that proteins could be separated using thermoresponsive microgels.^[116] They used regular pNIPAm microgels and observed that at $T > VPTT$ larger amounts of protein bound to the particles than at $T < VPTT$. The higher degree of protein adsorption at $T > VPTT$ was attributed to hydrophobic interaction between the protein and dehydrated polymer. In an approach that utilized Coulombic interactions, Elaissari et al. used cationically charged pNIPAm microgels for extraction of RNA. It was observed that the interaction between the cationic particles and negatively charged RNA decreased with an increase in pH, ionic strength and temperature, thereby indicating that adsorption was mainly governed by electrostatics.^[153] In an immunoseparation study, Kondo et al. synthesized poly(styrene/NIPAm/glycidyl methacrylate) microgels. These particles were designed such that they flocculated at high temperature and at high ionic strength. Using the glycidyl methacrylate co-monomer as a chemical handle for chemoligation, BSA was coupled to the particles, which were then used for immunoseparation of anti-BSA from serum. After incubation with the serum, the particles were separated by flocculation.^[154] Similarly, particles that contained magnetite were used by this group for separation and purification using a magnetic field to collect the particles.^[155]

Hydrogel nanoparticles have also been employed in a molecularly imprinted polymer (MIP) scheme. The principle behind MIP is based on both shape and molecular-recognition templating. When the polymerization is carried out in the presence of “template” molecules, it is envisioned that the polymer will rigidify around that template, forming a cavity that is optimized for binding of that molecule. After the templates are removed, it is hoped that the cavity retains that shape and is able to bind and detect that particular molecule or similar molecules in a complex mixture. Ye et al. have synthesized hydrogel nanoparticles in the presence of theophylline and 17 β -estradiol. The sensing molecules were dissolved in the mixture of methacrylic acid and trimethylolpropane trimethacrylate and then polymerized either thermally or by UV irradiation. In these studies they used radio ligand binding analysis to determine the sensitivity and selectivity of analyte binding.^[156] Competition binding experiments showed high selectivity for the analyte.

Daunert and coworkers in a recent report showed how biological processes can be used to tailor the response of hydrogels.^[157] A biological recognition unit was incorporated into the hydrogel structure and conformational changes in the unit in response to external factors resulted in volume changes in the hydrogel. Calmodulin (CaM), a protein, which undergoes different conformational changes on binding with Ca^{2+} (native to dumbbell-like), certain peptides or a certain class of drugs like phenothiazines (native to more constricted), was incorporated in the hydrogel by genetically engineering the protein to have a cysteine residue at the C-terminus, which was further conjugated to an allylamine in order to attain oriented immobilization of the protein in the hydrogel network. For incorporating phenothiazine in the polymer network,

a derivative having polymerizable acrylate group was synthesized. Free radical polymerization of the polymerizable protein and drug, an acrylamide monomer and a cross-linker N,N'-methylenebis(acrylamide) resulted in the desired hydrogels. The hydrogel showed reversible swelling which was dependent on the concentration of Ca^{2+} . On saturating the hydrogel with Ca^{2+} , the resulting conformational change in CaM and the phenothiazine binding site of CaM became accessible to the immobilized drug resulting in the increased cross-linking and shrinkage of the hydrogel. The gel swelled on Ca^{2+} removal, resulting from the release of the drug derivative from the binding site and also since the water uptake property of the polymer was changed due to modification of the hydrophobic surface of the protein. The hydrogel also showed response to phenothiazines. When the hydrogel was treated with free phenothiazine (chlorpromazine), the hydrogel swelled due the competitive binding of the free drug replacing the bound immobilized drug from the binding site of the conjugated protein. These protein and drug modified hydrogel biomaterials hold promise for microactuators and in microfluidics, as also demonstrated by the authors.

Miyata, et al., have demonstrated gels that respond to tumor markers.^[158] The gels were prepared by biomolecular imprinting, which involves functionalizing the gels with ligands that will interact and form cross-links upon recognition of a target molecule. In this work, the gels responded to the tumor specific marker α -fetoprotein, AFP. AFP is a glycoprotein used for serum diagnosis of primary hepatoma. Lectin (Con A) and polyclonal anti-AFP antibody was conjugated with N-succinimidylacrylate (NSA) to form polymerizable vinyl groups and the gels were formed by copolymerizing these groups with acrylamide in the presence of template AFP. This forms a lectin-AFP-

antibody complex, and the removal of the AFP creates the AFP-imprinted gel. It was shown that AFP-imprinted gels shrank upon exposure to AFP, as the lectin-AFP-antibody forms a gel cross-linking complex. Nonimprinted gels experienced slight swelling in AFP solutions. The gels were also shown to be specific to the glycoprotein, as the gels did not shrink, but actually swelled in ovalbumin solutions as well.

Wooley and co-workers have developed gadolinium-labeled shell-cross-linked nanoparticles for magnetic resonance imaging (MRI) applications.^[159] Gadolinium combined with the chelating agent diethylenetriaminepentaacetic acid (DTPA) is the predominant contrast agent used today for MRI. It is important to stabilize these agents within biological environments since gadolinium is highly toxic. The Wooley group complexed the gadolinium chelates to SCK nanoparticles to form particles with hydrodynamic diameters of 40 ± 3 nm. The SCKs possess a core-shell morphology comprised of diblock copolymers of poly(acrylic acid) and poly(methyl acrylate) after which the Gd-chelate was conjugated to the SCKs by carbodiimide coupling.

Khan has prepared magnetic nanoparticles of ~110 nm in diameter by a coprecipitation polymerization.^[160] These particles have a potential use as an MRI contrast agent or as a magnetically guided drug delivery agent. Oleic acid was reacted with the -OH groups on the surface of iron oxide particles. The prebound oleic acid allows excess oleic acid to adsorb, forming a hydrophobic shell. These particles will exist in aqueous phase after being dissolved in an NH_4OH solution, as the outer shell is transformed to an ammonium salt of oleic acid. A copolymer microgel shell of pNIPAm and polyacrylic acid can then be added by an emulsion polymerization reaction.

1.3.4. Biomaterials

Perhaps the broadest definition of biomaterials comes from the National Institutes of Health Consensus Development Conference: “[a biomaterial is] any substance (other than a drug) or combination of substances, synthetic or natural in origin, which can be used for any period of time, as a whole or part of a system which treats, augments or replaces any tissue, organ or function of the body”.^[161] Research in the field of biomaterials is often linked to developing a more biocompatible system, such as making an implant or surgical device less damaging to the body. In case of hydrogels, much of the effort has been put in coating the surface of the implants or devices with polymers or bulk gels. With the advent of responsive hydrogels, many researchers began working on making “smarter biomaterials”, where these materials can sense a change in the environment and respond in a programmed fashion to it. In this section we describe a few of those examples pertaining specifically to hydrogel nanoparticles.

As mentioned previously, Kawaguchi has studied the interaction of proteins with microgels extensively.^[116, 162, 163] For example, the group has studied the effect of temperature on the non-specific adsorption of proteins to thermoresponsive microgels. They have also investigated the activity of enzymes that are covalently bound to the microgels. In one example they attached trypsin peroxidase to pNIPAm microgels and studied its activity as a function of temperature.^[164] The enzyme activity decreased with increase in temperature due to the decrease in the pore size. This caused the decrease in the rate of diffusion of substrate to the enzyme. They also studied a similar system with a small molecule, ubiquinone, attached to the particle and observed similar temperature dependent results. Duracher et al. have studied the adsorption of HIV-1 capsid protein

p24 on polystyrene-core-pNIPAm-shell particles.^[165] As predicted by numerous studies, they observed higher adsorption at $T > VPTT$ of pNIPAm due to hydrophobic interactions. Similarly Urakami et al. studied the phagocytosis of polystyrene-co-polyacrylamide gel particles as a function of hydrophobicity. They observed that phagocytosis by granulocytes increased with the increase in polystyrene content of the particles, again presumably due to an increase in hydrophobic association with the granulocyte.^[166] In similar studies, Kimhi and Bianco-Peled used isothermal titration calorimetry (ITC) to study the adsorption of small molecules (aspartic acid and valine) to pNIPAm microgels as a function of temperature.^[167] They found that at 25 °C aspartic acid binds strongly to the polymer particles due to formation of hydrogen bonds and at 37 °C valine binds strongly due to the hydrophobic effect.

More advanced architectures can be prepared that take advantage of biocatalytic systems. For example, Ogawa et al. have synthesized pNIPAm microgels containing a pendant vinyl imidazole side-chain, which again allows for pH-tunable gel swelling.^[40] The enzyme urease, which catalyses the hydrolysis of urea into ammonia, was then physically entrapped in the particles. As the enzyme produced ammonia, the pH of the medium decreased. Hence, in the presence of urea the particles shrank due to increase in pH and subsequent deprotonation of the imidazole unit. When the substrate was removed, the particles swelled to their original size as the local pH equilibrated with the pH of the surrounding bath. To demonstrate the potential utility of such a biomechanical system, the authors incorporated these particles into a membrane. Upon introduction of urea to one of the solvent reservoirs, they observed that the permeability of the membrane increased as the particles shrank.

An important aspect of many implanted biomaterials relates to the ability of cells to adsorb and proliferate on the material surface. It is clear that even materials with low surface energies and hence low degrees of non-specific protein adsorption can tend to foul over time in cell culture or following implantation. Hence, it is important to evaluate fouling of biomaterials as well as to arrive at new strategies for mediating cellular recruitment at synthetic surfaces. Thus, in addition to the aforementioned protein adsorption studies, Kawaguchi and coworkers have also studied the effect of cell binding to thermoresponsive particles on a solid surface.^[116] They first deposited pNIPAm microspheres on a plate to produce a 2D array upon which the cell culture medium was seeded. They observed that the cells produced more reactive oxygen species at 37 °C than at 25 °C, indicating that the cells are under more mechanical stress at the higher temperature. This is presumably due to stronger attachment at $T > VPTT$. They also observed that the amount of reactive oxygen species produced when the system was heated from 25 °C to 37 °C was much higher than just incubation at 37 °C. This they attributed to the stimulus inflicted by the dynamic deswelling process. In addition to this system they have also used a ligand: receptor system to study the mechanical stress on the cells.^[116] Our group has fabricated particles in which the adsorption of the proteins to the particles is reduced by using PEG grafting.^[168] In this report we used pNIPAm-core/pNIPAm-shell particles and attached PEG either to the core or to the shell by copolymerization of PEG-monomethacrylate. Reduced protein adsorption was observed for both the core and shell-grafted PEG particles. It was further observed by NMR and protein adsorption measurements that at high temperature the PEG chains phase separate to the particle surface, and because of the polymer's hydrophilicity reduce protein

adsorption. In case of the particles in which the PEG is attached to the core, the PEG chains are able to penetrate the shell and phase separate to the surface, thus reducing the surface energy of the deswollen particles.

The Lyon group has prepared microgels for use as coatings for poly(ethylene terephthalate) (PET) discs to create non-fouling surfaces.^[169] Microgels were synthesized by free-radical precipitation polymerization with pNIPAm as the main monomer and poly(ethylene glycol) diacrylate as the cross-linker. The PET discs were functionalized with polyacrylic acid and benzophenone, and the particles were deposited by spin-coating. The discs were then irradiated with UV light to covalently link the particles to the PET. The microgels act to give the PET discs non-fouling property, as the bare PET support high levels of cell adhesion, while microgel coated PETs show no macrophage adhesion at 48 h.

The development of materials that can interact with cells and proteins is important for drug delivery devices and extracellular matrix (ECM) mimicking. Protease responsive hydrogels have been described in the literature, such as those developed by Moore and co-workers.^[170] In this work, hydrogel particles that are degraded by α -chymotrypsin were developed. They described a conjugation technique by which a disulfide transfer reaction under acidic conditions that allows for a cross-linker that contains peptide sequences to be synthesized. A methacrylamide containing a CYKC sequence was incorporated into polyacrylamide hydrogels. Hydrogels containing the CYKC cross-linker, which is sensitive to chymotrypsin, completely degraded in 20 minutes in the presence of the enzyme, while hydrogels containing a chymotrypsin-insensitive CSKC cross-linker remained intact.

In another example of core/shell particles that may have utility in biomaterials applications, the Lyon group has prepared a system in which the shell acts a barrier between the protein in the solution and a core-localized ligand buried under the shell.^[171] In this case a core has been synthesized, to which biotin is attached, followed by addition of a shell containing a degradable cross-linker. Initially the cross-linker density is high enough that the pore sizes are smaller than the size of the protein avidin. As the cross-linker is degraded, the average pore size increases and allows permeation of avidin to the core, where it can bind to biotin. We have also observed protein size dependent permeation *i.e.* for larger proteins, more cross-links have to be degraded to allow for binding. These systems are interesting from the view of the topological complexity and also because they may be a model system for a particle that can “express” a particular functionality at the surface following a biological or chemical signal, which disrupts shell-localized cross-links.

An interesting approach taken by researchers to form nanomaterials having unique properties is the conjugation of nanoparticles with ligands, which have the ability to mediate inter-particle interactions with substrates and direct their self assembly to form higher ordered nanostructures. Because of the ease of physical and chemical modification, directed self assembly of polymeric nanoparticles gives chemists an advantage of controlling and manipulating the shape and composition of the assembled material. Wooley and coworkers demonstrated that, conjugation of a peptide nucleic acid (PNA) to the surface of shell-cross-linked nanoparticles (by carbodiimide coupling methods) provides functionality for controlled self assembly of the nanoparticles into large assemblies.^[172] Higher order assemblies were obtained by inter-particle

complimentary base pairing of the PNA sequences on the nanoparticles. The size of the assemblies was controlled by controlling the number of PNAs on each nanoparticle. This assembly process has demonstrated an interesting way to assemble soft polymeric nanoparticles into desired arrays. One can also imagine having PNAs on the solid substrate surface that are complementary to the PNAs on the nanoparticles and thus directing the assembly of the nanoparticles onto a patterned substrate to form an array of soft materials with diverse functional regions.

1.4 Conclusions and Outlook

Towards the end of the last century, it was commonly thought that the term “nanotechnology” was coined exclusively for “hard materials” but this changed as polymeric materials became more common ingredients in nanometric systems. In this chapter we have discussed various types of hydrogel nanoparticles and their applications in nanotechnology. As more and more research is carried out in this field, it becomes clearer that these materials hold great promise on their own, and as a bridge between more traditional nanostructures and biological systems. For example, gels that respond to a change in their environment are potentially useful in the context of truly bioresponsive structures that may enable us to manipulate natural systems in a rational fashion.

Although many groups have worked in this field, many of the potential resources are still untapped. There are opportunities for new efforts in advanced synthetic approaches to complex hydrogel nanomaterials, both in colloid synthesis (e.g. size and shape control) and in new chemoligation methods for controlled bioconjugate synthesis. The rational design of multifunctional architectures will be enabled by such efforts,

thereby allowing the improvement of current applications areas, as well as the implementation of hydrogels in new arenas. In the case of core/shell particles reported by our group and others, the range of potential applications in which such materials can be applied is just beginning to be uncovered. Early studies of the detailed structure/function relationships in hydrogel particles are now leading to the design of primitive applications-oriented nanomaterials. These proof-of-concept studies can then feed back into the synthetic labs and provide guidance for the synthesis of the second generation of materials. In parallel, it will become increasingly important to perform detailed studies of cytotoxicity, immunogenicity, and pharmacokinetics, if these materials are to be employed in biotech applications. Finally, ground level integration between chemists, biochemists, engineers, and clinicians is desired to enable the design, synthesis, and testing of structures that are truly applicable in clinical applications such as drug delivery devices, implantable biomaterials, biosensors/assays, and targeted chemotherapeutic formulations. The following chapters will deal with our work in advancing the knowledge of nanogels as biomaterials, mainly as targeted delivery devices.

1.5 References

- [1] S. H. Gehrke, in *Adv. Polym. Sci., Vol. 110*, Springer-Verlag, Berlin, **1993**, pp. 82-144.
- [2] A. S. Hoffman, Hydrogels for biomedical applications. *Adv. Drug Deliv. Rev.* **2002**, *54*, 3-12.
- [3] K. Yeomans, Hydrogels- very versatile materials. *Chem. Rev.* **2000**, *10*, 2-5.
- [4] Y. Li, T. Tanaka, Study of the universality class of the gel network system. *J. Chem. Phys.* **1989**, *90*, 5161-5166.
- [5] Y. Li, T. Tanaka, Kinetics of swelling and shrinking of gels. *J. Chem. Phys.* **1990**, *92*, 1365-1371.
- [6] T. Tanaka, Kinetics of phase transition in polymer gels. *Physica A* **1986**, *140A*, 261-268.
- [7] W. E. Hennink, C. F. van Nostrum, Novel crosslinking methods to design hydrogels. *Adv. Drug Deliv. Rev.* **2002**, *54*, 13-36.
- [8] K. Dusek, W. Prins, Structure and elasticity of non-crystalline polymer networks. *Fortschritte der Hochpolymeren-Forschung* **1969**, *6*, 1-102.
- [9] W. R. Gombotz, S. Wee, Protein release from alginate matrixes. *Adv. Drug Deliv. Rev.* **1998**, *31*, 267-285.
- [10] M. F. A. Goosen, G. M. O'Shea, H. M. Gharapetian, S. Chou, A. M. Sun, Optimization of microencapsulation parameters: semipermeable microcapsules as a bioartificial pancreas. *Biotechnol. Bioeng.* **1985**, *27*, 146-150.
- [11] M. P. Lutolf, G. P. Raeber, A. H. Zisch, N. Tirelli, J. A. Hubbell, Cell-responsive synthetic hydrogels. *Adv. Mater.* **2003**, *15*, 888-892.
- [12] P. Gacesa, Alginates. *Carbohydr. Polym.* **1988**, *8*, 161-182.
- [13] T. Watanabe, A. Ohtsuka, N. Murase, P. Barth, K. Gersonde, NMR studies on water and polymer diffusion in dextran gels. Influence of potassium ions on microstructure formation and gelation mechanism. *Magnet. Reson. Med.* **1996**, *35*, 697-705.
- [14] D. Eagland, N. J. Crowther, C. J. Butler, Complexation between polyoxyethylene and poly(methacrylic acid). The importance of the molar mass of polyoxyethylene. *Eur. Polym. J.* **1994**, *30*, 767-773.

- [15] A. M. Mathur, K. F. Hammonds, J. Klier, A. B. Scranton, Equilibrium swelling of poly(methacrylic acid-g-ethylene glycol) hydrogels: Effect of swelling medium and synthesis conditions. *J. Control. Release* **1998**, *54*, 177-184.
- [16] S. Nagahara, T. Matsuda, Hydrogel formation via hybridization of oligodeoxyribonucleotides derivatized in water-soluble vinyl polymers. *Polym. Gels Netw.* **1996**, *4*, 111-127.
- [17] W. S. Dai, T. A. Barbari, Hollow fiber-supported hydrogels with mesh-size asymmetry. *J. Membrane Sci.* **2000**, *171*, 79-86.
- [18] N. A. Peppas, R. E. Benner, Jr., Proposed method of intracordal injection and gelation of poly(vinyl alcohol) solution in vocal cords: polymer considerations. *Biomaterials* **1980**, *1*, 158-162.
- [19] J. J. Sperinde, L. G. Griffith, Synthesis and Characterization of Enzymically-Crosslinked Poly(ethylene glycol) Hydrogels. *Macromolecules* **1997**, *30*, 5255-5264.
- [20] J. J. Sperinde, L. G. Griffith, Control and Prediction of Gelation Kinetics in Enzymatically Cross-Linked Poly(ethylene glycol) Hydrogels. *Macromolecules* **2000**, *33*, 5476-5480.
- [21] D. Gan, L. A. Lyon, Tunable Swelling Kinetics in Core-Shell Hydrogel Nanoparticles. *J. Am. Chem. Soc.* **2001**, *123*, 7511-7517.
- [22] C. D. Jones, L. A. Lyon, Synthesis and Characterization of Multiresponsive Core-Shell Microgels. *Macromolecules* **2000**, *33*, 8301-8306.
- [23] H. Staudinger, E. Husemann, *Ber. Dtsch. Chem. Ges.* **1935**, *68*, 16-18.
- [24] R. H. Pelton, Temperature-sensitive aqueous microgels. *Adv. Colloid. Interface Sci.* **2000**, *85*, 1-33.
- [25] B. R. Saunders, B. Vincent, Microgel particles as model colloids: theory, properties and applications. *Adv. Colloid Interface Sci.* **1999**, *80*, 1-25.
- [26] T. Tanaka, Collapse of Gels and the Critical Endpoint. *Physical Review Letters* **1978**, *40*, 820-823.
- [27] K. Dusek, K. Patterson, Transition on swollen polymer networks induced by intramolecular condensation. *Journal of Polymer Science, Polymer Physics Edition* **1968**, *6*, 1209-1216.

- [28] J. Moselhy, X. Y. Wu, R. Nicholov, K. Kodaria, In vitro studies of the interaction of poly(NIPAm/MAA) nanoparticles with proteins and cells. *J. Biomater. Sci., Polym. Ed.* **2000**, *11*, 123-147.
- [29] D. Duracher, F. Sauzedde, A. Elaissari, A. Perrin, C. Pichot, Cationic amino-containing N-isopropylacrylamide-styrene copolymer latex particles: 1 - Particle size and morphology vs. polymerization process. *Colloid Polym. Sci.* **1998**, *276*, 219-231.
- [30] D. Duracher, F. Sauzedde, A. Elaissari, C. Pichot, L. Nabzar, Cationic amino-containing N-isopropyl-acrylamide-styrene copolymer particles: 2-surface and colloidal characteristics. *Colloid Polym. Sci.* **1998**, *276*, 920-929.
- [31] M. J. Snowden, B. Z. Chowdhry, B. Vincent, G. E. Morris, Colloidal copolymer microgels of N-isopropylacrylamide and acrylic acid: pH, ionic strength and temperature effects. *J. Chem. Soc.-Faraday Trans.* **1996**, *92*, 5013-5016.
- [32] S. R. Sershen, S. L. Westcott, N. J. Halas, J. L. West, Temperature-sensitive polymer-nanoshell composites for photothermally modulated drug delivery. *J. Biomed. Mater. Res.* **2000**, *51*, 293-298.
- [33] S. R. Sershen, S. L. Westcott, N. J. Halas, J. L. West, Independent optically addressable nanoparticle-polymer optomechanical composites. *Appl. Phys. Lett.* **2002**, *80*, 4609-4611.
- [34] S. R. Sershen, S. L. Westcott, J. L. West, N. J. Halas, An opto-mechanical nanoshell-polymer composite. *Appl. Phys. B* **2001**, *73*, 379-381.
- [35] A. Suzuki, T. Ishii, Y. Maruyama, Optical switching in polymer gels. *J. Appl. Phys.* **1996**, *80*, 131-136.
- [36] A. Suzuki, T. Tanaka, Phase-Transition in Polymer Gels Induced by Visible-Light. *Nature* **1990**, *346*, 345-347.
- [37] T. Tanaka, I. Nishio, S. T. Sun, S. Ueno-Nishio, Collapse of gels in an electric field. *Science* **1982**, *218*, 467-469.
- [38] T. Miyata, N. Asami, T. Urugami, A reversibly antigen-responsive hydrogel. *Nature* **1999**, *399*, 766-769.
- [39] K. Ogawa, A. Nakayama, E. Kokufuta, Preparation and characterization of thermosensitive polyampholyte nanogels. *Langmuir* **2003**, *19*, 3178-3184.
- [40] K. Ogawa, B. Wang, E. Kokufuta, Enzyme-Regulated Microgel Collapse for Controlled Membrane Permeability. *Langmuir* **2001**, *17*, 4704-4707.

- [41] Y. Ogawa, K. Ogawa, B. Wang, E. Kokufuta, A biochemo-mechanical system consisting of polyampholyte gels with coimmobilized glucose oxidase and urease. *Langmuir* **2001**, *17*, 2670-2674.
- [42] J. Kim, S. Nayak, L. A. Lyon, Bioresponsive Hydrogel Microlenses. *J. Am. Chem. Soc.* **2005**, *127*, 9588-9592.
- [43] H. G. Schild, Poly(N-isopropylacrylamide): experiment, theory and application. *Prog. Polym. Sci.* **1992**, *17*, 163-249.
- [44] M. Heskins, J. E. Guillet, Solution properties of poly(N-isopropylacrylamide). *J. Macromol. Sci. Chem.* **1968**, *A2*, 1441-1455.
- [45] I. Berndt, W. Richtering, Doubly Temperature Sensitive Core-Shell Microgels. *Macromolecules* **2003**, *36*, 8780-8785.
- [46] I. Berndt, J. S. Pedersen, W. Richtering, Structure of Multiresponsive "Intelligent" Core-Shell Microgels. *J. Am. Chem. Soc.* **2005**, *127*, 9372-9373.
- [47] A. Matsumoto, S. Ikeda, A. Harada, K. Kataoka, Glucose-responsive polymer bearing a novel phenylborate derivative as a glucose-sensing moiety operating at physiological pH conditions. *Biomacromolecules* **2003**, *4*, 1410-1416.
- [48] D. Duracher, A. Elaissari, F. Mallet, C. Pichot, Preparation of thermosensitive latexes by copolymerization of N-isopropylmethacrylamide with a chelating monomer. *Macromol. Symp.* **2000**, *150*, 297-303.
- [49] D. Duracher, A. Elaissari, C. Pichot, Characterization of cross-linked poly(N-isopropylmethacrylamide) microgel latexes. *Colloid Polym. Sci.* **1999**, *277*, 905-913.
- [50] D. Duracher, A. Elaissari, C. Pichot, Preparation of poly(N-isopropylmethacrylamide) latexes kinetic studies and characterization. *J. Polym. Sci. Pol. Chem.* **1999**, *37*, 1823-1837.
- [51] F. M. Winnik, Quenching of fluorescence from pyrene-labeled poly(N-isopropylacrylamide) solutions heated above their lower critical solution temperature. *Macromolecules* **1990**, *23*, 1647-1649.
- [52] F. M. Winnik, Interaction of fluorescent dye labeled (hydroxypropyl)cellulose with nonionic surfactants. *Langmuir* **1990**, *6*, 522-524.
- [53] F. M. Winnik, Fluorescence studies of aqueous solutions of poly(N-isopropylacrylamide) below and above their LCST. *Macromolecules* **1990**, *23*, 233-242.

- [54] C. Wu, A comparison between the 'coil-to-globule' transition of linear chains and the "volume phase transition" of spherical microgels. *Polymer* **1998**, *39*, 4609-4619.
- [55] C. Wu, X. Qiu, Single Chain Core-Shell Nanostructure. *Phys. Rev. Lett.* **1998**, *80*, 620-622.
- [56] C. Wu, X. Wang, Globule-to-Coil Transition of a Single Homopolymer Chain in Solution. *Phys. Rev. Lett.* **1998**, *80*, 4092-4094.
- [57] C. Wu, S. Zhou, Laser Light Scattering Study of the Phase Transition of Poly(N-isopropylacrylamide) in Water. 1. Single Chain. *Macromolecules* **1995**, *28*, 8381-8387.
- [58] C. Wu, S. Zhou, Thermodynamically Stable Globule State of a Single Poly(N-isopropylacrylamide) Chain in Water. *Macromolecules* **1995**, *28*, 5388-5390.
- [59] C. Wu, S. Zhou, Internal Motions of both Poly(N-isopropylacrylamide) Linear Chains and Spherical Microgel Particles in Water. *Macromolecules* **1996**, *29*, 1574-1578.
- [60] X. Wang, X. Qiu, C. Wu, Comparison of the Coil-to-Globule and the Globule-to-Coil Transitions of a Single Poly(N-isopropylacrylamide) Homopolymer Chain in Water. *Macromolecules* **1998**, *31*, 2972-2976.
- [61] M. Arotcarena, B. Heise, S. Ishaya, A. Laschewsky, Switching the inside and the outside of aggregates of water-soluble block copolymers with double thermoresponsivity. *J. Am. Chem. Soc.* **2002**, *124*, 3787-3793.
- [62] M. Shibayama, T. Tanaka, in *Adv. Polym. Sci., Vol. 109*, Springer-Verlag, Berlin, **1993**, pp. 1-62.
- [63] T. Tanaka, D. J. Fillmore, Kinetics of Swelling of Gels. *J. Chem. Phys.* **1979**, *70*, 1214-1218.
- [64] T. Tanaka, D. J. Fillmore, S.-T. Sun, I. Nishio, G. Swislow, A. Shah, Phase Transition in Ionic Gels. *Phys. Rev. Lett.* **1980**, *45*, 1636-1639.
- [65] T. Tanaka, C. Wang, V. Pande, A. Y. Grosberg, A. English, S. Masamune, H. Gold, R. Levy, K. King, Polymer gels that can recognize and recover molecules. *Faraday Discuss.* **1995**, *101*, 201-206.
- [66] Q. Yan, A. S. Hoffman, Synthesis of macroporous hydrogels with rapid swelling and deswelling properties for delivery of macromolecules. *Poly. Commun.* **1995**, *36*, 887-889.

- [67] T. G. Park, A. S. Hoffman, Immobilization and characterization of beta-galactosidase in thermally reversible hydrogel beads. *J. Biomed. Mater. Res.* **1990**, *24*, 21-38.
- [68] S. Kim, K. E. Healy, Synthesis and Characterization of Injectable Poly(N-isopropylacrylamide-co-acrylic acid) Hydrogels with Proteolytically Degradable Cross-Links. *Biomacromolecules* **2003**, *4*, 1214-1223.
- [69] R. Pelton, Temperature-sensitive aqueous microgels. *Adv. Colloid. Interface Sci.* **2000**, *85*, 1-33.
- [70] E. Daly, B. R. Saunders, Temperature-dependent electrophoretic mobility and hydrodynamic radius measurements of poly(N-isopropylacrylamide) microgel particles: structural insights. *Phys. Chem. Chem. Phys.* **2000**, *2*, 3187-3193.
- [71] H. Ohshima, K. Makino, T. Kato, K. Fujimoto, T. Kondo, H. Kawaguchi, Electrophoretic Mobility of Latex-Particles Covered With Temperature-Sensitive Hydrogel Layers. *J. Colloid Interface Sci.* **1993**, *159*, 512-514.
- [72] J. D. Debord, L. A. Lyon, Thermoresponsive Photonic Crystals. *J. Phys. Chem. B* **2000**, *104*, 6327-6331.
- [73] H. Senff, W. Richtering, Temperature sensitive microgel suspensions: Colloidal phase behavior and rheology of soft spheres. *J. Chem. Phys.* **1999**, *111*, 1705-1711.
- [74] Z. Hu, X. Lu, J. Gao, Hydrogel opals. *Adv. Mater.* **2001**, *13*, 1708-1712.
- [75] T. Hellweg, C. D. Dewhurst, E. Bruckner, K. Kratz, W. Eimer, Colloidal crystals made of poly(N-isopropylacrylamide) microgel particles. *Colloid Polym. Sci.* **2000**, *278*, 972-978.
- [76] C. Wu, S. Zhou, Volume Phase Transition of Swollen Gels: Discontinuous or Continuous? *Macromolecules* **1997**, *30*, 574-575.
- [77] D. Gan, L. A. Lyon, Interfacial Nonradiative Energy Transfer in Responsive Core-Shell Hydrogel Nanoparticles. *J. Am. Chem. Soc.* **2001**, *123*, 8203-8209.
- [78] C. Wu, S. Zhou, Light scattering study of spherical poly(N-isopropylacrylamide) microgels. *J. Macromol. Sci., Phys.* **1997**, *B36*, 345-355.
- [79] Y. D. Yi, K. S. Oh, Y. C. Bae, Phase transition of submicron sized N-alkylacrylamide-derivative copolymer particles: applicability of photon correlation spectroscopy. *Polymer* **1997**, *38*, 3471-3476.

- [80] I. Varga, T. Gilanyi, R. Meszaros, G. Filipcsei, M. Zrinyi, Effect of Cross-Link Density on the Internal Structure of Poly(N-isopropylacrylamide) Microgels. *J. Phys. Chem. B* **2001**, *105*, 9071-9076.
- [81] A. Guillermo, J. P. C. Addad, J. P. Bazile, D. Duracher, A. Elaissari, C. Pichot, NMR investigations into heterogeneous structures of thermosensitive microgel particles. *J. Polym. Sci. Pt. B-Polym. Phys.* **2000**, *38*, 889-898.
- [82] B. R. Saunders, On the structure of poly(N-isopropylacrylamide) microgel particles. *Langmuir* **2004**, *20*, 3925-3932.
- [83] N. C. Woodward, B. Z. Chowdhry, M. J. Snowden, S. A. Leharne, P. C. Griffiths, A. L. Winnington, Calorimetric investigation of the influence of cross-linker concentration on the volume phase transition of poly(N-isopropylacrylamide) colloidal microgels. *Langmuir* **2003**, *19*, 3202-3211.
- [84] H. Senff, W. Richtering, Influence of crosslink density on rheological properties of temperature-sensitive microgel suspensions. *Colloid. Polym. Sci.* **2000**, *278*, 830-840.
- [85] H. Senff, W. Richtering, C. Norhausen, A. Weiss, M. Ballauff, Rheology of a temperature sensitive core-shell latex. *Langmuir* **1999**, *15*, 102-106.
- [86] S. Meyer, W. Richtering, Influence of Polymerization Conditions on the Structure of Temperature-Sensitive Poly(N-isopropylacrylamide) Microgels. *Macromolecules* **2005**, *38*, 1517-1519.
- [87] M. Stieger, W. Richtering, J. S. Pedersen, P. Lindner, Small-angle neutron scattering study of structural changes in temperature sensitive microgel colloids. *Journal of Chemical Physics* **2004**, *120*, 6197-6206.
- [88] X. Wu, R. H. Pelton, A. E. Hamielec, D. R. Woods, W. McPhee, The kinetics of poly(N-isopropylacrylamide) microgel latex formation. *Colloid Polym. Sci.* **1994**, *272*, 467-477.
- [89] T. Hoare, R. Pelton, Functional group distribution in carboxylic acid containing poly(N-isopropylacrylamide) microgels. *Langmuir* **2004**, *20*, 2123-2133.
- [90] R. H. Pelton, P. Chibante, Preparation Of Aqueous Lattices With N-Isopropylacrylamide. *Colloids Surface.* **1986**, *20*, 247-256.
- [91] S. Zhou, B. Chu, Synthesis and Volume Phase Transition of Poly(methacrylic acid-co-N-isopropylacrylamide) Microgel Particles in Water. *J. Phys. Chem. B* **1998**, *102*, 1364-1371.

- [92] K. Kratz, T. Hellweg, W. Eimer, Effect of connectivity and charge density on the swelling and local structural and dynamic properties of colloidal PNIPAM microgels. *Ber. Bunsen-Ges.* **1998**, *102*, 1603-1608.
- [93] H. Suzuki, B. Wang, R. Yoshida, E. Kokufuta, Potentiometric Titration Behaviors of a Polymer and Gel Consisting of N-Isopropylacrylamide and Acrylic Acid. *Langmuir* **1999**, *15*, 4283-4288.
- [94] K. Kratz, T. Hellweg, W. Eimer, Influence of charge density on the swelling of colloidal poly(N-isopropylacrylamide-co-acrylic acid) microgels. *Colloids Surf., A* **2000**, *170*, 137-149.
- [95] J. D. Debord, L. A. Lyon, Synthesis and Characterization of pH Responsive Copolymer Microgels with Tunable Volume Phase Transition Temperatures. *Langmuir* **2003**, *19*, 7662-7664.
- [96] J. Gao, B. J. Frisken, Cross-linker-free N-isopropylacrylamide gel nanospheres. *Langmuir* **2003**, *19*, 5212-5216.
- [97] J. Gao, B. J. Frisken, Influence of reaction conditions on the synthesis of self-cross-linked N-isopropylacrylamide microgels. *Langmuir* **2003**, *19*, 5217-5222.
- [98] S. Neyret, B. Vincent, The properties of polyampholyte microgel particles prepared by microemulsion polymerization. *Polymer* **1997**, *38*, 6129-6134.
- [99] K. McAllister, P. Sazani, M. Adam, M. J. Cho, M. Rubinstein, R. J. Samulski, J. M. DeSimone, Polymeric nanogels produced via inverse microemulsion polymerization as potential gene and antisense delivery agents. *J. Am. Chem. Soc.* **2002**, *124*, 15198-15207.
- [100] S. Kazakov, M. Kaholek, D. Kudasheva, I. Teraoka, M. K. Cowman, K. Levon, Poly(N-isopropylacrylamide-co-1-vinylimidazole) hydrogel nanoparticles prepared and hydrophobically modified in liposome reactors: Atomic force microscopy and dynamic light scattering study. *Langmuir* **2003**, *19*, 8086-8093.
- [101] N. Dingenouts, S. Seelenmeyer, I. Deike, S. Rosenfeldt, M. Ballau, P. Lindner, T. Narayanan, Analysis of thermosensitive core-shell colloids by small-angle neutron scattering including contrast variation. *Phys. Chem. Chem. Phys.* **2001**, *3*, 1169-1174.
- [102] X. C. Xiao, L. Y. Chu, W. M. Chen, S. Wang, R. Xie, Preparation of submicrometer-sized monodispersed thermoresponsive core-shell hydrogel microspheres. *Langmuir* **2004**, *20*, 5247-5253.
- [103] W. Stober, A. Fink, E. Bohn, Controlled Growth Of Monodisperse Silica Spheres In Micron Size Range. *Journal Of Colloid And Interface Science* **1968**, *26*, 62-69.

- [104] L. Zha, Y. Zhang, W. Yang, S. Fu, Monodisperse temperature-sensitive microcontainers. *Adv. Mater.* **2002**, *14*, 1090-1092.
- [105] J. H. Kim, T. R. Lee, Thermo- and pH-responsive hydrogel-coated gold nanoparticles. *Chem. Mater.* **2004**, *16*, 3647-3651.
- [106] C. D. Jones, L. A. Lyon, Dependence of shell thickness on core compression in acrylic acid modified poly(N-isopropylacrylamide) core/shell microgels. *Langmuir* **2003**, *19*, 4544-4547.
- [107] C. D. Jones, L. A. Lyon, Shell-Restricted Swelling and Core Compression in Poly(N-Isopropylacrylamide) Core-Shell Microgels. *Macromolecules* **2003**, *36*, 1988-1993.
- [108] D. Gan, L. A. Lyon, Fluorescence nonradiative energy transfer analysis of crosslinker heterogeneity in core-shell hydrogel nanoparticles. *Anal. Chim. Acta* **2003**, *496*, 53-63.
- [109] C. D. Jones, J. G. McGrath, L. A. Lyon, Characterization of Cyanine Dye-Labeled Poly(N-isopropylacrylamide) Core/Shell Microgels Using Fluorescence Resonance Energy Transfer. *J. Phys. Chem. B* **2004**, *108*, 12652-12657.
- [110] W. H. Blackburn, L. A. Lyon, Size Controlled Synthesis of Monodispersed, Core/Shell Nanogels. *Colloid Polym. Sci.* **2008**, *286*, 563-569.
- [111] S. Nayak, D. Gan, M. J. Serpe, L. A. Lyon, Hollow thermoresponsive microgels. *Small* **2005**, *1*, 416-421.
- [112] I. Berndt, J. S. Pedersen, P. Lindner, W. Richtering, Influence of Shell Thickness and Cross-Link Density on the Structure of Temperature-Sensitive Poly-N-Isopropylacrylamide-Poly-N-Isopropylmethacrylamide Core-Shell Microgels Investigated by Small-Angle Neutron Scattering. *Langmuir* **2006**, *22*, 459-468.
- [113] I. Berndt, J. S. Pedersen, W. Richtering, Temperature-sensitive core-shell microgel particles with dense shell. *Angewandte Chemie, International Edition* **2006**, *45*, 1737-1741.
- [114] I. Berndt, C. Popescu, F.-J. Wortmann, W. Richtering, Mechanics versus thermodynamics: swelling in multiple-temperature-sensitive core-shell microgels. *Angewandte Chemie, International Edition* **2006**, *45*, 1081-1085.
- [115] M. Kashiwabara, K. Fujimoto, H. Kawaguchi, Preparation of Monodisperse, Reactive Hydrogel Microspheres and Their Amphoterization. *Colloid Polym. Sci.* **1995**, *273*, 339-345.

- [116] H. Kawaguchi, K. Kisara, T. Takahashi, K. Achiha, M. Yasui, K. Fujimoto, Versatility of thermosensitive particles. *Macromol. Symp.* **2000**, *151*, 591-598.
- [117] T. Delair, F. Meunier, A. Elaissari, M.-H. Charles, C. Pichot, Amino-containing cationic latex-oligodeoxyribonucleotide conjugates: application to diagnostic test sensitivity enhancement. *Colloid. Surface. A* **1999**, *153*, 341-353.
- [118] T. J. Hu, Y. Z. You, C. Y. Pan, C. Wu, The coil-to-globule-to-brush transition of linear thermally sensitive poly(N-isopropylacrylamide) chains grafted on a spherical microgel. *J. Phys. Chem. B* **2002**, *106*, 6659-6662.
- [119] T. Hu, C. Wu, Grafting Density Induced Stretching and Collapse of Tethered Poly(ethylene oxide) Chains on a Thermally Sensitive Microgel. *Macromolecules* **2001**, *34*, 6802-6805.
- [120] F. Marcucci, F. Lefoulon, Active targeting with particulate drug carriers in tumor therapy: fundamentals and recent progress. *Drug Discov. Today* **2004**, *9*, 219-228.
- [121] G. Barratt, Colloidal drug carriers: Achievements and perspectives. *Cell. Mol. Life Sci.* **2003**, *60*, 21-37.
- [122] S. Hirosue, B. G. Muller, R. C. Mulligan, R. Langer, Plasmid DNA encapsulation and release from solvent diffusion nanospheres. *J. Control. Release* **2001**, *70*, 231-242.
- [123] H. Q. Mao, K. Roy, V. L. Troung-Le, K. A. Janes, K. Y. Lin, Y. Wang, J. T. August, K. W. Leong, Chitosan-DNA nanoparticles as gene carriers: synthesis, characterization and transfection efficiency. *J. Control. Release* **2001**, *70*, 399-421.
- [124] N. Wang, X. S. Wu, Preparation and characterization of agarose hydrogel nanoparticles for protein and peptide drug delivery. *Pharm. Dev. Technol.* **1997**, *2*, 135-142.
- [125] J. K. Li, N. Wang, X. S. Wu, Poly(vinyl alcohol) nanoparticles prepared by freezing-thawing process for protein/peptide drug delivery. *J. Control. Release* **1998**, *56*, 117-126.
- [126] I. S. Kim, Y. I. Jeong, S. H. Kim, Self-assembled hydrogel nanoparticles composed of dextran and poly(ethylene glycol) macromer. *Int. J. Pharm.* **2000**, *205*, 109-116.
- [127] K. Na, Y. H. Bae, Self-Assembled Hydrogel Nanoparticles Responsive to Tumor Extracellular pH from Pullulan Derivative/Sulfonamide Conjugate: Characterization, Aggregation, and Adriamycin Release in Vitro. *Pharmaceut. Res.* **2002**, *19*, 681-688.

- [128] N. J. Kavimandan, E. Losi, N. A. Peppas, Novel delivery system based on complexation hydrogels as delivery vehicles for insulin-transferrin conjugates. *Biomaterials* **2006**, 27, 3846-3854.
- [129] P. F. Kiser, G. Wilson, D. Needham, A synthetic mimic of the secretory granule for drug delivery. *Nature* **1998**, 394, 459-462.
- [130] M. L. Kraft, J. S. Moore, Surfactant-Induced Lysis of Lipid-Modified Microgels. *Journal of the American Chemical Society* **2001**, 123, 12921-12922.
- [131] G.-H. Hsiue, S.-h. Hsu, C.-C. Yang, S.-H. Lee, I. K. Yang, Preparation of controlled release ophthalmic drops, for glaucoma therapy using thermosensitive poly-N-isopropylacrylamide. *Biomaterials* **2001**, 23, 457-462.
- [132] P. K. Ghosh, Hydrophilic polymeric nanoparticles as drug carriers. *Indian J. Biochem. Bio.* **2000**, 37, 273-282.
- [133] U. Gaur, S. K. Sahoo, T. K. De, P. C. Ghosh, A. Maitra, P. K. Ghosh, Biodistribution of fluoresceinated dextran using novel nanoparticles evading reticuloendothelial system. *Int. J. Pharm.* **2000**, 202, 1-10.
- [134] S. Nayak, H. Lee, J. Chmielewski, L. A. Lyon, Folate-Mediated Cell Targeting and Cytotoxicity Using Thermoresponsive Microgels. *J. Am. Chem. Soc.* **2004**, 126, 10258-10259.
- [135] S. H. Choi, J. J. Yoon, T. G. Park, Galactosylated poly(N-isopropylacrylamide) hydrogel submicrometer particles for specific cellular uptake within hepatocytes. *J. Colloid Interf. Sci.* **2002**, 251, 57-63.
- [136] M. L. Becker, E. E. Remsen, D. Pan, K. L. Wooley, Peptide-derivatized shell-crosslinked nanoparticles. 1. synthesis and characterization. *Bioconjugate Chem.* **2004**, 15, 699-709.
- [137] M. L. Becker, L. O. Bailey, K. L. Wooley, Peptide-derivatized shell-crosslinked nanoparticles. 2. biocompatibility evaluation. *Bioconjugate Chem.* **2004**, 15, 710-717.
- [138] D. Pan, J. L. Turner, K. L. Wooley, Folic acid-conjugated nanostructured materials designed for cancer cell targeting. *Chem. Commun.* **2003**, 2400-2401.
- [139] M. Das, S. Mardyani, W. C. W. Chan, E. Kumacheva, Biofunctionalized pH-responsive microgels for cancer cell targeting: rational design. *Adv. Mater. (Weinheim, Germany)* **2006**, 18, 80-83.

- [140] H. Zhang, S. Mardyani, W. C. W. Chan, E. Kumacheva, Design of Biocompatible Chitosan Microgels for Targeted pH-Mediated Intracellular Release of Cancer Therapeutics. *Biomacromolecules* **2006**, 7, 1568-1572.
- [141] S. S. Jana, D. J. Bharali, P. Mani, A. Maitra, C. M. Gupta, D. P. Sarkar, Targeted cytosolic delivery of hydrogel nanoparticles into HepG2 cells through engineered Sendai viral envelopes. *FEBS Lett.* **2002**, 515, 184-188.
- [142] K. Na, K. H. Park, S. W. Kim, Y. H. Bae, Self-assembled hydrogel nanoparticles from curdlan derivatives: characterization, anti-cancer drug release and interaction with a hepatoma cell line (HepG2). *J. Control. Release* **2000**, 69, 225-236.
- [143] S. Mitra, U. Gaur, P. C. Ghosh, A. N. Maitra, Tumor targeted delivery of encapsulated dextran-doxorubicin conjugate using chitosan nanoparticles as carrier. *J. Control. Release* **2001**, 74, 317-323.
- [144] O. C. Farokhzad, J. Cheng, B. A. Teply, I. Sherifi, S. Jon, P. W. Kantoff, J. P. Richie, R. Langer, Targeted nanoparticle-aptamer bioconjugates for cancer chemotherapy in vivo. *Proceedings of the National Academy of Sciences of the United States of America* **2006**, 103, 6315-6320.
- [145] A. Rehor, H. Schmoekel, N. Tirelli, J. A. Hubbell, Functionalization of polysulfide nanoparticles and their performance as circulating carriers. *Biomaterials* **2008**, 29, 1958-1966.
- [146] J. Zhang, R. D. K. Mirsa, Magnetic drug-targeting carrier encapsulated with thermosensitive smart polymer: Core-shell nanoparticle carrier and drug release response. *Acta Biomaterialia* **2007**, 3, 838-850.
- [147] K. Akiyoshi, S. Kobayashi, S. Shichibe, D. Mix, M. Baudys, S. Wan Kim, J. Sunamoto, Self-assembled hydrogel nanoparticle of cholesterol-bearing pullulan as a carrier of protein drugs: Complexation and stabilization of insulin. *J. Control. Release* **1998**, 54, 313-320.
- [148] K. Akiyoshi, T. Nishikawa, S. Shichibe, J. Sunamoto, Stabilization of insulin upon supramolecular complexation with hydrophobized polysaccharide nanoparticle. *Chem. Lett.* **1995**, 707-708.
- [149] K. Akiyoshi, Y. Sasaki, J. Sunamoto, Molecular Chaperone-Like Activity of Hydrogel Nanoparticles of Hydrophobized Pullulan: Thermal Stabilization with Refolding of Carbonic Anhydrase B. *Bioconjugate Chem.* **1999**, 10, 321-324.
- [150] C. Nardin, S. Thoeni, J. Widmer, M. Winterhalter, W. Meier, Nanoreactors based on (polymerized) ABA-triblock copolymer vesicles. *Chemical Communications (Cambridge)* **2000**, 1433-1434.

- [151] A. Ranquin, W. Versees, W. Meier, J. Steyaert, P. Van Gelder, Therapeutic Nanoreactors: Combining Chemistry and Biology in a Novel Triblock Copolymer Drug Delivery System. *Nano Letters* **2005**, *5*, 2220-2224.
- [152] J. Kim, N. Singh, L. A. Lyon, Label-Free Biosensing with Hydrogel Microlenses. *Angew. Chemie Int. Ed.* **2006**, *45*, 1446-1449.
- [153] A. Elaissari, L. Holt, F. Meunier, C. Voisset, C. Pichot, B. Mandrand, C. Mabilat, Hydrophilic and cationic latex particles for the specific extraction of nucleic acids. *J. Biomat.Sci.-Polym. E.* **1999**, *10*, 403-420.
- [154] A. Kondo, T. Kaneko, K. Higashitani, Development and Application of Thermosensitive Immunospheres for Antibody Purification. *Biotechnol. Bioeng.* **1994**, *44*, 1-6.
- [155] A. Kondo, H. Kamura, K. Higashitani, Development and Application of Thermosensitive Magnetic Immunospheres for Antibody Purification. *Appl. Microbiol. Biot.* **1994**, *41*, 99-105.
- [156] L. Ye, P. A. G. Cormack, K. Mosbach, Molecularly imprinted monodisperse microspheres for competitive radioassay. *Anal. Commun.* **1999**, *36*, 35-38.
- [157] J. D. Ehrick, S. K. Deo, T. W. Browning, L. G. Bachas, M. J. Madou, S. Daunert, Genetically engineered protein in hydrogels tailors stimuli-responsive characteristics. *Nature Materials* **2005**, *4*, 298-302.
- [158] T. Miyata, M. Jige, T. Urugami, Tumor marker-responsive behavior of gels prepared by biomolecular imprinting. *Proc. Natl. Acad. Sci.* **2006**, *103*, 1190-1193.
- [159] J. L. Turner, D. Pan, R. Plummer, Z. Chen, A. K. Whitaker, K. L. Wooley, Synthesis of gadolinium-labeled shell-crosslinked nanoparticles for magnetic resonance imaging applications. *Adv. Funct. Mat.* **2005**, *15*, 1248-1254.
- [160] A. Khan, Preparation and characterization of magnetic nanoparticles embedded in microgels. *Materials Letters* **2008**, *62*, 898-902.
- [161] J. W. Boretos, M. Eden, Noyes Publications, Park Ridge, NJ, **1984**, pp. 232-233.
- [162] H. Kawaguchi, Functional polymer microspheres. *Prog. Polym. Sci.* **2000**, *25*, 1171-1210.
- [163] H. Kawaguchi, K. Fujimoto, Y. Mizuhara, Hydrogel Microspheres .3. Temperature-Dependent Adsorption of Proteins on Poly-N-Isopropylacrylamide Hydrogel Microspheres. *Colloid Polym. Sci.* **1992**, *270*, 53-57.

- [164] T. Shiroya, N. Tamura, M. Yasui, K. Fujimoto, H. Kawaguchi, Enzyme immobilization on thermosensitive hydrogel microspheres. *Colloid. Surface. B* **1995**, *4*, 267-274.
- [165] D. Duracher, A. Elaissari, F. Mallet, C. Pichot, Adsorption of modified HIV-1 capsid p24 protein onto thermosensitive and cationic core-shell poly(styrene)-poly(N- isopropylacrylamide) particles. *Langmuir* **2000**, *16*, 9002-9008.
- [166] Y. Urakami, Y. Kasuya, K. Fujimoto, M. Miyamoto, H. Kawaguchi, Phagocytosis of microspheres with modified surfaces. *Colloid. Surface. B* **1994**, *3*, 183-190.
- [167] O. Kimhi, H. Bianco-Peled, Microcalorimetry study of the interactions between poly(N-isopropylacrylamide) microgels and amino acids. *Langmuir* **2002**, *18*, 8587-8592.
- [168] D. Gan, L. A. Lyon, Synthesis and Protein Adsorption Resistance of PEG-Modified Poly(N-isopropylacrylamide) Core/Shell Microgels. *Macromolecules* **2002**, *35*, 9634-9639.
- [169] N. Singh, A. W. Bridges, A. J. Garcia, L. A. Lyon, Covalent tethering of functional microgel films on poly(ethylene terephthalate) surfaces, *Biomacromolecules* **2007**, *8*, 3271-3275.
- [170] K. N. Plunkett, K. L. Berkowski, J. S. Moore, Chymotrypsin responsive hydrogel: application of a disulfide exchange protocol for the preparation of methacrylamide containing peptides. *Biomacromolecules* **2005**, *6*, 632-637.
- [171] S. Nayak, L. A. Lyon, Ligand-Functionalized Core/Shell Microgels with Permselective Shells. *Angew. Chem. Int. Ed. Engl.* **2004**, *43*, 6706-6709.
- [172] J. L. Turner, M. L. Becker, X. Li, J.-S. A. Taylor, K. L. Wooley, PNA-directed solution- and surface-assembly of shell crosslinked (SCK) nanoparticle conjugates. *Soft Matter* **2005**, *1*, 69-78.

CHAPTER 2

THE USE OF AFFF-MALLS TO CHARACTERIZE MICROGEL PARTICLE SIZE

2.1 Introduction

Particle sizing can be accomplished by a number of analytical methods. These include optical or electron microscopy, Coulter counter, neutron scattering, and photon correlation spectroscopy. There are also methods based on the physical separation of particles, such as field flow fractionation (FFF) or capillary hydrodynamic chromatography (CHDF). All of these methods have problems however, which can lead to inaccuracy in measurements.^[1]

Optical microscopic techniques are limited in terms of particle size, as particles below 500 nm in diameter are very difficult to image. Transmission electron microscopy (TEM) does not encounter the same size problems, but the disadvantages include relatively slow measurement speed and difficulty in imaging soft nanoparticles such as hydrogels.^[1-3] The drawback to using a Coulter counter is that the instrument only sizes particles one at a time, not allowing for the sizing of a large ensemble of particles.^[1] Small angle neutron scattering (SANS) can size particles on the nanometer length scale, but can be difficult as a neutron source is required, meaning experiments are done at large scale facilities. The main disadvantage of PCS is that data analysis requires a number of assumptions in regards to the particle distribution.^[1] The data can be skewed if there is a broad distribution of particles, or if there is a multimodal particle set.

A well-established method for absolute determination of root mean square radii (rms) is multi-angle laser light scattering (MALLS).^[1-3] MALLS, when used on unseparated samples, will result in rms radius and mean molar mass of the particles. MALLS is classical light scattering, performed at several angles. It involves measuring the amount of light scattered by a sample at these angles to the incident laser. The scattering as a function of angle is called Rayleigh scattering, which for macromolecules has an angular dependence. It can give the rms radius, molar mass, and second virial coefficient (A_2). The theory used to describe the scattering of light by macromolecules in solution is called the Rayleigh-Gans-Debye theory.

Particles scatter light at various angles due to differences in each particle, leading to constructive or destructive interference. By measuring the interference at multiple angles, the angular dependence of scattered light can be determined. Knowing the angular dependence of scattered light allows the determination of particle size, measured as rms radius. The rms radius is a measure of particle size weighted by the mass distribution about the particle's center mass, and can also be called radius of gyration (R_z).

As described by Philip Wyatt^[1], Zimm^[4, 5] condensed the Rayleigh-Gans-Debye theory into an equation:

$$\frac{K * c}{R(\theta, c)} = \frac{1}{M_w P(\theta)} + 2A_2 c,$$

where $R(\theta, c)$ is excess Rayleigh ratio of solution as a function of scattering angle θ and concentration c , c is solute concentration, M_w is weight average molar mass, A_2 is second virial coefficient, K^* is an optical constant, and $P(\theta)$ is angular dependence of scattered light. $P(\theta)$ can be related to the rms radius by expansion to first order.

To measure the molar mass of particles in solution, it is necessary to know the change in refractive index (Δn) with the change in molecular concentration (Δc). This is known as the dn/dc , and can be measured with a refractive index detector. It is necessary to measure dn/dc because as a laser hits a particle in solution, an oscillating dipole is induced within the particle, which scatters the light. The intensity of scattered light to a detector is dependent on the dn/dc of the particles. By using the above equation, particle mass can also be determined.^[1, 6]

MALLS can be used to measure an ensemble of particles if combined with a separation technique. The separation will fractionate the particles in slices, each with narrow size distributions, which will be measured by MALLS. Asymmetric field flow fractionation (AFFF) is a separation technique based on hydrodynamic principles.^[1, 3, 7] Particles flow across a membrane, carried by a channel flow. The separation occurs as a cross flow acts perpendicularly to the channel flow, pushing the particles against the membrane. Translational diffusion causes the particles to migrate back into the channel flow. By choosing the appropriate cross flow, the particles can elute out of the channel, and on to a detector, such as a UV-vis or MALLS instrument. Particle retention against the membrane is a function of its size, as smaller particles will flow off of the membrane and to the detector faster than larger particles, thus creating the separation.

2.1.1 Uses of AFFF-MALLS

In this chapter, we will look at the many ways AFFF-MALLS has been used. Palmer and coworkers have used AFFF-MALLS to study the size, shape, and encapsulation efficiency of liposome-encapsulated actin-hemoglobin dispersions (LEAcHb).^[8] These LEAcHb dispersions were developed as potential blood substitutes, as a way to replace normal blood transfusions. Since cell free hemoglobin solutions induce vasoconstriction and renal toxicity, liposome-encapsulated hemoglobin systems have been developed. Liposomes were prepared via extrusion of a lipid film through polycarbonate membrane pores of either 400 or 600 nm in diameter. The dispersions were prepared as plain liposomes, liposome-encapsulated hemoglobin (LEHb), liposome-encapsulated actin (LEAc) or liposome-encapsulated actin-hemoglobin (LEAcHb). The shape, size, and encapsulation efficiency were measured at the same time by the AFFF-MALLS. Shapes were determined by fitting MALLS spectra to various form factors. Empty liposomes were spherical in shape, while liposomes containing actin were formed as a disk-like assembly. The size distributions were shown to increase for plain liposomes to liposomes containing hemoglobin, however the size did not change much for actin-containing particles that did or did not contain Hb. The same trends were seen for both liposomes extruded through the 400 or the 600 nm pore membranes. To determine encapsulation efficiency, the differential refractive index of eluting Hb was measured. The unencapsulated Hb was separated from the liposomes by the AFFF. LEAcHb prepared through 400 nm pore membranes had a Hb encapsulation efficiency of ~ 30%. LEAcHb prepared through 600 nm pore membranes showed an encapsulation efficiency of 46%.

Patton and Palmer have also used AFFF-MALLS to study “lipogels” as artificial blood substitutes.^[9] In this work, the particles were synthesized as poly(N-isopropylacrylamide) (pNIPAm) or poly(acrylamide) (pAm) hydrogels were prepared via UV-induced photopolymerization inside of a liposomal reactor. Egg-L- α -phosphatidylcholine (EPC) films were rehydrated in bovine hemoglobin, along with NIPAm or Am, cross-linker, and a photoinitiator in either Tris-HCl or phosphate buffered saline (PBS). Liposomes were formed by agitating the lipid film and then extruding the film through 200 nm pore diameter polycarbonate membranes, and then UV irradiation used to polymerize the hydrogels. AFFF-MALLS was then used to determine the particle size and shape. The lipogels were shown to be fairly monodisperse, as none of the constructs had a polydispersity index of much greater than 1. Also, the encapsulation of additional species did not effect the size, but lipogels extruded in PBS were larger but more monodisperse than those extruded in Tris. The pNIPAm and pAm lipogels ranged from 131 to 141 nm in radius. To determine shape, R_z/R_h was measured. While a ratio of 0.77 is seen for solid spheres, hollow spheres have an R_z/R_h near 1. Both pNIPAm and pAm lipogels had $R_z/R_h \leq 1$. The authors deduce from this that both sets of lipogels were spherical particles.

Middleberg and coworkers developed virus-like particles (VLPs) and used AFFF-MALLS to study their characteristics.^[10] VLPs are formed by self-assembly of viral structural proteins into biomolecular nanoparticles. VLPs have gained interested recently as a vaccine has been successfully developed against human papillomavirus.^[11, 12] An important issue involving VLPs is to have batch-to-batch consistency for regulatory acceptance. The use of AFFF-MALLS allows for quick and reliable characterization of

the VLPs. Marine polyomavirus VP1 DNA sequence was cloned into vectors and expressed in *Spodoptera frugiperda* (Sf9) cells and *Escherichia coli* (*E. coli*) cells. VLPs were collected from the cells. AFFF separation was done with a cross flow of 0.75 mL/min and the VLP fractions were then characterized by MALLS. Fraction sizes ranged up to 100 nm in radius with 69% of the VLPs from Sf9 between 15 and 35 nm. Less aggregation was seen from VLPs from *E. coli*, with 96% having a radius between 15 and 35 nm. To determine if there was VLP aggregation, cross flow was increased up to 1.50 mL/min to completely immobilize the particles on the membrane. There was no significant aggregation seen, even at these high cross flows. AFFF-MALLS was also used to monitor changes in the VLP quaternary structure. Differences in quaternary structure were evident from the fractions eluting after VLP disassembly. This disassembly is important for applications such as purification of encapsulated contaminants. This disassembly can thus be monitored by AFFF-MALLS.

Schimpf and coworkers have used AFFF-MALLS to study aggregation of the protein calsequestrin.^[13] Calsequestrin (CSQ) is a protein that functions both in the regulated release and sequestration of Ca^{2+} from the sarcoplasmic reticulum. CSQ, in response to increase Ca^{2+} concentration, forms aggregates in the form of dimers, then tetramers, and onto higher order aggregates. CSQ aggregation can be inhibited by increased K^+ concentration. Some small molecules are known to bind to CSQ, which could lead to cardiotoxic side effects. The authors have studied the aggregation of CSQ in the presence of Ca^{2+} and K^+ as well as the small molecule trifluoperazine (TFP). Canine cardiac CSQ was expressed in *E. coli* as an expression vector and purified. A cross flow of 2 mL/min that declined to 0 mL/min was used. The fractions eluted to the MALLS,

where molar mass was determined using light scattering and differential refractive index. In the presence of 3mM Ca^{2+} and 500 mM K^+ , 2 primary species eluted, with the masses indicating the species were dimers and tetramers. As K^+ is increased, the amount of tetramer decreases. When K^+ is held constant and Ca^{2+} concentration is increased, more dimer and tetramer exist, as well as hexamer. In their final experiments, Ca^{2+} and K^+ concentrations were held constant at 3 mM and 300 mM, respectively, while TFP was added. As TFP is increased, CSQ distribution shifts towards tetramer and hexamer formation. Thus, their findings indicate that small molecules like TFP can lead to CSQ aggregation.

Baalousha et al. have studied the size and shape of natural colloids. Natural soil colloids are important for contaminant adsorption, transport, and sedimentation in the aquatic environment.^[14] These colloids tend to have broad size distributions and can be any of a number of shapes. These characteristics control their mobility and how they interact with the environment. The use of AFFF-MALLS allows for shape and size determination of these colloids. The AFFF can accurately separate the many fractions of colloids, and as they elute to the MALLS, the size distributions of these fractions can be measured. Samples were obtained from drilled soil cores in northern Germany, and divided into two sample sets. An AFFF channel flow of 1.5 mL/min and cross flow of 0.75 mL/min were used for particle separation. The natural colloids showed a continuous distribution, until the cross flow was modified. By adjusting the cross flow on subsequent runs, the authors could elute peaks for the different sized colloids. Three different particle sizes were seen: small (50-150 nm), intermediate (200-350 nm), and large (> 350 nm). Shape was then inferred from R_g/R_h ratios. The small and intermediate sizes had ratios

of 0.85 and 0.775, respectively, suggesting spherical shapes. The large particles had ratios of 1.05, 2, and 2.7, depending on particle set. These suggest a deviation from spherical particles, toward a platelet shape.

Citkowitz et al. have studied VLPs for DNA delivery.^[15] VLPs were developed from the VP1 protein derived from human polyoma JC-virus (JCV) as it can be used to target a number of different cells, such as kidney epithelial cells. VLPs were expressed in Sf158 insect cells. After centrifugation of the cells, the VLPs were precipitated out of the supernatant with 8000 MW poly(ethylene glycol). After purification of the VLPs through a DEAE Sepharose column, the VLPs were collected. The VLPs were then dissociated to remove impurities, and then packaged with a reporter DNA containing green fluorescent protein. AFFF-MALLS was used to characterize the VLPs. The separation and subsequent molar mass measurements of the VLPs showed two populations, one of the VLPs, and a second of aggregated VP1 proteins. Initial packaging attempts of DNA seemed to suggest aggregation of the VLPs, as mass and radius were much larger than expected. The results suggested that 5-kB plasmids could not be encapsulated. Therefore, a 1.6-kB linear DNA was used. The packaged VLPs had a radius of 24 nm. This was ~ 1.5 nm larger than unpackaged VLPs. An interesting feature uncovered by AFFF-MALLS was that the larger radii packaged VLPs actually had a smaller molar mass than unpackaged VLPs. The authors explain this by describing the packaged DNA was near the VLP capsid, leaving the center of the particle “more empty”. The rigid capsid of the VLP keeps the outer radius fairly constant for each set of VLPs.

All of these uses demonstrate the capabilities of AFFF-MALLS. The remainder of this chapter will describe some of the work we have done with the instrument, characterizing microgel changes with the AFFF-MALLS.

2.1.2 Microgels

As described in Chapter 1, hydrogel colloids, or microgels, are randomly oriented, water-soluble, cross-linked polymer nanoparticles. This chapter will investigate responsive hydrogels, which can undergo a swollen to deswollen transition in response to external stimuli.^[16-23] One of the most interesting characteristics of pNIPAm-based microgels is the swelling/deswelling of the gels in water upon reaching the LCST. Below this temperature, the microgels are hydrophilic and swollen, but above this temperature, there is an entropically driven polymer phase transition, expelling the water and deswelling the gel.^[16, 19-21] Our group has optimized core/shell microgel synthesis over a wide range of sizes utilizing this behavior to drive the controlled nucleation growth of the particles. This behavior is also important in terms of particle characterization for this work, as we can use AFFF-MALLS to investigate particle sizes above and below the LCST.

The microgels used in this work are composed of a degradable cross-linker, *N,N'*-(1,2-dihydroxyethylene)bisacrylamide (DHEA). The use of DHEA allows for degradation by sodium periodate, which cleaves vicinal diols.^[24] By cleaving the DHEA in the core of the core/shell microgels, particles can be made “hollow”, which will lead to changes in radii for the particles at 25 °C and at temperatures above the LCST. Using the AFFF-MALLS, we have investigated these changes in particle size for both native core/shell microgels and the degraded core particles.

2.2 Experimental Section

2.2.1 Materials

All materials were purchased from Sigma-Aldrich unless otherwise noted. The monomer *N*-isopropylacrylamide (NIPAm) was recrystallized from hexane (J. T. Baker) before use. The cross-linkers *N,N'*-methylenebis(acrylamide) (BIS) and *N,N'*-(1,2-dihydroxyethylene)bisacrylamide (DHEA), as well as ammonium persulfate (APS), and sodium dodecyl sulfate (SDS), were all used as received. Water used in the experiments was distilled and then deionized using a Barnstead E-pure system operating at a resistance of 18 M Ω .

2.2.2 Microgel core synthesis

Microgel core particles were synthesized by free-radical precipitation polymerization as previously reported. In brief, monomer (NIPAm), cross-linker (DHEA), and surfactant (SDS) were dissolved in 100 mL of deionized water and the solution was then filtered. The solution was then heated to 70 °C in a three-neck round-bottom flask. The solution was purged with N₂ gas and stirred until the temperature remained stable. After 15 min, the reaction was initiated by adding 1-mL solution of initiator (APS). The solution turned turbid, indicating successful initiation, and the reaction continued for 4 h. After 4 h, the solution was allowed to cool to room temperature and filtered through a Whatman filter paper.

2.2.3 Microgel shell synthesis

Core particles were used as seeds to add a hydrogel shell, as previously reported. Briefly, 10 mL of the core microgel solution, SDS, and deionized water were added to a three-neck round-bottom flask and heated to 70 °C under N₂ gas. Separately, NIPAm and BIS were dissolved in 5 mL of deionized H₂O. This solution was added to the three-neck round-bottom flask. After the temperature stabilized, the reaction was initiated by the addition of a 1-mL solution of APS. The reaction proceeded for 4 h. After the synthesis, the solution was filtered through a Whatman filter paper and then centrifuged several times for purification.

2.2.4 Core degradation

Core degradation of the core/shell microgels was done by the addition of sodium periodate. Either a 1:1 or a 2X equivalent of periodate was added to the microgel solution. The amount of DHEA present in the particles was calculated from the pre-gel solution. The reaction was allowed to occur for either 2 h, or overnight, on a shaker table at room temperature. Particles were centrifuged after degradation to remove the degraded material.

2.2.5 Particle characterization

2.2.5.1 Static light scattering

In order to determine the distribution of z -average radii (R_z) for particles, multi-angle laser light scattering (MALLS; Wyatt Technology Corporation) detection following asymmetric field flow fractionation (AFFF) was used. AFFF separation uses a cross-flow method to separate particles as a function of hydrodynamic volume. The cross-flow forces larger particles against a cellulose membrane, while smaller particles elute to the MALLS detector faster. For all separations, a cross-flow of 1.0 mL/min was used, and a Peltier device was used to maintain a flow cell temperature at either 25 °C or 40 °C. The MALLS detector collects light from 16 different fixed angles as a function of peak intensity (V) to determine R_z of the particles. ASTRA 5.1.5.0 software was used to determine R_z of the particles, using the Debye fit method.

2.2.5.2 Photon correlation spectroscopy

Microgel hydrodynamic radii (R_h) were determined by photon correlation spectroscopy (Protein Solutions Inc.) equipped with a Peltier temperature control device. Scattered light is captured by the instrument at 90° with a single-mode optical fiber coupled to an avalanche photodiode detector. Samples were thermally equilibrated for 10 min, and then data was collected for at least 10 measurements with an acquisition time of 60 s per measurement. The data was analyzed with Dynamic Software version 5.25.44 (Protein Solutions). The hydrodynamic radii of the particles were calculated from the diffusion coefficient using the Stokes-Einstein equation.

2.3 Results and Discussion

The work presented here is a brief overview of the results that can be obtained with AFFF-MALLS. The remainder of this chapter will discuss some of the interesting results we have seen, and more significant AFFF-MALLS data will also be presented in Chapter 3.

Figure 2.1 shows the differential weight fraction of pNIPAm-co-DHEA core/shell microgels. This fraction represents the width of the entire peak eluting from the AFFF to the MALLS detector. This plot shows the excellent control we have over the synthesis, as the particles are extremely monodisperse. The AFFF allows for the particle separation before eluting to the detector, where the sizes are determined. With the monodispersity of this synthesis, the separation can be more highly defined by controlling the cross-flow across the membrane. By adjusting the cross-flow with a highly monodisperse sample, the particles do not elute at the same time, as they would with a polydisperse sample if a narrow peak is still desired. A separation to this degree with a polydisperse sample would lead to a very broad peak.

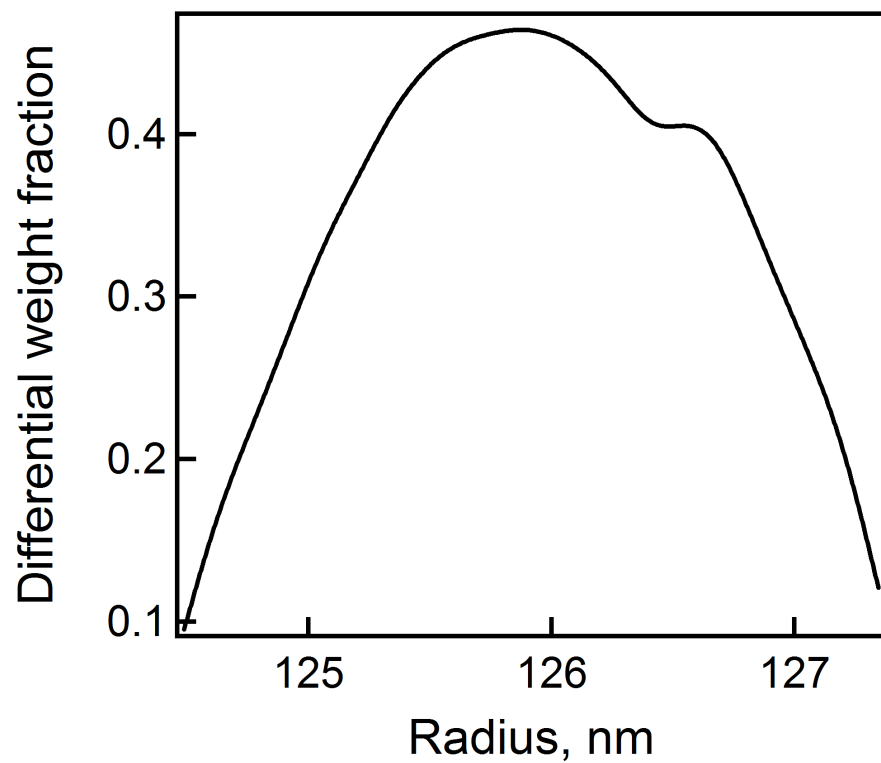


Figure 2.1. Differential weight fraction plot for pNIPAm-co-DHEA/pNIPAm core/shell particles, as determined by AFFF-MALLS.

Figure 2.2 shows the cleavage of DHEA by sodium periodate (NaIO_4). By using DHEA as a cross-linker in the core microgels, the addition of NaIO_4 will degrade the core material, which can be removed by cleaning the particles through centrifugation and removing the supernatant. Since the microgels are a core/shell structure, particles will hold their shape, but now as more “hollowed out” spheres.

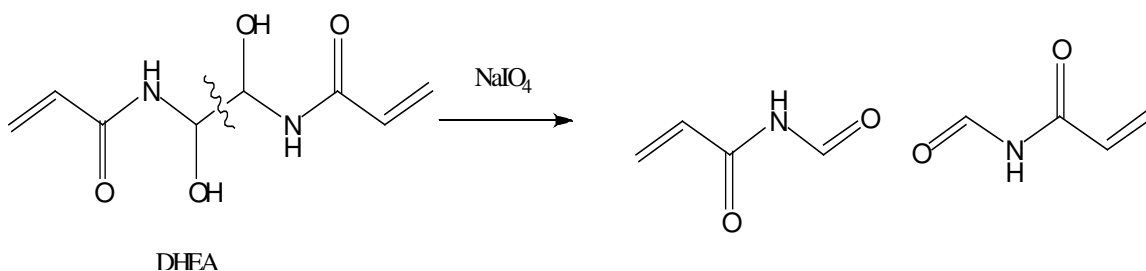


Figure 2.2. Scheme of DHEA cleavage by sodium periodate.

Figure 2.3 shows the visual turbidity changes that take place as the core is degraded. Native core/shell particles (vial 1) are very turbid, while the degraded core particles in vial 2 are much less turbid due to the removal of the core material. The cores in vial 2 particles were degraded overnight. While being able to visualize the change in turbidity, the changes in light scattering measurements are significant.



Figure 2.3. Picture of vials containing pNIPAm-co-DHEA core/pNIPAm shell microgels. Vial 1 contains native microgels. Vial 2 contains core-degraded microgels.

Table 2.1 shows the changes that take place with regard to size and light scattering as the particle cores are degraded. At 25 °C, core/shell particles see a slight increase in radius after the core is degraded. This should not be surprising as the particles will become more loose, as there is very little density in the core, meaning less connecting points to the shell which can restrict its size. As the temperature is increased to 40 °C, the particles deswell, as this is above the LCST. The degraded particles see a more dramatic decrease in size, as the core is not there to restrict the amount of deswelling. At both 25 °C and 40 °C, particles with a degraded core show a decrease in intensity, as there is less density and thus less light scattered. The overall increase in intensity from particles at 40 °C versus 25 °C is based on the deswollen particles scattering more light than swollen core/shell particles.

Table 2.1. Native and degraded core nanogel radii and peak intensity values.

	25 °C			40 °C		
	R _h (nm)	R _z (nm)	Peak Intensity (V)	R _h (nm)	R _z (nm)	Peak Intensity (V)
Native Core/shell	151	126	2.3	98	82	8.5
Degraded Core	153	132	1.2	89	74	5.6

Another interesting feature of these particles is the R_z/R_h ratio of the native core/shell and degraded core particles. As stated previously, the ratio for solid sphere is 0.77, while hollow spheres have an R_z/R_h near 1. For the native core/shell particles, the

R_z/R_h is 0.83. The degraded core particle ratio is slightly higher, at 0.86. While the difference is not huge, it does suggest that the degradation is causing the particles to become somewhat “hollowed out.”

2.4 Conclusions

AFFF-MALLS is a fairly quick and reliable tool that can be used to investigate particles in many different ways. In this chapter, it has been shown that degradable microgels can be synthesized and the size and shape studied with this instrument. The addition of DHEA in the microgels makes the cores of the particles degradable by sodium periodate. AFFF-MALLS shows exceptional control over the synthesis in terms of polydispersity. It also shows the size differences that occur after core degradation. The degraded particles show the ability to deswell more at high temperatures over the native particles, as the core material has been removed, allowing the particles more room to collapse. In addition to this, the R_z/R_h ratio for the degraded particles increases over that of the native particles, closer to 1. This suggests more of a hollow sphere shape for the degraded core particles. The AFFF-MALLS has proven to be a valuable instrument in our lab, and the next chapter will continue to show the excellent results we have gotten from it.

2.5 References

- [1] P. J. Wyatt, Submicrometer particle sizing by multiangle light scattering following fractionation, *Journal of Colloid and Interface Science*, 1998, **197**, 9-20.
- [2] P. J. Wyatt and D. N. Villalpando, High-Precision Measurement of Submicrometer Particle Size Distributions, *Langmuir*, 1997, **13**, 3913-3914.
- [3] D. W. Shortt, D. Roessner and P. J. Wyatt, Absolute measurement of diameter distributions of particles using a multiangle light scattering photometer coupled with flow field-flow fractionation, *American Laboratory*, 1996, **28**, 21-28.
- [4] B. H. Zimm, The scattering of light and the radial distribution function of high-polymer solutions, *Journal of Chemical Physics*, 1948, **16**, 1093-1099.
- [5] B. H. Zimm, Apparatus and methods for measurement and interpretation of the angular variation of light scattering; preliminary results on polystyrene solutions, *Journal of Chemical Physics*, 1948, **16**, 1099-1116.
- [6] J. Wen, T. Arakawa and J. S. Philo, Size-exclusion chromatography with online light-scattering, absorbance, and refractive index detectors for studying proteins and their interactions, *Analytical Biochemistry*, 1996, **240**, 155-166.
- [7] B. A. Korgel, J. H. Van Zanten and H. G. Monbouquette, Vesicle size distributions measured by flow field-flow fractionation coupled with multiangle light scattering, *Biophysical Journal*, 1998, **74**, 3264-3272.
- [8] S. Li, J. Nickels and A. F. Palmer, Liposome-encapsulated actin-hemoglobin (LEAcHb) artificial blood substitutes, *Biomaterials*, 2005, **26**, 3759-3769.
- [9] J. N. Patton and A. F. Palmer, Photopolymerization of Bovine Hemoglobin Entrapped Nanoscale Hydrogel Particles within Liposomal Reactors for Use as an Artificial Blood Substitute, *Biomacromolecules*, 2005, **6**, 414-424.
- [10] Y. P. Chuan, Y. Y. Fan, L. Lua and A. P. J. Middelberg, Quantitative analysis of virus-like particle size and distribution by field-flow fractionation, *Biotechnology and Bioengineering*, 2008, **99**, 1425-1433.

- [11] L. A. Koutsky, K. A. Ault, C. M. Wheeler, D. R. Brown, E. Barr, F. B. Alvarez, L. M. Chiacchierini, K. U. Jansen, K. Beutner, H. Buck, R. Edwards, D. Ferris, S. Gall, L. Miller, C. M. Peterson, Y. Wade, D. Wiley, E. Wiesmeier, P. Wood, D. Whitaker, F. Judson, A. Chatterjee, A. Giuliano, R. Kurman, B. Ronnett, M. Stoler, A. Ferenczy, R. Ashfaq, S. Selvaggi, M. Steinhoff, N. Kiviat, V. Santarsieri, D. Baker, D. King, M. Glant, C. Eisenhut, K. U. Jansen, F. Taddeo, A. DiCello, W. Li, J. Smith, R. Heffelfinger-Wenner, D. Campbell, R. Marchese, J. Erick, A. Lee, M. Kosinski, H. George, V. Goetz, P. De Phillips, Y. Wang, D. Volkin, L. Shi, P. K. Tsai, R. Sitrin, E. Barr, F. Alvarez, L. Chiacchierini, M. Dallas, M. Buiser, M. Swope, S. Schild, A. Thornton, G. Suhr, M. Nelson, P. Smith, C. Lightfoot, D. Johnson, K. Fujimori, C. Kirk, P. Krout, D. Pugliese and L. Zhang, A controlled trial of a human papillomavirus type 16 vaccine, *New England Journal of Medicine*, 2002, **347**, 1645-1651.
- [12] L. L. Villa, R. L. R. Costa, C. A. Petta, R. P. Andrade, J. Paavonen, O. E. Iversen, S. E. Olsson, J. Hoye, M. Steinwall, G. Riis-Johannessen, A. Andersson-Ellstrom, K. Elfgren, G. Von Krogh, M. Lehtinen, C. Malm, G. M. Tamms, K. Giacoletti, L. Lupinacci, R. Railkar, F. J. Taddeo, J. Bryan, M. T. Esser, H. L. Sings, A. J. Saah and E. Barr, High sustained efficacy of a prophylactic quadrivalent human papillomavirus types 6/11/16/18 L1 virus-like particle vaccine through 5 years of follow-up, *British Journal of Cancer*, 2006, **95**, 1459-1466.
- [13] S. E. Shadle, R. Rostock, L. Bonfrisco and M. E. Schimpf, Study of calsequestrin aggregation by flow field-flow fractionation with light scattering detection, *Journal of Liquid Chromatography & Related Technologies*, 2007, **30**, 1513-1523.
- [14] M. Baalousha, F. V. D. Kammer, M. Motelica-Heino, H. S. Hilal and P. Le Coustumer, Size fractionation and characterization of natural colloids by flow-field flow fractionation coupled to multi-angle laser light scattering, *Journal of Chromatography, A*, 2006, **1104**, 272-281.
- [15] A. Citkowicz, H. Petry, R. N. Harkins, O. Ast, L. Cashion, C. Goldmann, P. Bringmann, K. Plummer and B. R. Larsen, Characterization of virus-like particle assembly for DNA delivery using asymmetrical flow field-flow fractionation and light scattering, *Analytical Biochemistry*, 2008, **376**, 163-172.
- [16] M. Heskins and J. E. Guillet, Solution properties of poly(N-isopropylacrylamide), *J. Macromol. Sci. Chem.*, 1968, **A2**, 1441-1455.

- [17] S. Kim and K. E. Healy, Synthesis and Characterization of Injectable Poly(N-isopropylacrylamide-co-acrylic acid) Hydrogels with Proteolytically Degradable Cross-Links, *Biomacromolecules*, 2003, **4**, 1214-1223.
- [18] M. P. Lutolf, G. P. Raeber, A. H. Zisch, N. Tirelli and J. A. Hubbell, Cell-responsive synthetic hydrogels, *Advanced Materials*, 2003, **15**, 888-892.
- [19] R. H. Pelton and P. Chibante, Preparation of aqueous latexes with N-isopropylacrylamide, *Colloids and Surfaces*, 1986, **20**, 247-256.
- [20] H. G. Schild, Poly(N-isopropylacrylamide): experiment, theory and application, *Progress in Polymer Science*, 1992, **17**, 163-249.
- [21] T. Tanaka, Kinetics of phase transition in polymer gels, *Physica A*, 1986, **140A**, 261-268.
- [22] T. Tanaka and D. J. Fillmore, Kinetics of Swelling of Gels, *J. Chem. Phys.*, 1979, **70**, 1214 - 1218.
- [23] T. Tanaka, D. J. Fillmore, S.-T. Sun, I. Nishio, G. Swislow and A. Shah, Phase Transition in Ionic Gels, *Phys. Rev. Lett.*, 1980, **45**, 1636-1639.
- [24] S. Nayak, D. Gan, M. J. Serpe and L. A. Lyon, Hollow thermoresponsive microgels, *Small*, 2005, **1**, 416-421.

CHAPTER 3

SIZE CONTROLLED SYNTHESIS OF MONODISPERSED, CORE/SHELL NANOGELS

Adapted from Blackburn, W. H.; Lyon, L. A., Size-controlled synthesis of monodisperse core/shell nanogels. Colloid and Polymer Science 2008, 286, (5), 563-569.

In this chapter, we describe small, monodispersed nanogels (~ 50-nm radius) synthesized by free-radical precipitation polymerization and characterized using a suite of light scattering and chromatography methods. Nanogels were synthesized with either *N*-isopropylacrylamide or *N*-isopropylmethacrylamide as the main monomer, with acrylic acid or 4-acrylamidofluorescein as a co-monomer and *N, N'*-methylenebis(acrylamide) as a cross-linker. By varying the surfactant and initiator concentrations, particle size was controlled while maintaining excellent monodispersity. An amine-containing shell was added to these core particles to facilitate subsequent bioconjugation. Successful conjugation of folic acid to the particles was demonstrated as an example of how such materials might be employed in a targeted drug delivery system.

3.1 Introduction

As described in the previous chapters, poly(*N*-isopropylacrylamide) based hydrogel colloids, or nanogels are widely studied.^[1-4] Monodispersed nanogels over a wide range of sizes have been synthesized by a number of different methods,^[5-7] with

free-radical precipitation polymerization being the most common.^[1, 6, 8-12] The lower critical solution temperature (LCST) of pNIPAm nanogels in water is around 31 °C. Particles composed of poly(*N*-isopropylmethacrylamide) (pNIPMAm) behave in a similar manner, exhibiting an LCST around 44 °C, with the increased LCST arising from an increase in the rigidity of the pNIPMAm polymer, as is common for methacrylamides.^[13-17] This behavior is important to this work due to the fact that our group has optimized core/shell nanogel synthesis techniques that utilize this LCST behavior to drive the controlled nucleation and growth of the particles.

The focus of this chapter is related to the size control of a variety of core/shell nanogel constructs. Nanogels to be used for intravenous drug delivery applications such as targeted chemotherapy must be around 100 nm in diameter to be efficient vehicles. Particles of this size do not penetrate into healthy tissues, as pore sizes in the endothelia of blood vessels in most healthy tissues are ~2 nm, while ~6 nm pores are found in postcapillary venules.^[18] However, the same resistance to particle penetration is not encountered in tumor targeting, as the “leaky” discontinuous tumor vasculature has pore sizes ranging from 100 nm – 780 nm.^[18-20] Typically, this leaky vasculature enables what is called the “enhanced permeability and retention” (EPR) effect, which enables the enhanced deposition of nanoscale delivery vehicles at the site of a solid tumor.^[21-23] Another problem that delivery vehicles encounter is non-specific uptake by the reticuloendothelial system (RES). The surface characteristics of particles can affect uptake by the liver, spleen, and the rest of the RES.^[24, 25] Hydrophilic particles tend avoid the RES for much longer time periods than hydrophobic particles, thereby permitting longer circulation times, which allow the particles a greater chance to target the site of

interest.^[24] Thus, both size and surface chemistry should be controllable in order to enable the synthesis of effective tumor targeting vehicles.

The nanogels used in this chapter were synthesized by free-radical precipitation polymerization. In this approach, a free-radical initiator is used to initiate the reaction, while a surfactant is used to stabilize the growing polymer globule. Classically, one would expect that increasing both the surfactant and initiator concentrations would lead to a reduction in particle size.^[26] Ammonium persulfate (APS) is a free radical initiator, and as the reaction is heated, it creates free radicals and hence growing oligoradicals that act as nucleation sites onto which growing polymer can add. Increasing the initiator concentration leads to more free radicals being formed, and this leads to an increase in number of particles that can potentially be formed. Since the monomer is being consumed by more growing particles under such conditions, the final particle size will be smaller as the same amount of monomer is spread among more particles. Thus, we expect that an increase in the initiator concentration will yield a smaller average particle size. The second control parameter to be explored is that of surfactant concentration. Sodium dodecyl sulfate (SDS) is the surfactant used in the particle syntheses described below. SDS acts to stabilize the growing nuclei against aggregation early in the reaction. Thus, at lower [SDS], particles formed in the early stages of the reaction aggregate to form larger particles, decreasing the number of particles that are formed in a reaction. Conversely, an increase in [SDS] should increase the stability of the early nuclei, allowing them to grow without extensive aggregation and therefore increasing the particle number while decreasing the final particle size. Because of the simplicity of these reaction design considerations, these control parameters are commonly used in dispersion polymerization

to control particle size.^[26] In this chapter, we demonstrate the ability to synthesize small, monodisperse core/shell nanogel particles. The syntheses are very well controlled, and give us the ability to make a variety of particle sizes. We have also shown the ability to synthesize these small nanogels with different co-monomers thereby producing particles with multiple functionalities. These efforts were undertaken in support of our larger efforts in targeted chemotherapy wherein such synthetic control is critical.

3.2 Experimental Section

All materials were purchased from Sigma-Aldrich unless otherwise noted. The monomers *N*-isopropyl acrylamide (NIPAm) and *N*-isopropyl methacrylamide (NIPMAm) were recrystallized from hexane (J. T. Baker) before use. The cross-linker *N,N'*-methylenebis(acrylamide) (BIS), acrylic acid, *N*-(3-aminopropyl) methacrylamide hydrochloride (APMA) (Polysciences), ammonium persulfate (APS), and sodium dodecyl sulfate (SDS) were used as received. All water used in the experiments was distilled, and then deionized using a Barnstead E-pure system operating at a resistance of 18 M Ω . A 0.2 μ m filter was used to remove particulate matter. For folic acid conjugation, folic acid, 1-ethyl-3-methyl-(3-dimethylaminopropyl)carbodiimide (EDC) (Pierce), and ϵ -maleimidocaproic acid were used. The fluorescent monomer 4-acrylamidofluorescein (AFA) was synthesized via a previously reported procedure.^[27]

3.2.1 Nanogel Core Synthesis

Nanogel core/shell particles were synthesized by free-radical precipitation polymerization as reported previously.^[10, 11] For all particles, the molar composition of

core particles was 96% NIPAm (or 96% NIPMAm), 2% BIS, and 2% AAc, or 98% NIPAm (or 98% NIPMAm), 2% BIS, and 0.1 mM AFA. A total monomer concentration of 70 mM was used for NIPAm particles, while a total concentration of 140 mM was used for NIPMAm particles. All polymerizations were carried out in a three-neck round bottom flask. As described below, various concentrations of SDS were used as the surfactant, and various concentrations of APS were used to initiate the reaction. In a typical synthesis, 100 mL of a filtered, aqueous solution of monomer, BIS, and SDS were added to the flask and heated to 70 °C. The solution was purged with N₂ gas and stirred vigorously until the temperature remained stable. The AAc was then added (where appropriate). After 15 minutes, the reaction was initiated by adding a 1 mL solution of the desired concentration of APS. The solution turned turbid, indicating successful initiation. The reaction was allowed to continue for 4 hours while being purged by N₂ gas with constant stirring. For particles containing AFA, the AFA was added along with the main monomer and cross-linker. After the synthesis, the solution was filtered through a Whatman filter paper. Conditions for all of the core syntheses can be found in Tables 1 and 2. For all syntheses, the batch-to-batch size variation was within 10%. Differences from batch to batch can simply be attributed to slight thermal fluctuations during the synthesis.

3.2.2 Nanogel Shell Synthesis

Core particles were used as seeds for the addition of a shell hydrogel. The detailed procedure of the shell synthesis has been reported in previous publications.^[22, 23] In brief, 10 mL of the core nanogel solution, 2 mM SDS, and 35 mL of deionized H₂O were added

to a three-neck round bottom flask and heated under N₂ gas to 70 °C. Separately, a monomer mixture with the following molar ratios was dissolved in 5 mL of deionized H₂O: 97.5% NIPAm (or 97.5% NIPMAm), 2% BIS, and 0.5% APMA. This solution was added to the three-neck round bottom flask and heated to 70 °C. The reaction was initiated by a 1 mL solution of 0.5 mM APS and the reaction proceeded for four hours. Following the synthesis, the solution was filtered through a Whatman filter paper and then centrifuged several times for purification.

3.2.3 Particle Characterization

3.2.3.1 Static light scattering

Multi-angle laser light scattering (MALLS) (Wyatt Technology Corporation) detection following asymmetric field flow fractionation (AFFF) was used to determine the distribution of z-average radii (R_z) for all particles. The AFFF separation method uses a cross flow method to separate the particles as a function of hydrodynamic volume. The cross flow acts to force larger particles against a cellulose membrane, while smaller particles elute to the MALLS detector faster. For all separations, a cross flow of 0.5 mL/min was used. The MALLS detector is equipped with a Peltier device to maintain a flow cell temperature of 25 °C and collects scattered light from 16 different fixed angles to determine the R_z of the particles. By measuring R_z as a function of elution time, we construct a chromatogram that permits the determination of the weight fraction of particles as a function of radius, thereby providing a sample polydispersity. ASTRA 5.1.5.0 software was used to determine R_z values using the Debye fit method.

3.2.3.2 Fluorimetry

Particle LCST values were measured from turbidity curves collected on a steady-state fluorescence spectrophotometer (Photon Technology International), equipped with a Model 814 PMT photon-counting detector. Scattering was measured through slits that were set to attain a spectral bandwidth of 2 nm. The scattering was measured at a wavelength of 600 nm, and the temperature ramp was set from 25 °C to 60 °C. An integration time of 1 s was used and data was collected every 0.1 °C, with the temperature increasing at a rate of 1 °C per minute.

3.2.4 Folic acid conjugation

Nanogel core/shell particles were conjugated with folic acid by a method previously described by Dube et al.^[28] The core/shell nanogel solution was freeze-dried and then resuspended in 40 mL of 10 mM phosphate buffer pH 4.7. A 2:1 molar ratio of folic acid to amine in the shell was dissolved in 1 mL DMSO. To this, a 2X equivalent of EDC was added to activate the folic acid. This solution was mixed for 15 minutes, and then added to the core/shell nanogel solution. The reaction was stirred in the dark overnight. The particles were then centrifuged/resuspended several times for purification.

3.2.5 Absorbance measurements

The absorbance of folic acid, core/shell particles, and folate-conjugated core/shell particles was determined using a Shimadzu UV 1601 spectrophotometer. Freeze-dried samples were dissolved in DMSO for absorbance measurements.

Table 3.1. Parameters for pNIPAm core particle syntheses.

	Monomer	Cross-linker	Co-monomer	[Surfactant], mM	[Initiator], mM	[Total Monomer], mM	R_z , nm
1	pNIPAm- 96%	BIS- 2%	AAc- 2%	2	2	70	86
2	pNIPAm- 96%	BIS- 2%	AAc- 2%	3	3	70	73
3	pNIPAm- 96%	BIS- 2%	AAc- 2%	4	4	70	53
4	pNIPAm- 98%	BIS- 2%	AFA- 0.1 mM	4	4	70	57
5	pNIPAm- 95%	BIS- 5%	AFA- 0.1 mM	4	4	40	44

3.3 Results and Discussion

Table 3.1 shows the very straightforward progression we have followed in the synthesis of pNIPAm nanogels. These data show our ability to make core particles composed of p(NIPAm-co-acrylic acid), as well as pNIPAm core particles containing AFA as a fluorescent marker. For pNIPAm-co-AAc core particles, a 70 mM total monomer concentration was used for all reactions. The surfactant and initiator concentrations were gradually increased until the particle size approached the target 50-nm radius. As described above, MALLS coupled to the AFFF separation technique was used to characterize particle size and polydispersity. Examples of such data are shown in

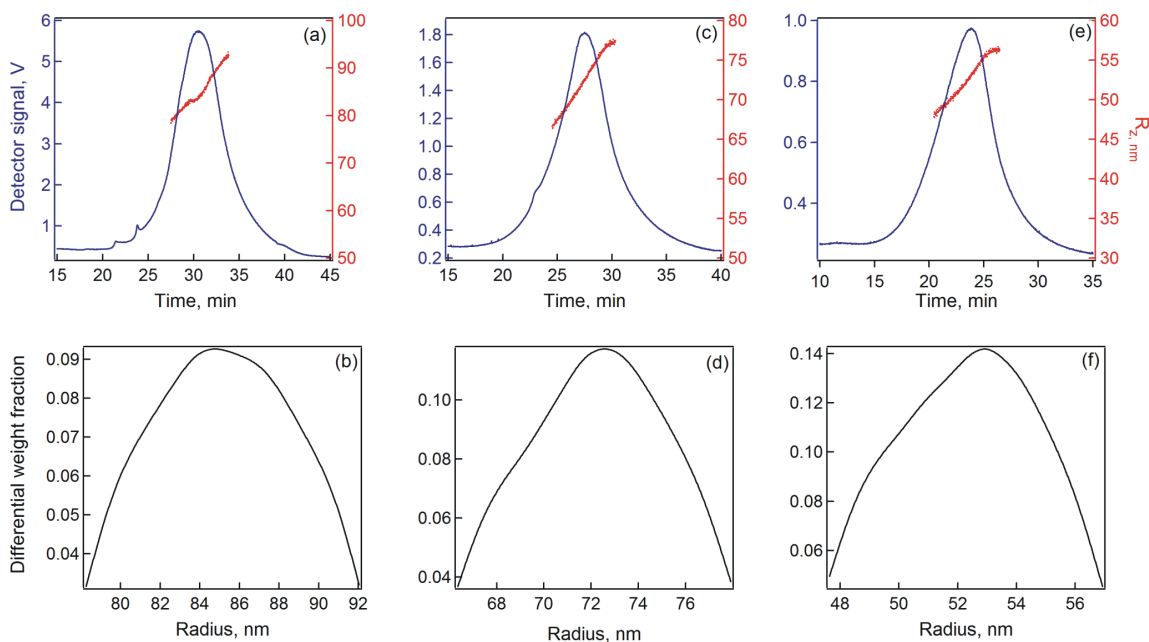


Figure 3.1. Overlay of radius data as sample elutes to detector and is shown as voltage (a,c,e) for pNIPAm-co-AAc core particles, and corresponding differential weight fraction plots, as determined by AFFF-MALLS (b,d,f). Synthetic parameters for (a,b) are shown in Table 3.1, row 1; (c,d) are shown in Table 3.1, row 2; (e,f) are shown in Table 3.1, row 3.

Figure 3.1, wherein highly monodisperse particle size distributions are evident from the differential weight fraction. Figure 3.1 also shows the overlay of the radius data with the raw detector signal, illustrating the high degree of monodispersity possible with these syntheses. The initial synthesis resulted in particles that were 86 nm in radius. This synthesis used 2 mM SDS and 2 mM APS. After increasing these concentrations to 3 mM each, the resulting particles were 73 nm in radius. Particles of appropriate size were synthesized when the SDS and APS concentrations were increased to 4 mM each. These particles had a radius of 53 nm. An interest in fluorescent tracking for future targeted chemotherapy studies led to our use of AFA as a co-monomer in the particle synthesis. Using the same synthesis conditions as described earlier, with the exception of 0.1 mM

AFA being used instead of 2 % AAc, the particles slightly increased in size to 57 nm in radius, still close to the desired particle size. This data is shown in Figure 3.2. A further attempt to decrease the core particle size was successful, (Figure 3.3) where the particle size was further reduced in size to 44 nm in radius for pNIPAm-co-AFA. The decrease in size was achieved by increasing [BIS] and decreasing the total monomer concentration. Increasing the [BIS] caused the particles to be more highly cross-linked, resulting in the tighter, smaller particles. The reduction of total monomer concentration results in smaller particles due to the decreased amount of monomer that can be added during the polymerization.

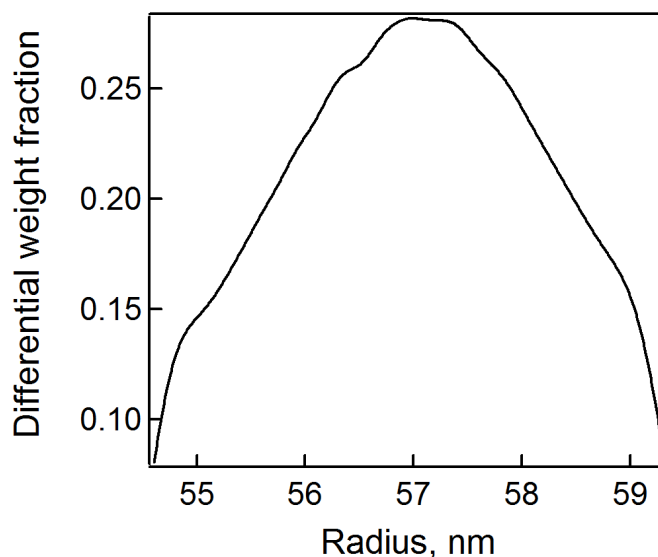


Figure 3.2. Differential weight fraction plot for pNIPAm-co-AFA core particles, as determined by AFFF-MALLS. Synthetic parameters are shown in Table 3.1, row 4.

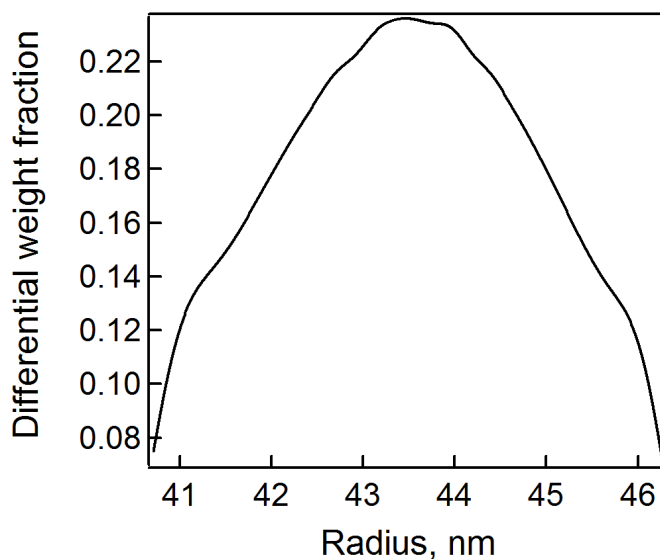


Figure 3.3. Differential weight fraction plots for pNIPAm-co-AFA core particles, as determined by AFFF-MALLS. Synthetic parameters are shown in Table 3.1, row 5.

Table 3.2 shows the synthetic progression for pNIPMAM nanogel syntheses. The introductory synthesis used the same conditions as that of the successful pNIPAM synthesis. However, using 70 mM total monomer concentration did not result in good particle formation. This was most likely due to the lower propagation rate constant for NIPMAM versus NIPAM, which would result in slower particle nucleation.^[29] The total monomer concentration was increased to 140 mM to achieve a successful synthesis. Since the synthesis required a higher monomer concentration, the surfactant and initiator concentrations had to be further increased to attain a particle size near 50 nm in radius. Figure 3.4 clearly shows that monodisperse particles can be made over a range of sizes using this straightforward synthetic approach. The progression of particle sizes is shown

with error bars that denote the full width of the differential weight fraction, indicating very monodisperse particles obtained from each synthesis. The pNIPMAm syntheses were also performed using AFA, for fluorescent tracking, instead of acrylic acid as a co-monomer. Figure 3.4 shows these particles also had a slight increase (51 nm radius) over the acrylic acid particles, but were still close to 50 nm in radius. A further attempt to decrease the core particle size was also successful with pNIPMAm-co-AFA (pNIPMAm-co-AFA #6, Figure 3.4). The particle size was decreased to 45 nm by increasing [BIS] and decreasing the total monomer concentration.

Table 3.2. Parameters for pNIPMAm core particle syntheses.

	Monomer	Cross-linker	Co-monomer	[Surfactant], mM	[Initiator], mM	[Total Monomer], mM	R_z , nm
1	pNIPMAm- 96%	BIS- 2%	AAc- 2%	4	4	70	N/A
2	pNIPMAm- 96%	BIS- 2%	AAc- 2%	4	4	140	137
3	pNIPMAm- 96%	BIS- 2%	AAc- 2%	6	6	140	60
4	pNIPMAm- 96%	BIS- 2%	AAc- 2%	8	8	140	48
5	pNIPMAm- 98%	BIS- 2%	AFA- 0.1 mM	8	8	140	51
6	pNIPMAm- 95%	BIS- 5%	AFA- 0.1 mM	8	8	100	45

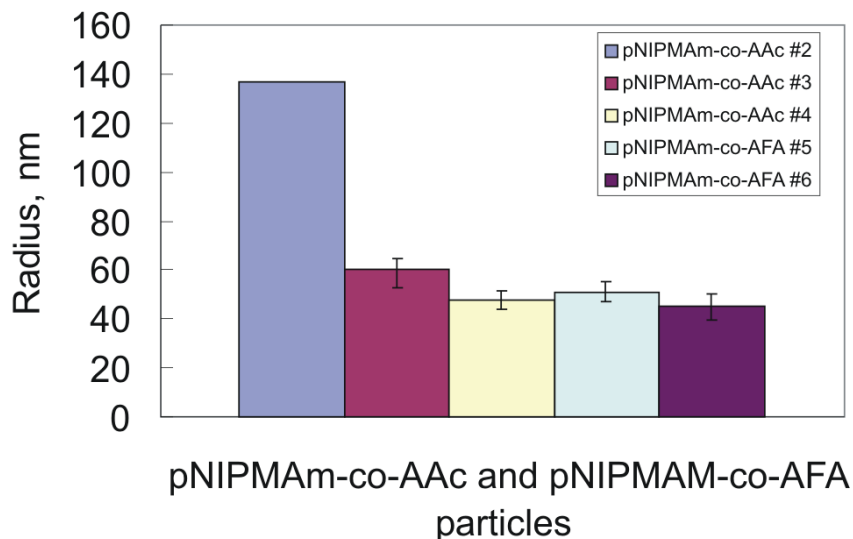


Figure 3.4. Particle sizes determined for the pNIPMAM core particle syntheses. Error bars do not indicate a standard deviation, but rather the total width of the differential weight fractions for each synthesis.

A thin, hydrogel shell was added to the 57 nm-radius pNIPAm-co-AFA core particles using a total monomer concentration of 20 mM in the feed solution. The shell consisted of pNIPAm, BIS, and APMA. The shell synthesis is a seeded precipitation polymerization reaction. The core particles are heated well above the LCST and the deswollen particles act as nuclei onto which growing polymer can be added. The thin shell compresses the core particle, and upon reswelling, the particle is actually smaller in size. Our group has previously shown shell compression, wherein the thin shell does not allow a complete reswelling of the core.^[24] Figure 3.5 shows that the shell compression creates a particle that is 52 nm in radius, versus the 57 nm radius core. The addition of

APMA incorporates primary amines in the shell to provide additional functionality to the particles.

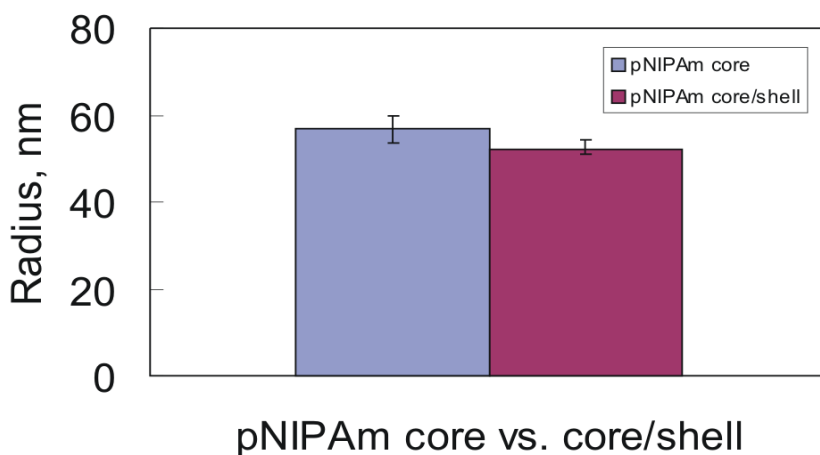


Figure 3.5. Change in size of pNIPAm core particles versus pNIPAm core/shell particles. Error bars indicate the total width of the differential weight fractions.

In order to add a shell to the 51 nm-radius pNIPMAm-co-AFA core, the shell's monomer concentration had to be increased from that of pNIPAm, to 50 mM. The shell consisted of pNIPMAm, BIS, and APMA. With the increase in monomer concentration, the particles did not see a dramatic compression as with the pNIPAm particles. Compression of the core most likely still occurs, but the increase in monomer concentration (and hence the increase in shell thickness) was enough to overtake the

amount of compression, and increase the total size of the particles. The pNIPMAm core/shell particles increased in size from 51 nm in radius for the core to 55 nm radius for the core/shell particles (Figure 3.6).

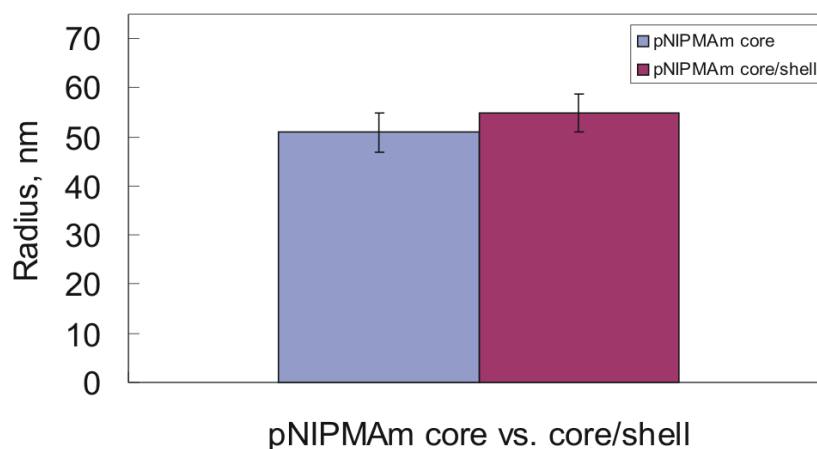


Figure 3.6. Change in size of pNIPMAm core particles versus pNIPMAm core/shell particles. Error bars indicate the total width of the differential weight fractions.

Figure 3.7 shows turbidity curves measured for both pNIPAm and pNIPMAm core/shell particles. The pNIPAm core/shell particles exhibited an LCST of ~ 31 °C, while the pNIPMAm core/shell particles exhibited an LCST of ~ 44 °C. Both of these values were as expected given the literature precedent referenced above. Future studies will compare targeting efficiencies of both sets of particles, as pNIPAm core/shell particles will be mainly deswollen at 37 °C, while pNIPMAm core/shell particles will be

mainly swollen at 37 °C. The deswollen pNIPAm particles are hydrophobic, which can lead to the particles being taken up by the RES. The swollen pNIPMAM particles are hydrophilic, which may lead to avoidance of the RES and longer circulation times in the body.

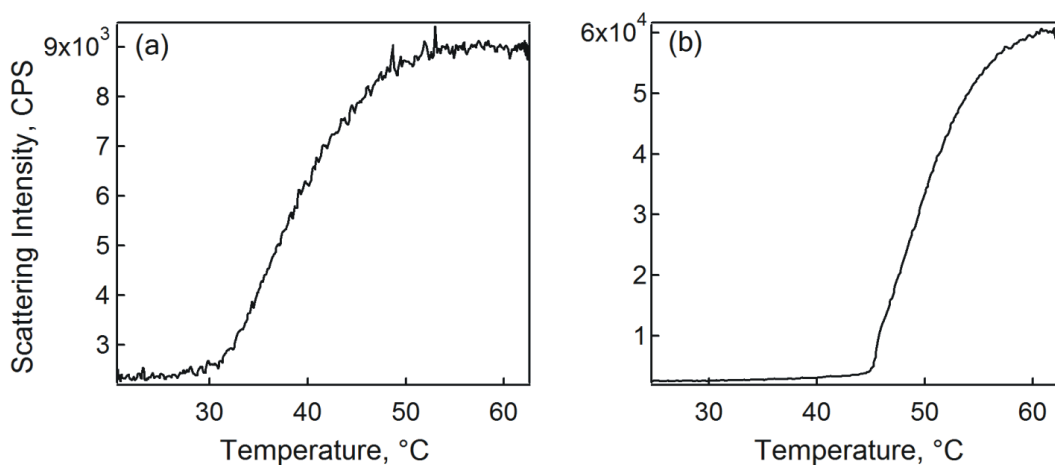


Figure 3.7. Temperature-dependent turbidity measurements for (a) pNIPAm core/shell particles and (b) pNIPMAM core/shell particles.

The core/shell particles are suitable for bioconjugation due to the amines incorporated in the shell. A variety of bioconjugation strategies can be used to create targeting moieties on the shell of the particles using pendant amines.^[29-32] In this case, we have used carbodiimide coupling to attach folic acid to the particles. Folic acid is biologically important, as it is needed by the body as vitamin B9. In addition, the folate

receptor is overexpressed in many tumor cells. This makes folic acid and its receptor a prime candidate for targeting studies. Figure 3.8 shows the incorporation of folic acid on the core/shell particles. Particles were conjugated with folic acid and cleaned several times by centrifugation to remove any free folic acid. Absorbance measurements for folic acid show a peak 285 nm. Unconjugated particles do not show this peak, while conjugated particles do show an absorbance peak at 285 nm, indicating folic acid has been conjugated to the particles. Future studies will use these bioconjugated core/shell particles for *in vitro* and *in vivo* targeting of cancer cells.

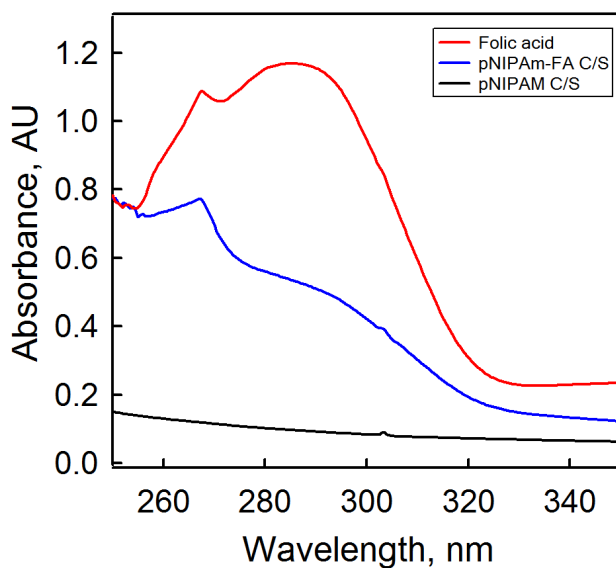


Figure 3.8. Absorbance of free folic acid (red), and pNIPAm core/shell particles before (black) and after (blue) folic acid conjugation.

3.4 Conclusions

In this chapter, it has been shown that small, bioconjugated nanogels can be produced using a very straightforward synthetic approach. Through our synthetic methods, we have shown control over particle size, with the ability to synthesize a wide range of diameters. The particles are highly monodisperse at all sizes and core/shell compositions. The ability to incorporate acrylic acid in the core allows greater functionality among the particles (i.e. for additional chemoligations), while the AFA-incorporated core allows fluorescent tracking. The incorporation of amines in the shell gives the particles multiple functionalities, allowing simple conjugation to acid groups present on a number of biologically important targeting moieties. We have illustrated this ability with the addition of folic acid to the particles in this contribution. The following chapters will describe the efficacy of these particles as drug carriers.

3.5 References

- [1] R. H. Pelton and P. Chibante, Preparation of aqueous latexes with N-isopropylacrylamide, *Colloids and Surfaces*, 1986, **20**, 247-256.
- [2] M. Heskins and J. E. Guillet, Solution properties of poly(N-isopropylacrylamide), *J. Macromol. Sci. Chem.*, 1968, **A2**, 1441-1455.
- [3] T. Tanaka, D. J. Fillmore, S.-T. Sun, I. Nishio, G. Swislow and A. Shah, Phase Transition in Ionic Gels, *Phys. Rev. Lett.*, 1980, **45**, 1636-1639.
- [4] S. Kim and K. E. Healy, Synthesis and Characterization of Injectable Poly(N-isopropylacrylamide-co-acrylic acid) Hydrogels with Proteolytically Degradable Cross-Links, *Biomacromolecules*, 2003, **4**, 1214-1223.
- [5] S. Nayak and L. A. Lyon, Soft nanotechnology with soft nanoparticles, *Angewandte Chemie, International Edition*, 2005, **44**, 7686-7708.
- [6] R. Pelton, Temperature-sensitive aqueous microgels, *Adv. Colloid. Interface Sci.*, 2000, **85**, 1-33.
- [7] B. R. Saunders and B. Vincent, Microgel particles as model colloids: theory, properties and applications, *Advances in Colloid and Interface Science*, 1999, **80**, 1-25.
- [8] M. J. Snowden and B. Vincent, The temperature-controlled flocculation of crosslinked latex particles, *Journal of the Chemical Society, Chemical Communications*, 1992, 1103-1105.
- [9] G. Zhou, A. Elaissari, T. Delair and C. Pichot, Synthesis and characterization of surface-cyano-functionalized poly(N-isopropylacrylamide) latexes, *Colloid and Polymer Science*, 1998, **276**, 1131-1139.
- [10] D. Gan and L. A. Lyon, Tunable Swelling Kinetics in Core-Shell Hydrogel Nanoparticles, *J. Am. Chem. Soc.*, 2001, **123**, 7511-7517.

- [11] C. D. Jones and L. A. Lyon, Synthesis and Characterization of Multiresponsive Core-Shell Microgels, *Macromolecules*, 2000, **33**, 8301-8306.
- [12] C. D. Jones and L. A. Lyon, Shell-Restricted Swelling and Core Compression in Poly(N-Isopropylacrylamide) Core-Shell Microgels, *Macromolecules*, 2003, **36**, 1988-1993.
- [13] I. Berndt, J. S. Pedersen, P. Lindner and W. Richtering, Structure of doubly temperature sensitive core-shell microgels based on poly-N-isopropylacrylamide and poly-N-isopropylmethacrylamide, *Progress in Colloid and Polymer Science*, 2006, **133**, 35-40.
- [14] I. Berndt, C. Popescu, F.-J. Wortmann and W. Richtering, Mechanics versus thermodynamics: swelling in multiple-temperature-sensitive core-shell microgels, *Angewandte Chemie, International Edition*, 2006, **45**, 1081-1085.
- [15] I. Berndt and W. Richtering, Doubly Temperature Sensitive Core-Shell Microgels, *Macromolecules*, 2003, **36**, 8780-8785.
- [16] D. Duracher, A. Elaissari and C. Pichot, Characterization of cross-linked poly(N-isopropylmethacrylamide) microgel latexes, *Colloid and Polymer Science*, 1999, **277**, 905-913.
- [17] D. Duracher, A. Elaissari and C. Pichot, Preparation of poly(N-isopropylmethacrylamide) latexes kinetic studies and characterization, *Journal of Polymer Science, Part A: Polymer Chemistry*, 1999, **37**, 1823-1837.
- [18] D. C. Drummond, O. Meyer, K. Hong, D. B. Kirpotin and D. Papahadjopoulos, Optimizing liposomes for delivery of chemotherapeutic agents to solid tumors, *Pharmacological Reviews*, 1999, **51**, 691-743.
- [19] S. K. Hobbs, W. L. Monsky, F. Yuan, W. G. Roberts, L. Griffith, V. P. Torchilin and R. K. Jain, Regulation of transport pathways in tumor vessels: role of tumor type and microenvironment, *Proceedings of the National Academy of Sciences of the United States of America*, 1998, **95**, 4607-4612.
- [20] F. Yuan, M. Dellian, D. Fukumura, M. Leunig, D. A. Berk, V. P. Torchilin and R. K. Jain, Vascular permeability in a human tumor xenograft: molecular size dependence and cutoff size, *Cancer Research*, 1995, **55**, 3752-3756.

- [21] Y. Matsumura and H. Maeda, A new concept for macromolecular therapeutics in cancer chemotherapy: mechanism of tumor-tropic accumulation of proteins and the antitumor agent smancs, *Cancer Research*, 1986, **46**, 6387-6392.
- [22] H. Maeda, The enhanced permeability and retention (EPR) effect in tumor vasculature: The key role of tumor-selective macromolecular drug targeting, *Advances in Enzyme Regulation*, 2001, **41**, 189-207.
- [23] H. Maeda, L. W. Seymour and Y. Miyamoto, Conjugates of anticancer agents and polymers: advantages of macromolecular therapeutics in vivo, *Bioconjugate Chemistry*, 1992, **3**, 351-362.
- [24] L. Brannon-Peppas and J. O. Blanchette, Nanoparticle and targeted systems for cancer therapy, *Advanced Drug Delivery Reviews*, 2004, **56**, 1649-1659.
- [25] G. Storm, S. O. Belliot, T. Daemen and D. D. Lasic, Surface modification of nanoparticles to oppose uptake by the mononuclear phagocyte system, *Advanced Drug Delivery Reviews*, 1995, **17**, 31-48.
- [26] G. Odian, Principles of Polymerization, 4th Edition, 2004.
- [27] M. J. Serpe, C. D. Jones and L. A. Lyon, Layer-by-layer deposition of thermoresponsive microgel thin films, *Langmuir*, 2003, **19**, 8759-8764.
- [28] D. Dube, M. Francis, J.-C. Leroux and F. M. Winnik, Preparation and Tumor Cell Uptake of Poly(N-isopropylacrylamide) Folate Conjugates, *Bioconjugate Chemistry*, 2002, **13**, 685-692.
- [29] S. Nayak, H. Lee, J. Chmielewski, L. A. Lyon, *J. Am. Chem. Soc.*, 2004, **126**, 10258-10259.
- [30] C. P. Leamon, S. R. Cooper and G. E. Hardee, Folate-liposome-mediated antisense oligodeoxynucleotide targeting to cancer cells: Evaluation in vitro and in vivo, *Bioconj. Chem.*, 2003, **14**, 738-747.
- [31] C. P. Leamon and P. S. Low, Delivery of Macromolecules into Living Cells - a Method That Exploits Folate Receptor Endocytosis, *Proc. Natl. Acad. Sci. U. S. A.*, 1991, **88**, 5572-5576.

- [32] C. P. Leamon and P. S. Low, Folate-mediated targeting: from diagnostics to drug and gene delivery, *Drug Discov. Today*, 2001, **6**, 44-51.

CHAPTER 4

TARGETED NANOGEL DELIVERY OF siRNA TO CANCER CELLS

4.1 Introduction

Many different types of delivery vehicles have been explored for *in vivo* applications. Among these are liposomes^[1-5], block co-polymer micelles^[6-10], and polymeric nanoparticles.^[11-21] For each of these, the same set of design rules tends to be followed. The aim of one of these rules is to have a long circulation time of the particles in the blood. To increase circulation time, the particles need to resist protein adsorption and opsonization, which leads to clearance by the reticuloendothelial system (RES).^[4, 22] Particle surface characteristics can be designed to avoid the RES longer by increasing the hydrophilicity of the particles.

Another important design feature of targeted delivery vehicles is size. Particles must be near 100 nm in diameter for efficient delivery through the vasculature for intravenous delivery applications.^[23-25] Particles that are this size are unable to penetrate healthy tissues, which have pore sizes of ~2 nm in the endothelia of blood vessels, and ~6-nm pores in postcapillary venules.^[26] This pore size exclusion is not seen in tumor vasculature though. Pore sizes range from 100 to 780 nm in the leaky vasculature of tumors.^[26-28] The leakiness leads to the enhanced permeability and retention effect (EPR), allowing the deposition of particles in this size range at the site of the tumor.^[29-31]

Another important consideration for particle size is to avoid lymphatic drainage. Particles that are too small (tens of nm) tend to be rapidly cleared by this pathway.^[23-25] Particles in the range of 50-100 nm can efficiently avoid lymphatic drainage.^[23-25]

In an attempt to follow these design rules, researchers have utilized several structures as delivery vehicles. Many researchers have used liposomes to deliver materials^[1-5], but instability can make liposomes a less than ideal carrier system. Block-co-polymer micelles have been investigated^[6-10], but toxicity issues hold this approach back. Difficult synthetic approaches make dendrimer carriers unsuitable for scalable manufacture of drug delivery devices.^[23, 32, 33]

For the applications in this chapter, nanogels will be investigated as delivery vehicles. As described in previous chapters, nanogels have unique features that lend the particles to many uses. Chapter 3 detailed nanogels composed of poly(N-isopropylmethacrylamide) (pNIPMAm) have a lower critical solution temperature (LCST) ~44 °C. Below this temperature, the particles are hydrophilic and swollen. Above this temperature, the water is expelled, due to an entropically-driven polymer phase separation.^[34-37] These particles are mainly swollen at body temperature (37 °C). The use of pNIPMAm nanogels at 37 °C would make the particles very hydrophilic, which could be advantageous in permitting longer circulation times in the body, as described earlier.

Another important design rule for delivery devices is to have a targeting moiety so particles can effectively reach their destination. For this investigation, we will utilize cell receptors for targeting. The Eph family of receptors and their ephrin ligands play important roles in neural development, vascular development, and are critical in pathological forms of angiogenesis.^[38] The erythropoietin-producing hepatocellular

(EphA2) receptor is expressed in the vasculature of human tumors. EphA2 is also up-regulated in the cells of a number of tumors, including ovarian, prostate, breast, skin, colon, and esophageal cancers. The ability to mimic an ephrin ligand would allow targeting of cancer cells through delivery vehicles. The Pasquale group has found a peptide mimic that binds EphA2 and stimulates its receptor tyrosine kinase activity.^[38] This peptide mimic is twelve amino acids long, and has a sequence of YSAYPDSVPMMS. We have added a C-terminal cysteine for aiding in conjugation to core/shell nanogel particles (YSAYPDSVPMMSC) (the “YSA” peptide).

The up-regulation of EphA2, combined with the EPR effect, could lead to targeting by anti-cancer drug containing vehicles. Nanogels designed around 100 nm in diameter could therefore be used as efficient delivery vehicles. Bioconjugation of the YSA peptide to the nanogels could then make these targeted delivery vehicles. In this work, we will describe the use of nanogels encapsulated with siGLO Red Transfection Indicator (siGLO), a non-targeted siRNA linked with the fluorophore DY-547, and their targeted delivery to cancer cells.

4.2 Experimental Section

4.2.1 Materials

All materials were purchased from Sigma-Aldrich unless otherwise noted.

4.2.2 Nanogel core synthesis

Nanogel core particles were synthesized by free-radical precipitation polymerization, as previously reported.^[39, 40] The molar composition was 98% *N*-isopropylmethacrylamide (NIPMAm), 2% *N,N'*-methylenebis(acrylamide) (BIS), and 0.1mM acrylamidofluorescein (synthesized previously).^[41] A total monomer concentration of 140 mM was used. Polymerizations were carried out in a three-neck round-bottom flask. A total of 8 mM sodium dodecylsulfate (SDS) was used to stabilize the reaction, while 8 mM ammonium persulfate (APS) was used to initiate the reaction. For the synthesis, 100 mL of a filtered, aqueous solution of NIPMAm, BIS, and SDS was added to the flask and heated to 70 °C. The solution was purged with N₂ gas and stirred vigorously until the temperature remained stable. The AFA was added and after 10 minutes, the reaction was initiated by the addition of a 1-mL solution of 8 mM APS. The solution turned turbid, indicating successful initiation. The reaction was allowed to continue for 4 h under N₂ gas. After the synthesis, the solution was filtered through a Whatman filter paper.

4.2.3 Nanogel shell synthesis

Core particles were used as seeds for the addition of a shell hydrogel. The detailed procedure of the shell synthesis has been reported previously.^[39, 40] Briefly, 10 mL of core nanogel solution, 2 mM SDS, and 35 mL of deionized H₂O were added to a three-neck round-bottom flask and heated under N₂ gas to 70 °C. Separately, a 50 mM mixture with the molar ratios of 97.5% NIPMAm, 2% BIS, and 0.5% APMA (Polysciences) were dissolved in 5 mL of deionized H₂O. The solution was added to the three-neck round-

bottom flask, and the temperature was allowed to stabilize at 70 °C. The reaction was initiated by a 1 mL solution of 0.5 mM APS. The reaction proceeded for 4 h under N₂ gas. Following the synthesis, the solution was filtered through a Whatman filter paper. The particles were purified by centrifugation.

4.2.4 YSA synthesis

The YSA peptide (YSAYPDSVPMMSK) was synthesized using standard Fmoc chemistry as described previously^[42]. Peptide synthesis was carried out by K.D. Clark, University of Georgia. Following synthesis, the resin-peptide was cleaved and deprotected for 4 h in reagent K after air-drying. The peptide was purified using a series of 5 mL injections onto a preparatory HPLC column (10-μm; particle size, 21.2 mm 25 cm, Jupiter C18; Phenomenex Inc.) using HPLC-grade H₂O and a linear gradient of acetonitrile (0–70 min, 10–80%) at 5 mL per min. Both the acetonitrile and H₂O contained 0.05% trifluoroacetic acid. The desired peak was identified by matrix-assisted laser desorption ionization time-of-flight mass spectrometry, and the peaks from multiple runs were pooled, lyophilized, and stored at 4 °C in solid form. On other occasions, the YSA peptide was also purchased from GenScript Corp.

4.2.5 Peptide conjugation

The YSA peptide or scrambled YSA peptide (GenScript) was conjugated to the nanogels via maleimide coupling to the cysteine residue on the C-terminal end of the peptide. A solution of EDC (Pierce) and NHS were added to ε-maleimidocaproic acid in

pH 6.0 MES buffer to activate the acid groups for 30 min at room temperature. This solution was then added to particles and reacted for 2 h on a shaker table. The particles were centrifuged to remove any unreacted material, and then the peptide was added to the particles and reacted overnight. Particles were then cleaned by centrifugation as described above.

4.2.6 siGLO encapsulation

A solution of siGLO (Dharmacon) was prepared in phosphate buffered saline (PBS). Lyophilized particles were dissolved in this solution at a concentration of 4 mg to 250 μ L of 20 mM siGLO and allowed to shake overnight. After shaking, the particles were then centrifuged to remove any free siGLO, and then followed by resuspension in PBS.

4.2.7 Particle characterization

4.2.7.1 Static light scattering

Multi-angle laser light scattering (MALLS; Wyatt Technology Corporation) detection following asymmetric field flow fractionation (AFFF) was performed as described in Chapter 3.2.3.1.

4.2.7.2 Absorbance measurements

A standard curve for increasing concentrations of siRNA was made by measuring the absorbance at 260 nm using a Shimadzu UV 1601 spectrophotometer. After siRNA

was encapsulated in the particles and the particles were then centrifuged, the absorbance of the supernatant was then measured to determine the amount taken up by the particles.

4.2.7.3 Fluorimetry

Particle LCST values were measured using a steady-state fluorescence spectrophotometer (Photon Technology International), equipped with a Model 814 PMT photon-counting detector as described in Chapter 3.2.3.2.

4.2.8 Cell culture

Hey cells were provided by Gordon W. Mills, Department of Molecular Therapeutics, the University of Texas, M. D. Anderson Cancer Center. Hey cells were cultured in RPMI 1640 (Mediatech) supplemented with 10% v/v heat-inactivated fetal calf serum (Invitrogen), 2 mM L-glutamine (Mediatech), 10 mM HEPES buffer (Mediatech), penicillin (100 U/ml), and streptomycin (100 µg/ml). Human umbilical vein endothelial cells (HUVEC) were purchased from Lonza. HUVECs were grown as adherent cultures in EGM-2 medium (Lonza) supplemented with penicillin (100 U/ml) and streptomycin (100 µg/ml) (Sigma). All cells were grown under standard conditions (37 °C, 5% CO₂ humidified atmosphere) and were serially passaged following detachment with 0.25% trypsin plus EDTA. Passages two through eight were used to insure experimental continuity for HUVECs.

4.2.9 Particle/transfection experiments

4.2.9.1 siGLO-encapsulated particle transfection

Hey cells were plated onto an 8-well chamber slide (5×10^3 cells/well) and allowed to adhere overnight at 37 °C and 5% CO₂. After washing the wells with PBS and replacing the media, siGLO-loaded/YSA-conjugated nanogels, unloaded YSA-conjugated nanogels, pNIPMAm nanogels and siGLO only were added to wells. Cells were incubated with nanogels for 4 h. Cells were then washed with PBS, and media replaced. The cells were then fixed by adding paraformaldehyde for 30 min. The wells were then aspirated and the chamber removed. A cover slip was placed on the slide for microscopic imaging.

4.2.9.2 Ephrin competition assay

Hey cells were plated onto an 8-well chamber slide (5×10^3 cells/well) and allowed to adhere overnight at 37 °C and 5% CO₂. After washing the wells with PBS and replacing the media, Ephrin was added to 4 of the wells, at a 1:10 ephrin volume to media volume dilution. To the ephrin containing wells, siGLO-loaded/YSA-conjugated nanogels were added to 2 wells, and unloaded pNIPMAm nanogels were added to 2 wells. Two other wells were incubated with siGLO-loaded/YSA-conjugated nanogels, and the final 2 wells were untreated cells. Cells were incubated with nanogels for 4 h. Cells were then washed with PBS, and media replaced. The cells were then fixed by adding paraformaldehyde for 30 min. The wells were then aspirated and the chamber removed. A cover slip was placed on the slide for microscopic imaging.

4.2.9.3 Scrambled peptide targeting

Hey cells were plated onto an 8-well chamber slide (5×10^3 cells/well) and allowed to adhere overnight at 37 °C and 5% CO₂. After washing the wells with PBS and replacing the media, scrambled YSA-conjugated nanogels, unloaded YSA-conjugated nanogels, and pNIPMAm nanogels were added to wells; 4 wells were untreated. Cells were incubated with nanogels for 4 h. Cells were then washed with PBS, and media replaced. The cells were then fixed by adding paraformaldehyde for 30 min. The wells were then aspirated and the chamber removed. A cover slip was placed on the slide for microscopic imaging.

4.2.10 Confocal Microscopy

A Zeiss LSM510 confocal microscope was used to take cell images. Cells were incubated with or without particles encapsulated with siGLO for 4 h. After 4 h, the cells were washed and then fixed on the slide. An Ar⁺ laser was used to excite the AFA in particles in the cells. A HeNe laser was used to excite the siGLO that was delivered to the cells by the particles. LSM510 software was used to view the images.

4.3 Results and Discussion

Small, monodispersed nanogels (~ 50-nm radius) were synthesized by free-radical precipitation polymerization. These nanogels were designed with a core/shell architecture, using N-isopropylmethacrylamide as the main monomer. The core contains 4-acrylamidofluorescein (AFA) for visualization during cell studies. The shell contains N-

(3-aminopropyl) methacrylamide to provide chemical handles at the surface of the nanogels for bioconjugation. The use of pNIPMAm nanogels provides swollen particles at body temperature (37 °C), as these particles have a LCST of around 44 °C.

Lyophilized nanogels were dissolved in a concentrated solution of siGLO, and shaken overnight. The volume of solution is just enough to completely dissolve the nanogels, forcing the siGLO into the gels in a technique known as “breathing-in.” After overnight shaking, the nanogels are centrifuged and the supernatant aspirated to remove any non-encapsulated siGLO. The absorbance of the supernatant was measured to detect the amount of siGLO that was not encapsulated in the nanogels, and ~ 80-95% (by mass) of the siGLO in solution is retained in the particles. The absorbance measurements were compared to a standard curve of siGLO in solution.

The siGLO-loaded nanogels were then incubated with Hey and BG-1 cells. Hey and BG-1 cells were incubated overnight in an 8-well chamber slide. Cells were incubated with siGLO-loaded/YSA-conjugated nanogels, unloaded YSA-conjugated nanogels, non-targeted pNIPMAm nanogels, or siGLO only for 4 h. The cells were then washed and the slides fixed for confocal microscopy imaging. Figure 4.1 shows cells targeted with YSA-conjugated nanogels show significant particle uptake (D-F), and cells incubated with siGLO-loaded/YSA-conjugated nanogels show significant uptake of particles and siGLO (A-C).

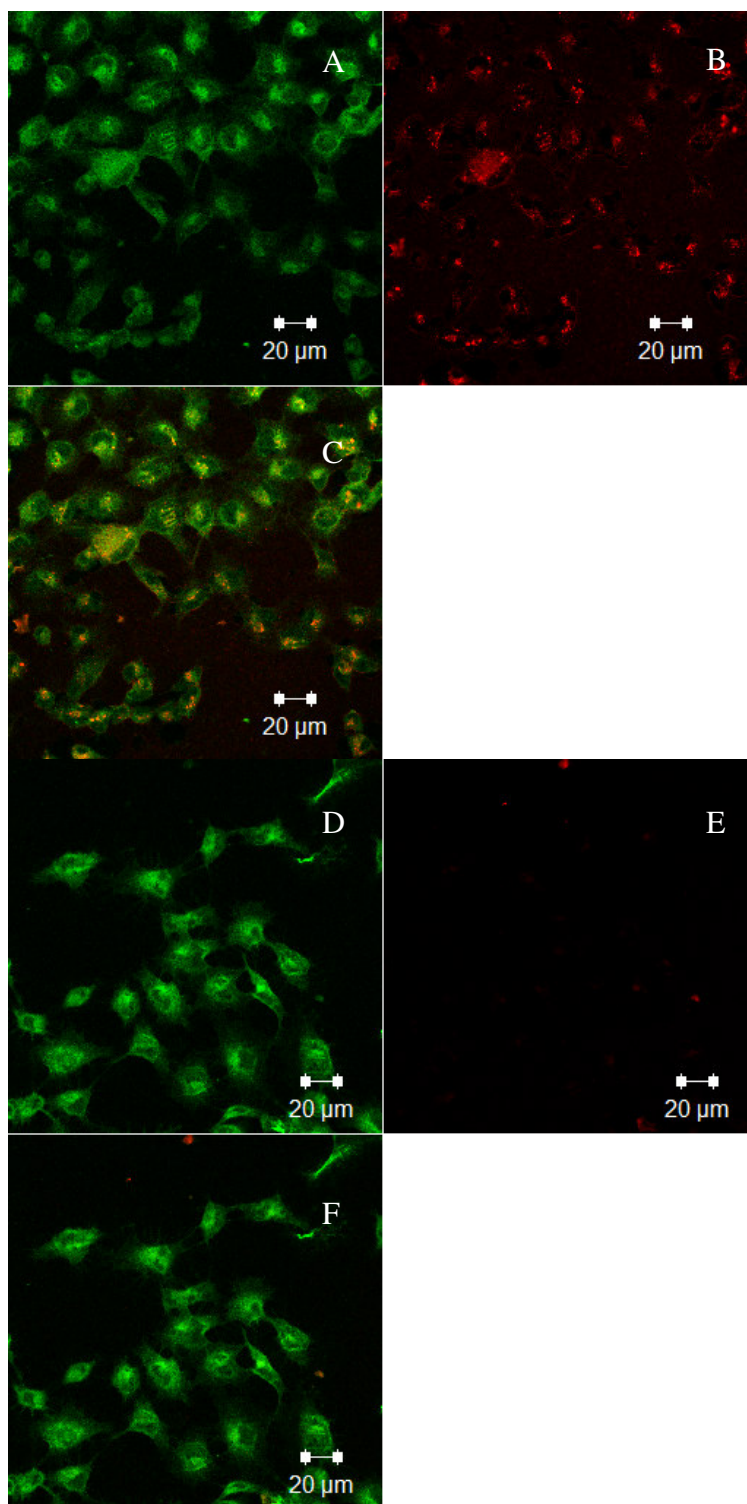


Figure 4.1. Confocal microscopy images of Hey cells following exposure to siGLO-loaded/YSA-conjugated nanogels. (A) shows the green (AFA) channel and (B) shows the red (siGLO) channel. (C) is an overlay of these channels. (D) shows the green channel and (E) shows red channel following exposure of Hey cells to unloaded YSA-conjugated nanogels. (F) is an overlay of these images.

Nanogel and siGLO uptake was higher in Hey cells versus BG-1 cells as Hey cells have 10-fold higher EphA2 receptor over BG-1 cells. The same procedure was used as with Hey cells. Figure 4.2 shows siGLO-loaded/YSA-conjugated nanogels are taken up by BG-1 cells, as well, despite the lower degree of receptor expression.

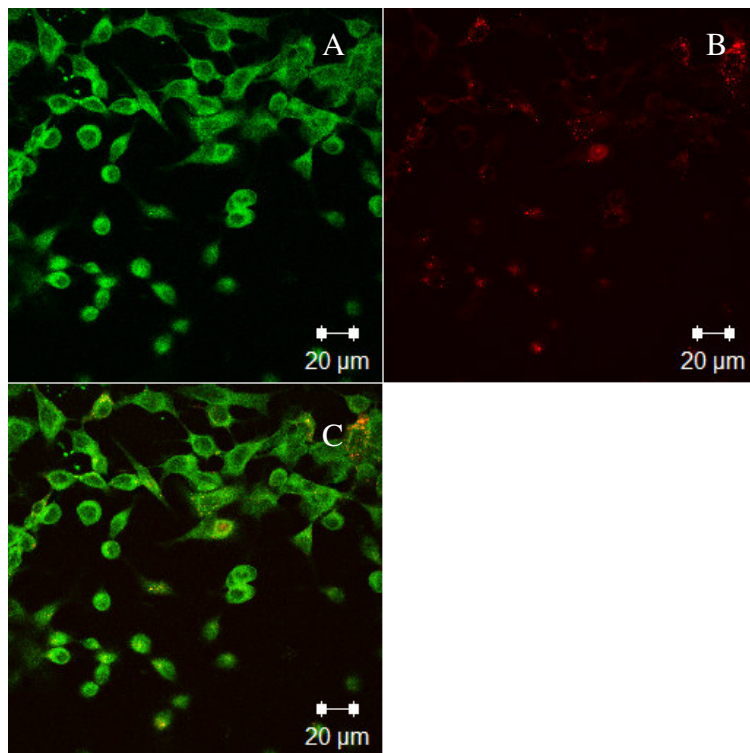


Figure 4.2. Confocal microscopy images of BG-1 cells following exposure to siGLO-loaded/YSA-conjugated nanogels. (A) shows the green (AFA) channel and (B) shows the red (siGLO) channel. (C) is an overlay of these channels.

For both Hey and BG-1 cells, non-targeted nanogels show very little cell uptake. Figure 4.3 is a representative image showing the lack of nanogel uptake. This figure

shows unloaded pNIPMAm nanogels targeted to Hey cells. It appears that there is some non-specific uptake of the nanogels, but this amount is insignificant as compared to YSA-conjugated nanogels. Similar results are seen with BG-1 cells targeted by unloaded pNIPMAm nanogels (image not shown). To ensure that siGLO could not enter the cells without a carrier, Hey and BG-1 cells were also incubated with the siGLO only. For both cells, the images show no uptake on either green or red channels (images not shown).

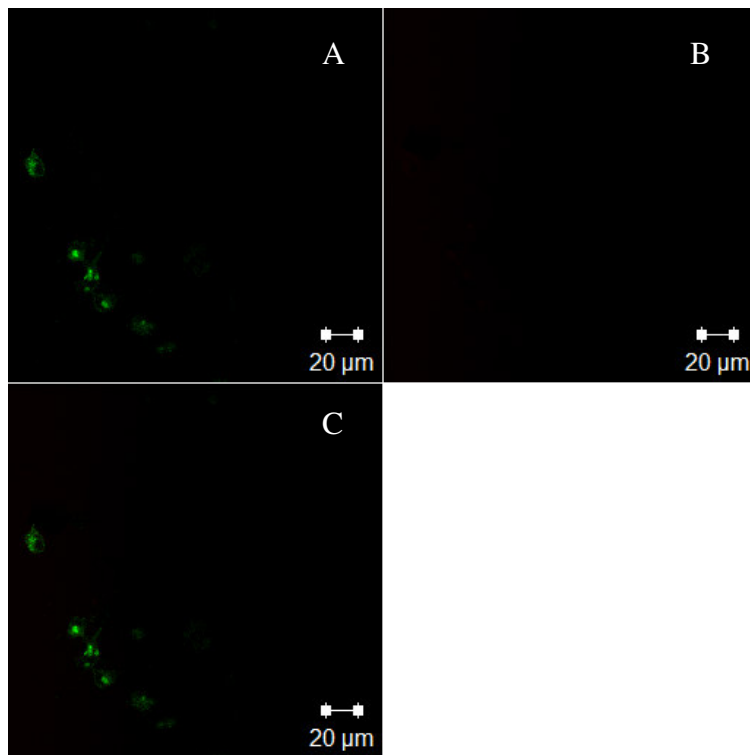


Figure 4.3. Confocal microscopy images of Hey cells following exposure to non-targeting pNIPMAm nanogels. (A) shows the green (AFA) channel and (B) shows the red (siGLO) channel. (C) is an overlay of these channels.

While these results suggest that targeting of EphA2 receptor is the mode of entry for the nanogels, it was necessary to further explore cell uptake. To do this, Hey cells were pre-incubated with the natural ligand for EphA2, ephrin, before nanogel delivery. If cell uptake of nanogels is receptor-mediated, the uptake after cell exposure to ephrin should be greatly reduced, as the EphA2 receptor will be internalized and less available for nanogel uptake. Hey cells were incubated overnight in an 8-well chamber slide. To 2 wells, 2 μg of ephrin was added, and the cells were incubated for 1 h. After ephrin incubation, siGLO-loaded/YSA-conjugated nanogels were added to the ephrin and non-ephrin incubated wells. The cells were incubated for 4 h and then washed and the slide fixed for confocal microscopy imaging. Figure 4.4 A-C shows the cells incubated with ephrin. These wells do show some uptake of nanogels and siGLO after ephrin was added, but wells D-F show much brighter fluorescence for siGLO loaded nanogels added without ephrin, indicating higher uptake by the cells. These results suggest that nanogel uptake is mediated by the EphA2 receptor.

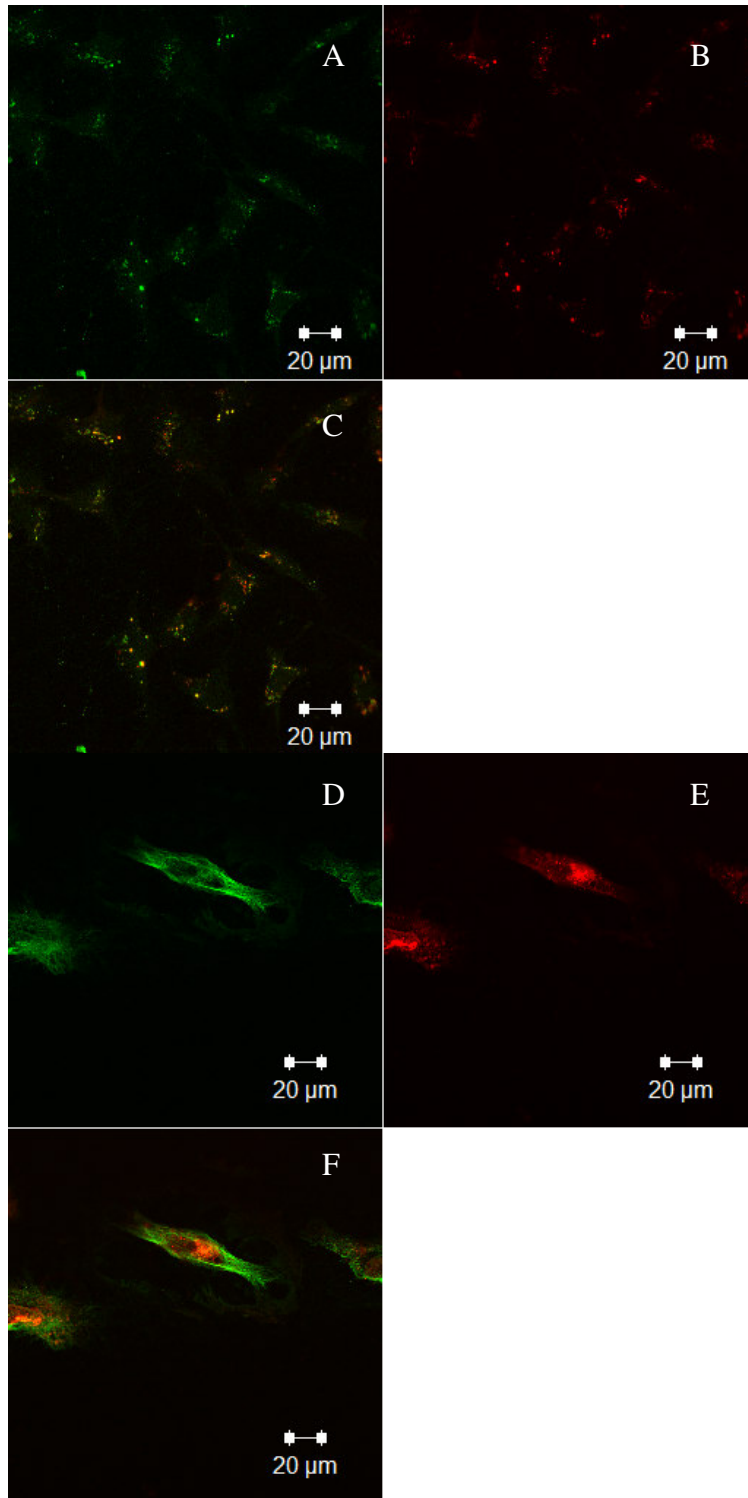


Figure 4.4. Confocal microscopy images of Hey cells following exposure to siGLO-loaded/YSA-conjugated nanogels after 1 h ephrin incubation. (A) shows the green (AFA) channel and (B) shows the red (siGLO) channel. (C) is an overlay of these channels. (D) shows the green channel and (E) shows red channel following exposure of Hey cells to siGLO-loaded/YSA-conjugated nanogels (no ephrin). (F) is an overlay of these images.

4.4 Conclusions

The results shown in this chapter describe the efficient uptake of siGLO and delivery to cells by nanogels. Nanogels conjugated with YSA preferentially target the EphA2 receptor present on Hey and BG-1 cells, while the cells do not take up unconjugated nanogels as readily. The ability to encapsulate high concentrations of siGLO allows its delivery to the cells via the nanogels. The results also suggest that the uptake of targeted nanogels is receptor mediated, as the delivery of the natural ligand to EphA2 reduces uptake of the particles. The use of nanogels therefore has potential to be drug or gene delivery agents, and this will be further investigated in the following chapters.

4.5 References

- [1] D. A. Eavarone, X. Yu and R. V. Bellamkonda, Targeted drug delivery to C6 glioma by transferrin-coupled liposomes, *J. Biomed. Mater.*, 2000, **51**, 10-14.
- [2] R. J. Lee and P. S. Low, Delivery of liposomes into cultured KB cells via folate receptor-mediated endocytosis, *J. Biol. Chem.*, 1994, **269**, 3198-3204.
- [3] F. J. Martin, Stealth liposomes: a pharmaceutical perspective, *Microspheres, Microcapsules & Liposomes*, 1999, **2**, 435-461.
- [4] G. Storm, S. O. Belliot, T. Daemen and D. D. Lasic, Surface modification of nanoparticles to oppose uptake by the mononuclear phagocyte system, *Advanced Drug Delivery Reviews*, 1995, **17**, 31-48.
- [5] D. Uyar, B. Kulp, G. Peterson, K. Zanotti, M. Markman and J. Belinson, Cardiac safety profile of prolonged (≥ 6 cycles) pegylated liposomal doxorubicin administration in patients with gynecologic malignancies, *Gynecol. Oncol.*, 2004, **94**, 147-151.
- [6] O. Carion, B. Mahler, T. Pons and B. Dubertret, Synthesis, encapsulation, purification and coupling of single quantum dots in phospholipid micelles for their use in cellular and in vivo imaging, *Nat. Protoc.*, 2007, **2**, 2383-2390.
- [7] M. H. Dufresne, D. Le Garrec, V. Sant, J. C. Leroux and M. Ranger, Preparation and characterization of water-soluble pH-sensitive nanocarriers for drug delivery, *Int. J. Pharm.*, 2004, **277**, 81-90.
- [8] R. Rossin, D. Pan, K. Qi, L. Turner Jeffrey, X. Sun, L. Wooley Karen and J. Welch Michael, ^{64}Cu -labeled folate-conjugated shell cross-linked nanoparticles for tumor imaging and radiotherapy: synthesis, radiolabeling, and biologic evaluation, *J Nucl Med*, 2005, **46**, 1210-1218.
- [9] K. B. Thurmond, II, H. Huang, C. G. Clark, Jr., T. Kowalewski and K. L. Wooley, Shell crosslinked polymer micelles: stabilized assemblies with great versatility and potential, *Colloids Surf., B*, 1999, **16**, 45-54.

- [10] F. van Nostrum Cornelus, Polymeric micelles to deliver photosensitizers for photodynamic therapy, *Adv Drug Deliv Rev*, 2004, **56**, 9-16.
- [11] J. Cheng, A. Teply Benjamin, I. Sherifi, J. Sung, G. Luther, X. Gu Frank, E. Levy-Nissenbaum, F. Radovic-Moreno Aleksandar, R. Langer and C. Farokhzad Omid, Formulation of functionalized PLGA-PEG nanoparticles for in vivo targeted drug delivery, *Biomaterials*, 2007, **28**, 869-876.
- [12] W. Cho Yong, A. Park Soo, H. Han Tae, H. Son Dai, S. Park Ji, J. Oh Seung, H. Moon Dae, K.-J. Cho, C.-H. Ahn, Y. Byun, I.-S. Kim, C. Kwon Ick and Y. Kim Sang, In vivo tumor targeting and radionuclide imaging with self-assembled nanoparticles: mechanisms, key factors, and their implications, *Biomaterials*, 2007, **28**, 1236-1247.
- [13] M. Das, S. Mardyani, W. C. W. Chan and E. Kumacheva, Biofunctionalized pH-responsive microgels for cancer cell targeting: Rational design, *Adv. Mater.*, 2006, **18**, 80-83.
- [14] K.-i. Fukukawa, R. Rossin, A. Hagooley, E. D. Pressly, J. N. Hunt, B. W. Messmore, K. L. Wooley, M. J. Welch and C. J. Hawker, Synthesis and Characterization of Core-Shell Star Copolymers for In Vivo PET Imaging Applications, *Biomacromolecules*, 2008, **9**, 1329-1339.
- [15] D. E. Owens and N. A. Peppas, Opsonization, biodistribution, and pharmacokinetics of polymeric nanoparticles, *Int. J. Pharm.*, 2006, **307**, 93-102.
- [16] E. D. Pressly, R. Rossin, A. Hagooley, K.-I. Fukukawa, B. W. Messmore, M. J. Welch, K. L. Wooley, M. S. Lamm, R. A. Hule, D. J. Pochan and C. J. Hawker, Structural Effects on the Biodistribution and Positron Emission Tomography (PET) Imaging of Well-Defined ⁶⁴Cu-Labeled Nanoparticles Comprised of Amphiphilic Block Graft Copolymers, *Biomacromolecules*, 2007, **8**, 3126-3134.
- [17] V. G. Sergeev, O. A. Novoskoltseva, O. A. Pyshkina, A. A. Zinchenko, V. B. Rogacheva, A. B. Zezin, K. Yoshikawa and V. A. Kabanov, Secondary Structure of DNA Is Recognized by Slightly Cross-Linked Cationic Hydrogel, *J. Am. Chem. Soc.*, 2002, **124**, 11324-11333.
- [18] V. P. Torchilin, PEG-based micelles as carriers of contrast agents for different imaging modalities, *Adv. Drug Delivery Rev.*, 2002, **54**, 235-252.

- [19] S. Vinogradov, E. Batrakova and A. Kabanov, Poly(ethylene glycol)-polyethylenimine NanoGel particles: novel drug delivery systems for antisense oligonucleotides, *Colloids Surf., B*, 1999, **16**, 291-304.
- [20] S. V. Vinogradov, Colloidal microgels in drug delivery applications, *Curr. Pharm. Des.*, 2006, **12**, 4703-4712.
- [21] J. Zhang and R. D. K. Misra, Magnetic drug-targeting carrier encapsulated with thermosensitive smart polymer: core-shell nanoparticle carrier and drug release response, *Acta Biomater*, 2007, **3**, 838-850.
- [22] L. Brannon-Peppas and J. O. Blanchette, Nanoparticle and targeted systems for cancer therapy, *Advanced Drug Delivery Reviews*, 2004, **56**, 1649-1659.
- [23] A. K. Boal and V. M. Rotello, Fabrication and Self-Optimization of Multivalent Receptors on Nanoparticle Scaffolds, *J. Am. Chem. Soc.*, 2000, **122**, 734-735.
- [24] R. Minchin, Sizing up targets with nanoparticles, *Nature Nanotechnology*, 2008, **3**, 12-13.
- [25] A. Rehor, H. Schmoekel, N. Tirelli and J. A. Hubbell, Functionalization of polysulfide nanoparticles and their performance as circulating carriers, *Biomaterials*, 2008, **29**, 1958-1966.
- [26] D. C. Drummond, O. Meyer, K. Hong, D. B. Kirpotin and D. Papahadjopoulos, Optimizing liposomes for delivery of chemotherapeutic agents to solid tumors, *Pharmacological Reviews*, 1999, **51**, 691-743.
- [27] S. K. Hobbs, W. L. Monsky, F. Yuan, W. G. Roberts, L. Griffith, V. P. Torchilin and R. K. Jain, Regulation of transport pathways in tumor vessels: role of tumor type and microenvironment, *Proceedings of the National Academy of Sciences of the United States of America*, 1998, **95**, 4607-4612.
- [28] F. Yuan, M. Dellian, D. Fukumura, M. Leunig, D. A. Berk, V. P. Torchilin and R. K. Jain, Vascular permeability in a human tumor xenograft: molecular size dependence and cutoff size, *Cancer Research*, 1995, **55**, 3752-3756.

- [29] H. Maeda, The enhanced permeability and retention (EPR) effect in tumor vasculature: The key role of tumor-selective macromolecular drug targeting, *Advances in Enzyme Regulation*, 2001, **41**, 189-207.
- [30] H. Maeda, L. W. Seymour and Y. Miyamoto, Conjugates of anticancer agents and polymers: advantages of macromolecular therapeutics in vivo, *Bioconjugate Chemistry*, 1992, **3**, 351-362.
- [31] Y. Matsumura and H. Maeda, A new concept for macromolecular therapeutics in cancer chemotherapy: mechanism of tumor-tropic accumulation of proteins and the antitumor agent smancs, *Cancer Research*, 1986, **46**, 6387-6392.
- [32] A. Mecke, I. Lee, J. R. Baker, M. M. B. Holl and B. G. Orr, Deformability of poly(amidoamine) dendrimers, *European Physical Journal E*, 2004, **14**, 7-16.
- [33] J. A. Ryan, K. W. Overton, M. E. Speight, C. M. Oldenburg, L. Loo, W. Robarge, S. Franzen and D. L. Feldheim, Cellular uptake of gold nanoparticles passivated with BSA-SV40 large T antigen conjugates, *Analytical Chemistry*, 2007, **79**, 9150-9159.
- [34] M. Heskins and J. E. Guillet, Solution properties of poly(N-isopropylacrylamide), *J. Macromol. Sci. Chem.*, 1968, **A2**, 1441-1455.
- [35] R. H. Pelton and P. Chibante, Preparation of aqueous latexes with N-isopropylacrylamide, *Colloids and Surfaces*, 1986, **20**, 247-256.
- [36] H. G. Schild, Poly(N-isopropylacrylamide): experiment, theory and application, *Progress in Polymer Science*, 1992, **17**, 163-249.
- [37] T. Tanaka, Kinetics of phase transition in polymer gels, *Physica A*, 1986, **140A**, 261-268.
- [38] M. Koolpe, M. Dail and E. B. Pasquale, An Ephrin Mimetic Peptide That Selectively Targets the EphA2 Receptor, *J. Biol. Chem.*, 2002, **277**, 46974-46979.
- [39] D. Gan and L. A. Lyon, Tunable Swelling Kinetics in Core-Shell Hydrogel Nanoparticles, *J. Am. Chem. Soc.*, 2001, **123**, 7511-7517.

- [40] C. D. Jones and L. A. Lyon, Synthesis and Characterization of Multiresponsive Core-Shell Microgels, *Macromolecules*, 2000, **33**, 8301-8306.
- [41] M. J. Serpe, C. D. Jones and L. A. Lyon, Layer-by-layer deposition of thermoresponsive microgel thin films, *Langmuir*, 2003, **19**, 8759-8764.
- [42] K. D. Clark, B. F. Volkman, H. Thoetkiattikul, D. King, Y. Hayakawa and M. R. Strand, Alanine-scanning mutagenesis of plasmatocyte spreading peptide identifies critical residues for biological activity, *J Biol Chem*, 2001, **276**, 18491-18496.

CHAPTER 5

CHEMOTHERAPEUTIC POTENTIAL OF PROTEIN KNOCKDOWN BY NANOGEL DELIVERY OF siRNA

5.1 Introduction

Genetic engineering is a field that has gained much interest in recent years as a way to treat disease. The goal of genetic engineering is to successfully transfer genetic information to targeted tissues, with the clinical goal of recovering a healthy tissue, or destroying an irreparably damaged one (e.g. as in cancer). This is not a simple proposition though, as naked genes are degraded by nucleases and not easily delivered across the cell membrane.^[1, 2] These issues lead to the need for an efficient delivery vehicle to successfully transport a therapeutic gene to its targeted site of interest. Genetic engineering can refer to gene delivery, as a way to gain function, or for tracking experiments by adding a gene that will express a protein such as green fluorescent protein.^[1, 2] Genetic engineering can also refer to a loss of function. Loss of function experiments can allow for the study of a gene of interest, or lead to the knockout of a harmful gene.^[1, 2]

RNA interference (RNAi) is a relatively new approach to gene silencing *in vitro* and *in vivo*. This naturally occurring mechanism was discovered by Fire and Mello et al. in Nobel prize winning work first published in 1998.^[3] RNAi employs small 21-25 nucleotide long double stranded RNAs (dsRNA) to lead to inhibition of gene expression.

These small RNAs are known as small interfering RNAs (siRNA). Gene silencing by siRNA begins by cleavage of the double stranded RNA to single strands by the enzyme Dicer. The single stranded RNAs are then assembled into the RNA Induced Silencing Complex (RISC), and lined up with a complementary sequence on the target mRNA.^[4] The target mRNA can then be degraded, leading to gene silencing. The use of siRNA for therapeutic applications could therefore be very effective at specifically shutting down genes both in cell culture and *in vivo*.

Artificial siRNA can be delivered to cells to get the same silencing response as naturally occurring RNA. The RNAi response is triggered by the presence of the dsRNA. However, the introduction of long dsRNA can lead to the initiation of the anti-viral interferon response and global protein expression shutdown.^[5] This response can be avoided though by delivering small double stranded siRNA. From this point, the siRNA interacts with Dicer and enters RISC.

The delivery of siRNA across the cell membrane is a problem that has led to much research. The polyanionic nature of siRNA, due to the phosphates, along with its high molecular weight (~13 kDa), keeps the small RNAs from freely crossing the cell membrane.^[5] Therefore, a delivery system must be utilized to effectively target siRNA into the cell. These problems are part of a larger effort in the development of effective delivery vehicles for genetic information. Many non-viral transport have been developed to carry DNA or RNA to cells.^[1] One approach has been to covalently attach the genetic material to folate ^[6, 7] or peptides ^[8, 9] for cell targeting. However, these methods do not protect the naked genetic material from nucleases, so an optimal vehicle should act as a carrier that can shield the material from degradation. An approach taken by Kakizawa

and Kataoka has been to synthesize block-co-polymer micelles composed of poly-L-lysine (PLL), poly(ethylenimine) (PEI), and poly(di-methylaminoethyl methacrylate) (PAMA) to encapsulate DNA.^[10] Perez et al. have used poly(lactic acid) (PLA)-poly(ethylene glycol) (PEG) polymer microspheres^[11] while Dass has used liposomes to deliver DNA to cells.^[12]

One of the most popular methods for delivering siRNA has been the use of commercial lipid carriers. These carriers have been developed by several industrial companies, but have drawbacks such as toxicity issues and difficulties in cell targeting.^[13] Therefore, researchers are looking to alternative delivery methods for siRNA as well. Schiffelers et al. have used an RGD (Arg-Gly-Asp peptide ligand)-PEG-PEI complex to target siRNA to tumor neovasculature. Song et al. used a protamine-antibody fusion protein using the Fab fragment of HIV-1 envelope antibody for siRNA delivery.^[14] Another targeting motif has been the use of liposomes in the form of an immunoliposome complex in work performed by Pirollo et al.^[15]

While these siRNA carriers have shown certain degrees of success, there are still issues of toxicity and payload capacity. We have utilized nanogels to encapsulate and deliver siRNA to ovarian cancer cells. As described in previous chapters, nanogels composed of poly(*N*-isopropylmethacrylamide) (pNIPMAm) could be ideal delivery vehicles. The nanogels are swollen at body temperature, leading to high payload capacity and making the particles hydrophilic in nature, which could lead to longer circulation times. The conjugation of the YSA (YSAYPDMMSC) peptide to the nanogels preferentially targets the nanogels to the EphA2 receptor, as shown in Chapter 4, and non-targeted siRNA linked with a red dye can be effectively encapsulated and targeted to

Hey and BG-1 cells. This chapter will show that siRNA can be delivered to knockdown epidermal growth factor receptor (EGFR) expression. Knockdown of EGFR is non-lethal on its own, but has been shown to increase drug sensitivity to previously drug resistant ovarian carcinomas.^[16, 17] After delivery of siRNA to cancer cells to knockdown EGFR, we have treated the cells with taxol to determine the chemotherapeutic potential of the combination therapy approach.

The targeting of EphA2 for particle uptake, combined with siRNA targeting EGFR for protein silencing is by design. It has been shown that EGFR can regulate EphA2 levels, as the activation of EGFR increases EphA2 mRNA levels.^[18] EphA2 is a direct transcriptional target of EGFR signaling in some cancer cells.^[19, 20] Therefore, the presence of EGFR in Hey cells leads to an increase in EphA2, making it an ideal target. It has also been shown that EphA2 localizes with EGFR at the cell membrane.^[18] EphA2 also plays a role in cell migration induced by EGF. Knockdown of EphA2 inhibits EGF-induced cell migration.^[18] Uptake of particles by the EphA2 receptor could therefore have the added benefit of inhibiting cell migration. All of these factors led to utilizing both receptors for this study.

5.2 Experimental Section

5.2.1 Materials

All materials were purchased from Sigma-Aldrich unless otherwise noted.

5.2.2 Nanogel core synthesis

Nanogel core particles were synthesized as described in Chapter 4.2.2.

5.2.3 Nanogel shell synthesis

Nanogel shell addition was performed as described in Chapter 4.2.3.

5.2.4 Peptide conjugation

The YSA peptide (GenScript or provided by K. D. Clark, University of Georgia) was conjugated to the nanogels via maleimide coupling to the cysteine residue on the C-terminal end of the peptide. A solution of EDC (Pierce) and NHS was added to ϵ -maleimidocaproic acid in pH 6.0 MES buffer to activate the acid groups for 30 min at room temperature. This solution was then added to particles and reacted for 2 h on a shaker table. The particles were centrifuged to remove any unreacted material, and then the peptide was added to the particles and reacted overnight. Particles were then cleaned by centrifugation as described above.

5.2.5 siRNA encapsulation

A solution of EGFR siRNA (Dharmacon) or siGLO (Dharmacon) was prepared in phosphate buffered saline (PBS). Lyophilized particles were dissolved in this solution at a concentration of 4 mg to 250 μ L of 20 mM siRNA and allowed to shake overnight. After shaking, the particles were then centrifuged to remove any free siRNA, and then followed by resuspension in PBS.

5.2.6 Particle characterization

5.2.6.1 Absorbance measurements

Absorbance measurements were made using a Shimadzu UV 1601 spectrophotometer, as described in Chapter 4.2.7.2.

5.2.7 Cell culture

Hey cells and human umbilical vein endothelial cells (HUVEC) were cultured as described in Chapter 4.2.8.

5.2.8 Particle/transfection experiments

5.2.8.1 Commercial agent transfection

Hey cells were plated onto 6-well plates (5×10^5 cells/well) and allowed to adhere overnight at 37 °C and 5% CO₂. For studies with a commercial transfection reagent, RNAiFect (Qiagen) was used. Before the transfection, 12 µL of 100 nmol/L siRNA was added to 73 µL of EC-R buffer. To this, 15 µL of RNAiFect was added. This solution was allowed to incubate at room temperature for 15 min, and then added to each well. The cells were incubated at 37 °C and 5% CO₂ in wells for 24, 48, 72, 96, and 120 h experiments.

5.2.8.2 siGLO-encapsulated particle transfection

For protein level determination, Hey cells were plated onto 6-well plates (5×10^5 cells/well) and allowed to adhere overnight at 37 °C and 5% CO₂. Particles encapsulated with siGLO were added to the appropriate wells and allowed to incubate for 4 h. The wells were then aspirated and washed with PBS. Fresh medium was added and the cells were incubated at 37 °C and 5% CO₂ in wells for 72 h. Control wells were set up to include non-targeted pNIPMAM particles, unloaded YSA-conjugated particles, and untreated cells.

5.2.8.3 EGFR-siRNA-encapsulated particle transfection

Hey cells were plated onto 6-well plates (5×10^5 cells/well) and allowed to adhere overnight at 37 °C and 5% CO₂. EGFR-siRNA encapsulated particles were added to the appropriate wells and allowed to incubate for 4 h. The wells were then aspirated and washed with PBS. Fresh medium was added and the cells were incubated at 37 °C and 5% CO₂ in wells for 24, 48, 72, 96, and 120 h experiments. Control wells were set up to include non-targeted, siRNA-encapsulated pNIPMAM particles, unloaded YSA-conjugated particles, unloaded pNIPMAM particles, and untreated cells.

In order to transfect different concentrations of siRNA to the cells, the same loading procedure was used, but the concentration of particles delivered to each well was varied. The same concentration of siRNA-encapsulated particles as the time point experiments was added to a well. The concentration of the next 3 wells was reduced by 10 fold each. After 4 h incubation with the particles, wells were cleaned and the medium replaced. The cells were then incubated for 72 h.

Nanogels were also targeted to human umbilical vein endothelial cells (HUVECs). HUVECs were plated onto an 8-well chamber slide (5×10^3 cells/well) and allowed to adhere overnight at 37 °C and 5% CO₂. After washing the wells with PBS and replacing the media, YSA-conjugated nanogels and pNIPMAm nanogels were added to cells to incubate for 4 h, and wells were set up with untreated cells. Cells were then washed with PBS, and the media was replaced. The cells were then fixed by adding paraformaldehyde for 30 min. The wells were then aspirated and the chamber removed. A cover slip was placed on the slide for microscopic imaging.

5.2.9 Toxicity Studies

5.2.9.1 Trypan Blue Exclusion Assay

Hey cells were plated onto 6-well plates (5×10^5 cells/well) and allowed to adhere overnight at 37 °C and 5% CO₂. The media was aspirated, and then wells were washed with PBS. The PBS was then aspirated and the media replaced. Wells were set up at each of the 4 concentrations of siRNA-loaded nanogels used in the protein knockdown experiments, unloaded YSA-conjugated nanogels, and a well of untreated cells. The cells were incubated with the nanogels for 4 h. The wells were then aspirated, washed with PBS, and the media replaced. The cells were then incubated for 72 h to allow siRNA treatment to occur. After siRNA treatment, wells were aspirated, washed with PBS, and then aspirated again. A 1-mL solution of trypan blue was diluted to 4 mL in PBS, and 400 µL added to each well. Each well was then viewed via optical microscopy to determine the number of stained (dead) cells.

5.2.9.2 Tox 8 Assay

Hey cells were plated onto 96-well plates (1×10^4 cells/well) and allowed to adhere overnight at 37 °C and 5% CO₂. The media was aspirated, and then wells were washed with PBS. The PBS was then aspirated and the media replaced. Wells were set up in triplicate to include each concentration of delivered siRNA-loaded nanogels, unloaded YSA-conjugated nanogels, unloaded pNIPMAM nanogels, and untreated cells. The cells were incubated with the nanogels for 4 h. The wells were then aspirated, washed with PBS, and the media replaced. The cells were then incubated for 72 h to allow siRNA treatment to occur.

For the chemotherapy studies, wells were set up in triplicate to include 0 nM, 0.1 nM, 1 nM, 10 nM, 100 nM, and 1000 nM taxol and the cells incubated for 4 d. The same concentrations of taxol were also used after nanogel delivery of siRNA at siRNA concentrations of 16 µg, 1.6 µg, 160 ng, and 16 ng. Cells were incubated with nanogels for 4 h, then the cells washed and media replaced. At 48 h of siRNA treatment, cells were washed and media replaced, and then taxol was added.

After these treatments, wells were aspirated, washed with PBS, and 100 µL of media was added back to the wells. To this, 10 µL of Tox 8 was added. Upon addition of Tox 8, the cells were incubated for 50 min. The fluorescence was then measured ($\lambda_{em} = 560$ nm, $\lambda_{ex} = 590$ nm) by a Spectramax Gemini Fluorescence Microplate Reader (Molecular Devices).

5.2.10 Confocal Microscopy

A Zeiss LSM510 confocal microscope was used to take cell images as described in Chapter 4.2.10.

5.2.11 Western blot analysis

Hey cells were plated into 6 well plates (5×10^5 / well) and allowed to adhere overnight at 37°C, 5% CO₂. Cells were lysed with 100 µl of lysis buffer (50 mM Tris-HCl, pH 7.5, 150 mM NaCl, 2 mM EDTA (Fisher), 2 mM EGTA (Fisher), 1 mM sodium orthovanadate, 2.5 mM sodium pyrophosphate, 1 mM β-glycerolphosphate, 1 mM phenylmethanesulfonyl fluoride, 10 µg/ml aprotinin, 10 µg/ml leupeptin, 1% Triton X-100, and 5% glycerol), and the lysates were sonicated four times for 5 seconds each. The lysates were cleared by centrifugation at 11,000 rcf for 15 min at 4 °C. To the lysates, 90 µL of Laemmli 2X sample buffer was added and the samples were then heated to 90 °C for 5 min.

For whole cell lysates, the proteins were separated by SDS-PAGE and transferred onto nitrocellulose. The blots were blocked with either 5% nonfat dry milk (NFDM) or 5% bovine serum albumin (BSA) in 10 mM Tris-buffered saline, pH 7.5 plus 1% Tween 20 (BioRad) (TBST) for 1 hour at room temperature. Blots were probed with anti-EGF-r antibody (Cell Signaling, cat. no. 4405) or with anti-β-actin antibody (Chemicon, Mab1501) diluted in 5% NFDM or 5% BSA overnight, with shaking at 4 °C. Blots were washed three times with TBST and probed with goat anti-rabbit IgG (Santa Cruz, sc-2004) or with goat anti-mouse IgG (Santa Cruz, sc-2005) linked to horseradish

peroxidase (HRP). Bands were visualized on film (Pierce) using the ECL reagent, picowest (Pierce).

5.3 Results and Discussion

As described in previous chapters, pNIPMAm nanogels around 100 nm in diameter were synthesized.^[21] These particles have an LCST of ~ 44 °C, so the nanogels will be mostly swollen at body temperature. In this swollen state, the nanogels should be ideal for encapsulation. The results in Chapter 4 show that siGLO can be efficiently encapsulated within the particles, with roughly 80-95 % of siGLO in solution (20 μ M) being taken up by the nanogels.

Since these high concentrations could be imbibed by the nanogels, it was necessary to have a better understanding of how long the siGLO would stay in the nanogels. A 1 mL solution of 20 μ M siGLO was used to resuspend 9.0 mg of YSA-conjugated nanogels. The nanogels were shaken overnight and then divided into six 150 μ L aliquots. The first of these samples was designated as timepoint 0 h. The sample was centrifuged and 10 μ L of the supernatant was used for absorbance measurements. The 10 μ L of supernatant was diluted to 1 mL in water and the absorbance was measured. The same procedure was done for each sample, following at timepoints 1 h, 2 h, 4 h, 8 h, and 24 h. The results are shown in Table 5.1. They show that at each timepoint, the amount of siGLO released is consistent and low, corresponding to less than 9 % siGLO loss for each sample. It is interesting to note that one of the highest amounts is actually timepoint 0 h. While the highest amount is the 24 h timepoint, it is just 2 % more siGLO than the lowest amount, timepoint 8 h. These small differences are most likely due to the nanogels being

near a saturation point, and small amounts of siGLO will remain in solution. It appears that the siGLO is strongly held by the nanogels for at least 24 h in PBS at room temperature.

Table 5.1 Absorbance measurements of supernatant from siGLO-loaded nanogels.

Timepoint	Absorbance at 260 nm	% siGLO loss
0 h	0.054	8.2
1 h	0.039	7.0
2 h	0.048	7.7
4 h	0.054	8.2
8 h	0.038	6.8
24 h	0.063	8.8

The successful delivery of siGLO via targeted nanogels to Hey and BG-1 cells (Chapter 4) led to the attempt to deliver siRNA targeting epidermal growth factor receptor (EGFR). The EGFR siRNA was encapsulated at similar rates to siGLO. For these attempts we used Hey cells. The siRNA was encapsulated in YSA-conjugated nanogels and non-conjugated pNIPMAm nanogels by the breathing-in technique. Hey cells were incubated in 6-well plates overnight. After removing the media and washing the wells with PBS, the media was replaced and then the cells were incubated with nanogels for 4 h. The media was then removed and the wells were washed with PBS. The media was then replaced, and time points of 24, 48, 72, 96, and 120 h were set up in separate wells. Controls included cells incubated with siRNA-loaded, non-conjugated

pNIPMAm nanogels, unloaded YSA-conjugated nanogels, unloaded pNIPMAm nanogels, and untreated cells. After the 4 h incubation time, the cells were incubated at 37 °C for the required time point, with controls incubating for 48 h. At each time, the media was removed and cells washed with PBS. The PBS was then aspirated, and the cells were lysed. Protein levels for EGFR were then measured by immunoblot. Figure 5.1 shows percent knockdown at each time point, with controls showing little knockdown. The results show an average of 3 blots, with error bars representing the standard deviation. The 24 h timepoint shows high error. This is due to one blot showing little knockdown at 24 h. This could be due to error during development of the film, or it could be that knockdown begins near the 24 h timepoint, and for this experiment, protein knockdown was not seen until after 24 h. Low levels of knockdown of EGFR by commercial transfection of siRNA was seen (results not shown).

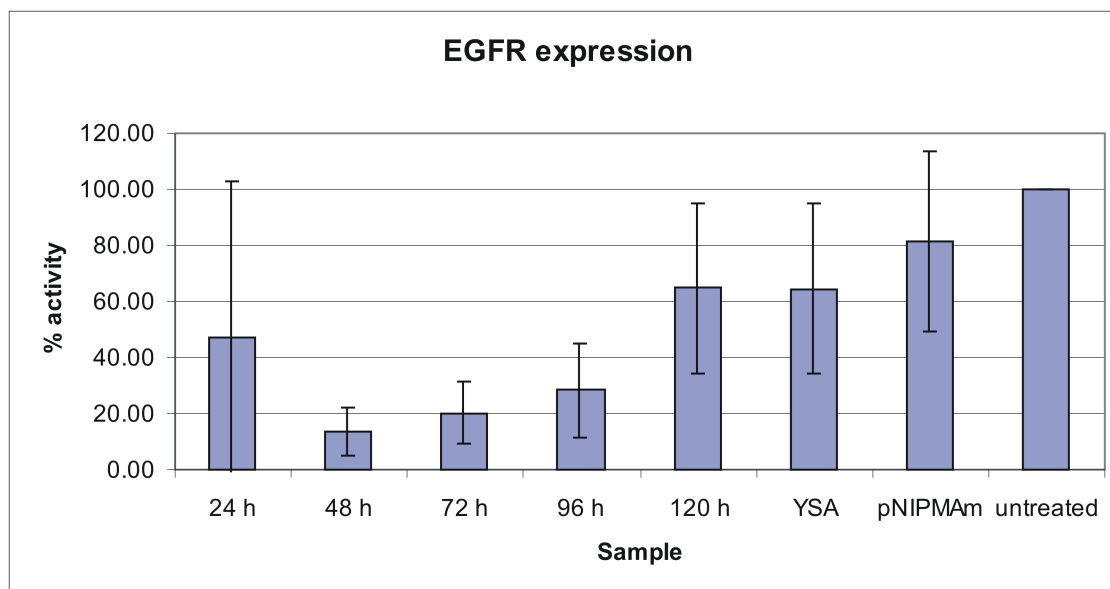


Figure 5.1. The knockdown of EGFR by nanogel-delivered siRNA at 24, 48, 72, 96, and 120 h incubation times. Controls shown are unloaded YSA-conjugated particles and pNIPMAm particles, as well as untreated cells. Untreated cells were set at 100% activity.

The knockdown achieved in Figure 5.1 was using very high concentrations of siRNA, up to 1000-fold higher than used with commercial transfection reagents. The next step was to determine if lower concentrations would still have the same protein knockdown effect. The same breathing-in technique was used to encapsulate the siRNA within the nanogels, using the same concentrations as the previous experiments. In order to reduce the concentration of delivered siRNA, the amount of nanogels delivered to each well was reduced 10 fold until reaching concentrations used by commercial transfection reagents. The experiments were carried out in the same manner as the time point studies, with the concentration studies using a 72 h incubation time. Significant knockdown is

seen at each of the three highest concentrations, as seen in figure 5.2. The concentrations designate the amount of siRNA delivered to each well.

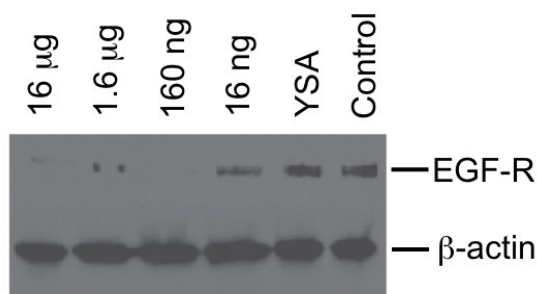


Figure 5.2. Immunoblot showing EGFR knockdown by various concentrations of siRNA delivered via nanogels. “YSA” designates unloaded YSA-conjugated nanogels, while the control is untreated cells. The β -actin levels show equal protein loading among each well.

Along with successful transfection of Hey cells with siRNA via nanogels, it was necessary to determine the toxicity of the particles. Two different cell viability assays were performed on each concentration of siRNA delivered by nanogels. A trypan blue exclusion assay was performed first. Hey cells were incubated overnight in 6-well plates. The following day, nanogels were incubated with the cells. After 4 h, the wells were washed with PBS, then aspirated and the media replaced. The cells were then incubated for 72 h to complete the nanogel/siRNA treatment. The wells were then aspirated and cleaned with PBS. A 1 mL solution of trypan blue was diluted to 4 mL in PBS, and 400 μ L of this was added to each well. Dead cells will become stained by trypan blue as it the

dye can cross the ruptured cell membrane. Viewing several fields via optical microscopy showed no stained cells among any concentration of siRNA delivered by nanogels (results not shown). No stained cells were seen among unloaded, YSA-conjugated nanogels or pNIPMAm nanogels.

The second cell viability assay was a Tox 8 viability/proliferation assay. This assay was also performed on each nanogel-delivered siRNA concentration. It is a resazurin-based assay that allows for spectrophotometric measurement of cell metabolic activity. Hey cells were incubated in 96-well plates overnight. Nanogel were then delivered to the cells for 4 h. Wells were then washed with PBS, and 100 μ L of media was added to the wells. Figure 5.3 shows that spectrophotometric analysis of the wells reveals no statistically significant difference for any treatment versus untreated cells. Controls of unloaded, YSA-conjugated nanogels and pNIPMAm nanogels are also not significantly different than untreated cells.

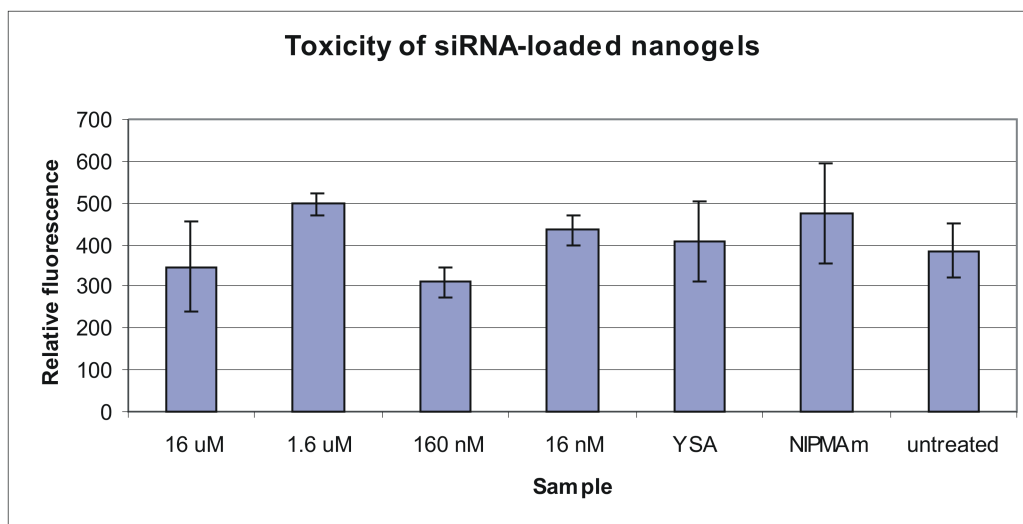


Figure 5.3. Tox 8 assay on siRNA-loaded nanogel delivery to Hey cells. The fluorescence indicates cell activity. Concentrations denote siRNA delivered by nanogels. Controls are unloaded YSA-conjugated nanogels, unloaded pNIPMAm nanogels, and untreated cells.

To ensure that protein silencing was not a side-effect of the nanogels and was caused by the EGFR siRNA, a non-targeting siRNA was delivered. The siRNA used in this experiment was siGLO. The same procedure was used as with EGFR siRNA delivery. The concentration of siGLO corresponded to the highest amount used in the knockdown studies. Hey cells were incubated with the nanogels for 4 h, then the wells were washed and the media replaced. Protein levels were measured at 72 h. No knockdown of EGFR by siGLO was observed (results not shown).

With the successful knockdown of EGFR by nanogel delivery of siRNA, we next investigated the effects of taxol on the cells, with and without nanogel targeting. To determine the effects of taxol alone, Hey cells were incubated in a 96-well plate overnight. Taxol was then added to wells at concentrations of 0.1 nM, 1 nM, 10 nM, 100

nM and 1000 nM. After 4 d, a Tox 8 assay was performed. Figure 5.4 (black line) shows the concentration dependent cytotoxicity of taxol on Hey cells. Toxic effects were seen as taxol concentration was increased to 100 nM. To determine if EGFR knockdown by siRNA could increase sensitivity of the cells to taxol, siRNA-loaded nanogels at the previously discussed concentrations were added. The siRNA treatment proceeded for 48 h before taxol was added. At 4 d, a Tox 8 assay was performed. Unfortunately, experimental error led to some inconsistencies in the results. However, this preliminary study shows promise. Interestingly, the best results were seen with 160 ng siRNA delivery by the nanogels. The results (Figure 5.4 red line) suggest that toxic effects may be seen at concentrations as low as 1 nM. These studies should be a major focus of future work with this project, as these early results are very promising.

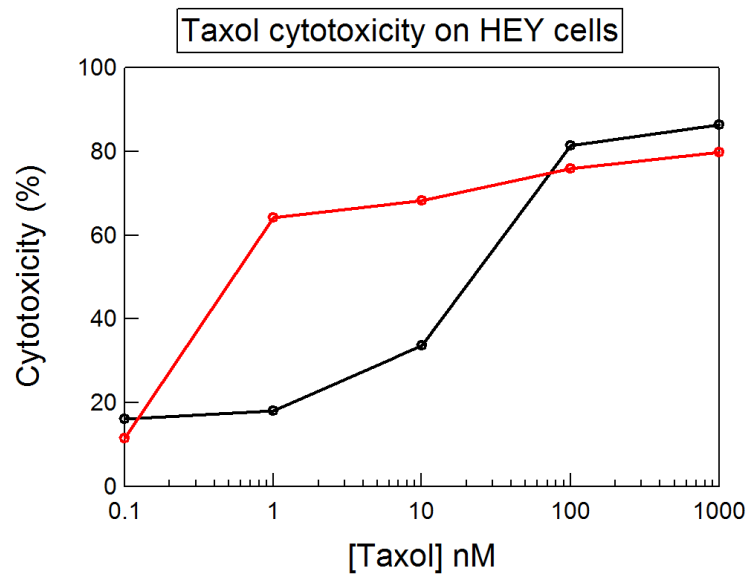


Figure 5.4. Cytotoxic effects of taxol with (red) and without (black) siRNA delivery by nanogels.

5.4 Conclusions

In this chapter, it has been shown that siRNA can be efficiently delivered to Hey cells via nanogels. Through the breathing-in method, high concentrations of siRNA can be encapsulated in the nanogels. Peptide conjugation of the nanogels allows targeting to ovarian cancer cells, and thus the delivery of siRNA. The siRNA knocks down EGFR expression at multiple timepoints and concentrations, as the nanogels are able to enter the cells within 4 h and deliver their payload. The delivery of siRNA-loaded nanogels shows no toxic effects compared to untreated cells. However, Hey cells seem to become more sensitive to taxol, if added after EGFR knockdown. This therapy should be further explored, as it holds promise as a low-dose chemotherapy treatment.

5.5 References

- [1] J.-i. Jo and Y. Tabata, Non-viral gene transfection technologies for genetic engineering of stem cells, *European Journal of Pharmaceutics and Biopharmaceutics*, 2008, **68**, 90-104.
- [2] T. A. Ratko, J. P. Cummings, J. Blebea and K. A. Matuszewski, Clinical gene therapy for nonmalignant disease, *Am. J. Med.*, 2003, **115**, 560-569.
- [3] A. Fire, S. Xu, M. K. Montgomery, S. A. Kostas, S. E. Driver and C. C. Mello, Potent and specific genetic interference by double-stranded RNA in *Caenorhabditis elegans*, *Nature*, 1998, **391**, 806-811.
- [4] J. Martinez, A. Patkaniowska, H. Urlaub, R. Luhrmann and T. Tuschl, Single-stranded antisense siRNAs guide target RNA cleavage in RNAi, *Cell*, 2002, **110**, 563-574.
- [5] S. Akhtar and I. F. Benter, Nonviral Delivery of synthetic siRNAs in vivo, *The Journal of Clinical Investigation*, 2007, **117**, 3623-3632.
- [6] K. A. Mislick, J. D. Baldeschwieler, J. F. Kayyem and T. J. Meade, Transfection of Folate-Polylysine DNA Complexes: Evidence for Lysosomal Delivery, *Bioconjugate Chem.*, 1995, **6**, 512-515.
- [7] X. B. Zhao and R. J. Lee, Tumor-selective targeted delivery of genes and antisense oligodeoxyribonucleotides via the folate receptor, *Adv. Drug Delivery Rev.*, 2004, **56**, 1193-1204.
- [8] S. L. Hart, R. P. Harbottle, R. Cooper, A. Miller, R. Williamson and C. Coutelle, Gene delivery and expression mediated by an integrin-binding peptide, *Gene Therapy*, 1995, **2**, 552-554.
- [9] E. Wagner, M. Cotten, R. Foisner and M. L. Birnstiel, Transferrin-polycation-DNA complexes: the effect of polycations on the structure of the complex and DNA delivery to cells, *Proc. Natl. Acad. Sci. U. S. A.*, 1991, **88**, 4255-4259.
- [10] Y. Kakizawa and K. Kataoka, Block copolymer micelles for delivery of gene and related compounds, *Adv. Drug Delivery Rev.*, 2002, **54**, 203-222.

- [11] C. Perez, A. Sanchez, D. Putnam, D. Ting, R. Langer and M. J. Alonso, Poly(lactic acid)-poly(ethylene glycol) nanoparticles as new carriers for the delivery of plasmid DNA, *J. Controlled Release*, 2001, **75**, 211-224.
- [12] C. R. Dass, Lipoplex-mediated delivery of nucleic acids: factors affecting in vivo transfection, *Journal of Molecular Medicine*, 2004, **82**, 579-591.
- [13] S. Spagnou, A. D. Miller and M. Keller, Lipidic carriers of siRNA: Differences in the formulation, cellular uptake, and delivery with plasmid DNA, *Biochemistry*, 2004, **43**, 13348-13356.
- [14] E. Song, P. Zhu, S.-K. Lee, D. Chowdhury, S. Kussman, D. M. Dykxhoorn, Y. Feng, D. Palliser, D. B. Weiner, P. Shankar, W. A. Marasco and J. Lieberman, Antibody mediated in vivo delivery of small interfering RNAs via cell-surface receptors, *Nat. Biotechnol.*, 2005, **23**, 709-717.
- [15] K. F. Pirollo, A. Rait, Q. Zhou, S. H. Hwang, J. A. Dagata, G. Zon, R. I. Hogrefe, G. Palchik and E. H. Chang, Materializing the Potential of Small Interfering RNA via a Tumor-Targeting Nanodelivery System, *Cancer Res.*, 2007, **67**, 2938-2943.
- [16] P. H. Thaker, M. Deavers, J. Celestino, A. Thornton, M. S. Fletcher, C. N. Landen, M. S. Kinch, P. A. Kiener and A. K. Sood, EphA2 expression is associated with aggressive features in ovarian carcinoma, *Clin Cancer Res*, 2004, **10**, 5145-5150.
- [17] P. H. Thaker, S. Yazici, M. B. Nilsson, K. Yokoi, R. Z. Tsan, J. Q. He, S. J. Kim, I. J. Fidler and A. K. Sood, Antivascular therapy for orthotopic human ovarian carcinoma through blockade of the vascular endothelial growth factor and epidermal growth factor receptors, *Clinical Cancer Research*, 2005, **11**, 4923-4933.
- [18] A. B. Larsen, M. W. Pedersen, M.-T. Stockhausen, M. V. Grandal, B. Van Deurs and H. S. Poulsen, Activation of the EGFR gene target EphA2 inhibits epidermal growth factor-induced cancer cell motility, *Molecular Cancer Research*, 2007, **5**, 283-293.
- [19] M. Macrae, R. M. Neve, P. Rodriguez-Viciano, C. Haqq, J. Yeh, C. Chen, J. W. Gray and F. McCormick, A conditional feedback loop regulates Ras activity through EphA2, *Cancer Cell*, 2005, **8**, 111-118.

- [20] J. Wykosky, D. M. Gibo, C. Stanton and W. Debinski, Interleukin-13 Receptor alpha 2, EphA2, and Fos-Related Antigen 1 as Molecular Denominators of High-Grade Astrocytomas and Specific Targets for Combinatorial Therapy, *Clinical Cancer Research*, 2008, **14**, 199-208.
- [21] W. H. Blackburn and L. A. Lyon, Size-controlled synthesis of monodisperse core/shell nanogels, *Colloid and Polymer Science*, 2008, **286**, 563-569.

CHAPTER 6

Ag-ENCAPSULATED NANOGELS FOR *IN VIVO* IMAGING

6.1 Introduction

Non-invasive bioimaging modalities, such as magnetic resonance imaging (MRI) or ultrasound, have led to significant developments in modern medicine.^[1] Techniques like these can lead to identification of abnormal tissue, disease diagnosis, and tracking disease progress. Optical imaging is a technique that offers complementary information, and leads to improved spatial resolution over ultrasound and MRI.^[2] Multidimensional optical imaging allows for identification and localization of different tissue types and can provide true 3-D images. However, a drawback for this technique exists as optical probes used for imaging must be appropriate for clinical use. Therefore, new optical probes must be developed for improvements to be seen with *in vivo* imaging.

In vivo tumor imaging has become a major and necessary tool in cancer diagnosis and research. The number of imaging systems and their applications has rapidly expanded over the last few decades. Imaging systems can be grouped based on their spatial resolution as either macroscopic or microscopic, or they can be grouped by the information obtained, as anatomical, physiological, cellular, or molecular systems.^[3] Macroscopic imaging techniques, such as ultrasound^[4-8] and MRI^[3, 9-12], offer anatomical and physiological information that are used both clinically and in research. Approaches at the molecular level include positron-emission tomography (PET)^[13-18], fluorescence-mediated tomography (FMT)^[2, 19-21], and bioluminescence.^[21-25] Now approaches are

being combined to take advantage of the strengths of multiple techniques. These approaches, such as PET-MRI are being used to improve data visualization.^[26, 27]

Fluorescence bioimaging is a fast growing technique that is being used both preclinically and clinically. Fluorescent markers can be combined with microscopic techniques to visualize multiple cells or molecules at the same time, or to view targets deep in tissues. Fluorescence approaches include fluorescence reflectance imaging (FRI) and tomographic reflectance.^[1] FRI approaches give a two-dimensional image and are limited to shallow tissue depths. Tomographic reflectance systems provide 3-D images, but complicated algorithms that construct the images have made these approaches slow to move into clinical use.^[2, 19-21] These drawbacks then lead to the need to improve development of molecular probes. Probes that emit in the red to near-IR region can lead to greater image depth, quantification, and, with the use of tunable probes, multi-color imaging. Improved probes can also lead to higher resolution, which can allow the visualization of small cancer foci that may not be seen by traditional approaches such as PET.

Recently, research has focused on delivery of metal nanoparticles for bioimaging.^[28-30] Several researchers have used gold nanoparticles for tumor modeling, which has advantages of biocompatibility, photostability, and ease of coating. However, the coating must provide enough coverage to prevent aggregation of the gold nanoparticles.^[29] Corr et al. have used the polyelectrolyte, polysodium-4-styrene sulfonate (PSSS), to produce stable magnetic nanoparticles suspensions in water.^[31] The suspensions were created by adding a solution of iron to PSSS. Composites of 1:2, 3:1, and 6:1 PSSS to magnetic iron nanoparticles were used to create a chain-like assembly of

magnetic nanoparticles. These composites showed good biocompatibility and potential for *in vivo* MRI agents. The drawbacks to this system are little knowledge of the system's tissue localization, and lack of targeting. Chung et al. have modified silver nanoparticles with phosphoryl disulfides.^[32] Sodium borohydride was used to reduce the disulfide bonds and silver ions, which created nanoclusters as the thiol groups generated reacted with silver atoms. Phosphorylcholine and phosphorylethanolamine was used to make the particles biocompatible. These nanoclusters were shown to be taken up by platelets and fibroblast cells. This method also lacks targeting, and since the studies are in the early stages, much is still unknown about their potential as imaging agents. Khan has developed magnetically responsive microgels by embedding iron oxide nanoparticles in poly(N-isopropylacrylamide)-co-acrylic acid particles.^[33] A colloidal magnetic solution was added to a solution of pNIPAm, AAc and methylene bisacrylamide, and then the reaction was initiated with ammonium persulfate. The microgels were around 115 nm in diameter, and TEM shows the magnetic nanoparticles in the microgels. These particles could prove effective as contrast agents for MRI.

The results in this chapter describe the use of poly(N-isopropylmethacrylamide) nanogels for silver nanocluster delivery *in vivo*. As described in previous chapters, the nanogels are effective at encapsulation and targeting *in vitro*. We will investigate the ability of the nanogels to encapsulate the silver nanoclusters, and then target the nanogels to MatrigelTM plugs in mice.

6.2 Experimental Section

6.2.1 Materials

All materials were purchased from Sigma-Aldrich unless otherwise noted. The monomers *N*-isopropylacrylamide (NIPAm) and *N*-isopropylmethacrylamide (NIPMAm) were recrystallized from hexane (J. T. Baker) before use. The cross-linker *N,N'*-methylenebis(acrylamide) (BIS), acrylic acid, *N*-(3-aminopropyl) methacrylamide hydrochloride (APMA) (Polysciences), ammonium persulfate (APS), sodium dodecyl sulfate (SDS), and phosphate buffered saline (PBS) were used as received. All water used in the experiments was distilled, and then deionized using a Barnstead E-pure system operating at a resistance of 18 M Ω . A 0.2 μ m filter was used to remove particulate matter. For peptide conjugation, the YSA peptide (YSAYPDSVPMMS) (Genscript), 1-ethyl-3-(3-dimethylaminopropyl)carbodiimide (EDC) (Pierce), and dimethyl sulfoxide (DMSO) (Fisher) were used. The fluorescent monomer 4-acrylamidofluorescein (AFA) was synthesized via a previously reported procedure.^[34] Silver nanoclusters (Ag nanodots) in solution were synthesized by Sungmoon Choi in Robert M. Dickson's lab, Department of Chemistry, Georgia Tech. The Ag nanodots are composed of fewer than ten Ag atoms, stabilized by short, single stranded DNA strands. The Ag nanodots were provided in 250 μ L aliquots (300 nM).

6.2.2 Nanogel core synthesis

Nanogel core particles were synthesized as described in Chapter 4.2.2.

6.2.3 Nanogel shell synthesis

Nanogel shell addition was performed as described in Chapter 4.2.3.

6.2.4 Peptide conjugation

The YSA peptide was conjugated to the nanogels via maleimide coupling to the cysteine residue on the C-terminal end of the peptide. A solution of EDC (Pierce) and NHS were added to ϵ -maleimidocaproic acid to activate the acid group for 30 min. This solution was then added to particles and reacted for 2 h on a shaker table. The particles were centrifuged to remove any unreacted material, and then the peptide was added to the particles and reacted overnight. Particles were then cleaned by centrifugation as described above.

6.2.5 Ag nanodot encapsulation

Lyophilized particles were dissolved in a solution of Ag nanodots at a concentration of 4 mg to 250 μ L of 300 nM nanodots and allowed to shake overnight. After shaking, the particles were then centrifuged to remove any free Ag nanodots, followed by resuspension in 0.5 mL PBS.

6.2.6 Static light scattering

Multi-angle laser light scattering (MALLS; Wyatt Technology Corporation) detection following asymmetric field flow fractionation (AFFF) was performed as described in Chapter 3.2.3.1.

6.2.7 Fluorescence microscopy

Fluorescence microscopy was used to image nanogels and Ag nanodots in solution and targeted MatrigelTM plugs. An Olympus IX 70 inverted microscope equipped with a Mercury Arc lamp was used. An Olympus 100x UplanFl 1.30 NA oil immersion objective was used for imaging. Images were captured with a Cooke Cooperation Pixelfly color CCD camera. For observation of green fluorescence, a 40 nm band pass filter centered at 470 nm for excitation was used with a 515 nm long pass filter. To visualize red fluorescence, a 50 nm band pass filter centered at 535 nm for excitation was used with a 590 nm long pass filter for emission.

6.2.8 Targeting to MatrigelTM plug

All *in vivo* experiments were performed by Erin B. Dickerson, Department of Biology, Georgia Tech. MatrigelTM (250 μ L) was injected subcutaneously over the right flank of 8-12 week old female *nu/nu* mice and permitted to solidify. Subsequently (after 30–60 min), mice were anesthetized and a small (0.3-0.5 cm) nick was made in the skin using a #15 surgical blade. A smaller nick was then made in the MatrigelTM plug. A sterilized polyvinyl sponge (2 x 2 x 1.5 mm) containing approximately 10^5 Hey or OVCAR-3 ovarian tumor cells was introduced through the nick in the MatrigelTM and placed in the center of the plug using forceps. The wound was closed with a suture. Mice were observed after 24 h to monitor condition of the wound. Mice were injected via the tail vein with 800-1000 μ g of nanogel particles in a volume of 200 μ L. Nanogels were allowed to circulate for the times indicated, and the plugs were recovered. Plugs were

stored in formalin and vessels containing nanogels were visualized under fluorescent light.

6.3 Results and Discussion

As described in the previous chapters, pNIPMAm core/shell nanogels were synthesized by free-radical precipitation polymerization. These nanogels were near 100 nm in diameter, for efficient delivery through the vasculature and uptake by cells.^[35] The nanogels were conjugated with the YSA peptide in order to target the particles to the Hey or OVCAR-3 cells and new vasculature forming in the MatrigelTM plug, which have the EphA2 receptor, the target of YSA.

The nanogels were lyophilized in preparation for Ag nanodot encapsulation. The Ag nanodots were supplied by the Dickson lab at Georgia Tech in 250 μ L aliquots at a concentration of 300 nM. The Ag nanodots used in this study emitted in the red region of the spectrum at \sim 600 nm. To encapsulate the Ag nanodots, the nanogels were dissolved in the solution of nanodots and shaken overnight. The nanogels were centrifuged to remove any unencapsulated Ag nanodots, and then resuspended in PBS. To determine whether the Ag nanodots were encapsulated, fluorescence microscopy was done to image both the nanogels and nanodots. Particles were diluted at 1:200, and then dried on a coverslip. Figure 6.1 shows images for both green and red emission from the same field of view on a fluorescent microscope. It shows that both the red (Ag nanodots) and green (AFA from nanogels) overlay each other, suggesting that the Ag nanodots are localized in the nanogels. The encapsulation of the Ag nanodots most likely occurs due to two reasons. The solution volume is just enough to dissolve the entire mass of particles. The

solution becomes very viscous, so the particles are forced to take up whatever is in solution. With the particles taking up the nanodots, they are then held in by hydrogen bonding. The amide groups of the nanogels offer multiple opportunities for hydrogen bonding with the DNA strands of the Ag nanodots.

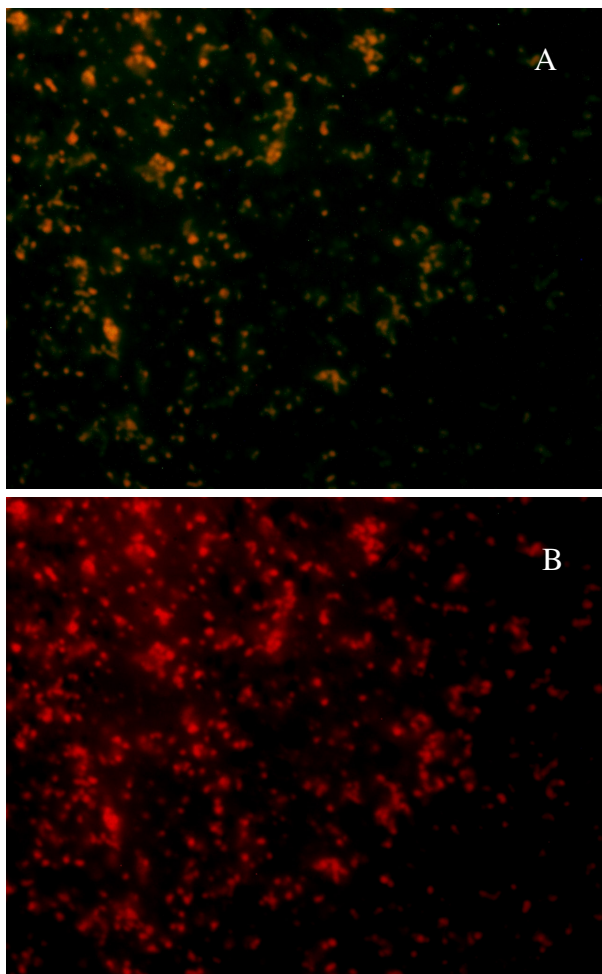


Figure 6.1. Fluorescence microscopy image of Ag nanodot encapsulated nanogels at day 1. Panel A shows the green channel (AFA). Panel B shows the red channel (Ag nanodots).

We next wanted to see how efficiently the nanogels held the Ag nanodots. After the initial encapsulation, unused particles were stored in the dark at 4 °C for 5 d. The particles were once again centrifuged to remove any Ag nanodots that were not encapsulated. Figure 6.2 again shows the green and red emitting fluorescent images of the particles. Once again, it is seen that the Ag nanodots are overlaid with the nanogels, suggesting that a good deal of the nanodots remain entrapped in the nanogels.

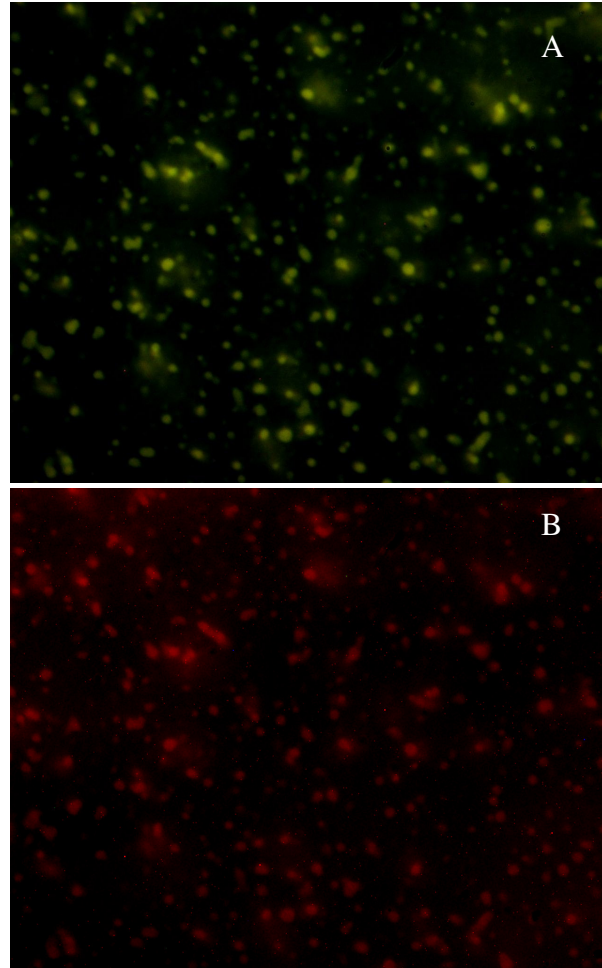


Figure 6.2. Fluorescence microscopy image of Ag nanodot encapsulated nanogels at day 5. Panel A shows the green channel (AFA). Panel B shows the red channel (Ag nanodots).

After it was determined that the Ag nanodots could be efficiently encapsulated in the nanogels, we attempted to deliver the particles *in vivo* to MatrigelTM plugs. MatrigelTM was injected into mice subcutaneously, and allowed to solidify. Then, a sponge containing either Hey or OVCAR-3 cells was introduced into a nick cut into the plug. After closing the suture and observing the wound, the mice were injected with a solution of Ag nanodot-encapsulated YSA-conjugated nanogels or Ag nanodot-encapsulated pNIPMAm nanogels via the tail vein. Nanogels were allowed to circulate for 2 h, at which point the MatrigelTM plugs were removed and imaged. Figure 6.3 shows the fluorescence from the nanogels and Ag nanodots in the vasculature of the plug. The top panel shows the dual fluorescence image. The vasculature shows bright green fluorescence, indicating the presence of nanogels. There are also some spots of yellow, indicating an overlay of green and red fluorescence. This suggests that nanogels containing Ag nanodots are present in the MatrigelTM plug. The bottom panel is red fluorescence, which shows a similar pattern to the green fluorescence. This red fluorescence is indicative of the Ag nanodots being present in plug. Future studies should be done to increase the Ag nanodot concentration and therefore the signal to background in these images. For these studies, similar results were seen among both the YSA-conjugated and pNIPMAm nanogels. This is most likely due to vasculature leakiness, but future studies must be done to get a better understanding of *in vivo* targeting.

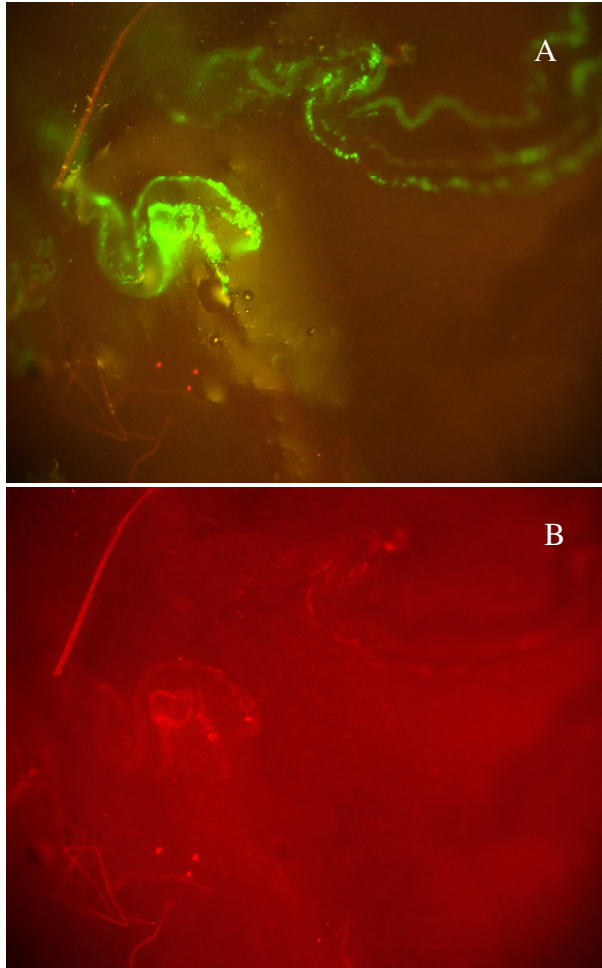


Figure 6.3. Fluorescence microscopy image of MatrigelTM plug. Panel A shows dual fluorescence in vessels. Panel B shows the red channel.

Figure 6.4 shows another dual fluorescence image of the Matrigel™ plug. This image shows the vasculature of the plug in more detail. Once again, there is bright fluorescence in the vessels, indicating very effective targeting of the nanogels to the Matrigel™ vasculature.

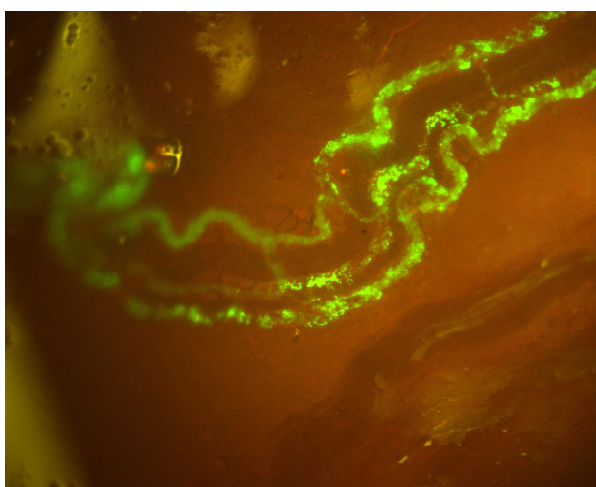


Figure 6.4. Dual fluorescence microscopy image of vessels in Matrigel™ plug.

6.4 Conclusions

The results in this chapter show that targeted nanogel delivery *in vivo* holds promise as a bioimaging technique. As shown in previous chapters, nanogels are proving to be very effective encapsulation entities. This trend has continued with the encapsulation of Ag nanodots. The nanogels effectively hold the Ag nanodots for at least

5 d. Chapters 4 and 5 showed that YSA-conjugated nanogels also effectively target the EphA2 receptor on Hey cells. We have also targeted the nanogels to Hey cells and neovasculature *in vivo*, as they both have EphA2 receptor. However, unconjugated nanogels also seem to localize in the Matrigel™ plugs. This is most likely due to the leakiness of vasculature growing into the plugs. While these results are very preliminary, Ag nanodot encapsulated nanogels could show promise as imaging agents. Future studies should continue in order to increase Ag nanodot concentration and gain a better understanding of *in vivo* targeting.

6.4 References

- [1] R. Weissleder and M. J. Pittet, Imaging in the era of molecular oncology, *Nature*, 2008, **452**, 580-589.
- [2] V. Ntziachristos, C. Bremer and R. Weissleder, Fluorescence imaging with near-infrared light: new technological advances that enable in vivo molecular imaging, *Eur Radiol*, 2003, **13**, 195-208.
- [3] M. G. Harisinghani, J. Barentsz, P. F. Hahn, W. M. Deserno, S. Tabatabaei, C. H. van de Kaa, J. de la Rosette and R. Weissleder, Noninvasive detection of clinically occult lymph-node metastases in prostate cancer, *N Engl J Med*, 2003, **348**, 2491-2499.
- [4] M. F. Muller, C. Meyenberger, P. Bertschinger, R. Schaer and B. Marincek, Pancreatic tumors: evaluation with endoscopic US, CT, and MR imaging, *Radiology*, 1994, **190**, 745-751.
- [5] J. Ophir, I. Cespedes, H. Ponnekanti, Y. Yazdi and X. Li, Elastography: a quantitative method for imaging the elasticity of biological tissues, *Ultrasonic imaging*, 1991, **13**, 111-134.
- [6] L. Palazzo, G. Roseau, B. Gayet, V. Vilgrain, J. Belghiti, F. Fekete and J. A. Paolaggi, Endoscopic ultrasonography in the diagnosis and staging of pancreatic adenocarcinoma. Results of a prospective study with comparison to ultrasonography and CT scan, *Endoscopy*, 1993, **25**, 143-150.
- [7] T. Rosch, R. Lorenz, C. Braig, S. Feuerbach, J. R. Siewert, V. Schusdziarra and M. Classen, Endoscopic ultrasound in pancreatic tumor diagnosis, *Gastrointest Endosc*, 1991, **37**, 347-352.
- [8] A. T. Stavros, D. Thickman, C. L. Rapp, M. A. Dennis, S. H. Parker and G. A. Sisney, Solid breast nodules: use of sonography to distinguish between benign and malignant lesions, *Radiology*, 1995, **196**, 123-134.
- [9] C. K. Kuhl, P. Mielcareck, S. Klaschik, C. Leutner, E. Wardelmann, J. Gieseke and H. H. Schild, Dynamic breast MR imaging: are signal intensity time course data useful for differential diagnosis of enhancing lesions?, *Radiology*, 1999, **211**, 101-110.

- [10] M. D. Rifkin, E. A. Zerhouni, C. A. Gatsonis, L. E. Quint, D. M. Paushter, J. I. Epstein, U. Hamper, P. C. Walsh and B. J. McNeil, Comparison of magnetic resonance imaging and ultrasonography in staging early prostate cancer. Results of a multi-institutional cooperative trial, *N Engl J Med*, 1990, **323**, 621-626.
- [11] D. A. Sipkins, D. A. Cheresch, M. R. Kazemi, L. M. Nevin, M. D. Bednarski and K. C. P. Li, Detection of tumor angiogenesis in vivo by alpha vbeta 3-targeted magnetic resonance imaging, *Nat. Med.*, 1998, **4**, 623-626.
- [12] V. P. Torchilin, PEG-based micelles as carriers of contrast agents for different imaging modalities, *Adv. Drug Delivery Rev.*, 2002, **54**, 235-252.
- [13] T. Beyer, D. W. Townsend, T. Brun, P. E. Kinahan, M. Charron, R. Roddy, J. Jerin, J. Young, L. Byars and R. Nutt, A combined PET/CT scanner for clinical oncology, *Journal of Nuclear Medicine*, 2000, **41**, 1369-1379.
- [14] M. K. Gould, C. C. Maclean, W. G. Kushner, C. E. Rydzak and D. K. Owens, Accuracy of positron emission tomography for diagnosis of pulmonary nodules and mass lesions: a meta-analysis, *The Journal of the American Medical Association*, 2001, **285**, 914-924.
- [15] R. M. Pieterman, J. W. van Putten, J. J. Meuzelaar, E. L. Mooyaart, W. Vaalburg, G. H. Koeter, V. Fidler, J. Pruim and H. J. Groen, Preoperative staging of non-small-cell lung cancer with positron-emission tomography, *N Engl J Med*, 2000, **343**, 254-261.
- [16] M. L. Schipper, Z. Cheng, S.-W. Lee, L. A. Bentolila, G. Iyer, J. Rao, X. Chen, A. M. Wu, S. Weiss and S. S. Gambhir, microPET-based biodistribution of quantum dots in living mice, *J. Nucl. Med.*, 2007, **48**, 1511-1518.
- [17] A. F. Shields, J. R. Grierson, B. M. Dohmen, H. J. Machulla, J. C. Stayanoff, J. M. Lawhorn-Crews, J. E. Obradovich, O. Muzik and T. J. Mangner, Imaging proliferation in vivo with [F-18]FLT and positron emission tomography, *Nat. Med.*, 1998, **4**, 1334-1336.
- [18] R. L. Wahl, R. L. Cody, G. D. Hutchins and E. E. Mudgett, Primary and metastatic breast carcinoma: initial clinical evaluation with PET with the radiolabeled glucose analogue 2-[F-18]-fluoro-2-deoxy-D-glucose, *Radiology*, 1991, **179**, 765-770.

- [19] C. Bremer, V. Ntziachristos, B. Weitkamp, G. Theilmeyer, W. Heindel and R. Weissleder, Optical Imaging of Spontaneous Breast Tumors Using Protease Sensing 'Smart' Optical Probes, *Invest. Radiol.*, 2005, **40**, 321-327.
- [20] X. Montet, J.-L. Figueiredo, H. Alencar, V. Ntziachristos, U. Mahmood and R. Weissleder, Tomographic fluorescence imaging of tumor vascular volume in mice, *Radiology*, 2007, **242**, 751-758.
- [21] K. Shah, A. Jacobs, X. O. Breakefield and R. Weissleder, Molecular imaging of gene therapy for cancer, *Gene Ther.*, 2004, **11**, 1175-1187.
- [22] C. H. Contag and B. D. Ross, It's not just about anatomy: in vivo bioluminescence imaging as an eyepiece into biology, *J Magn Reson Imaging*, 2002, **16**, 378-387.
- [23] P. Ray, A. De, J.-J. Min, R. Y. Tsien and S. S. Gambhir, Imaging tri-fusion multimodality reporter gene expression in living subjects, *Cancer Res*, 2004, **64**, 1323-1330.
- [24] A. Rehemtulla, L. D. Stegman, S. J. Cardozo, S. Gupta, D. E. Hall, C. H. Contag and B. D. Ross, Rapid and quantitative assessment of cancer treatment response using in vivo bioluminescence imaging, *Neoplasia*, 2000, **2**, 491-495.
- [25] M. Vooijs, J. Jonkers, S. Lyons and A. Berns, Noninvasive imaging of spontaneous retinoblastoma pathway-dependent tumors in mice, *Cancer Res.*, 2002, **62**, 1862-1867.
- [26] B. J. Pichler, M. S. Judenhofer, C. Catana, J. H. Walton, M. Kneilling, R. E. Nutt, S. B. Siegel, C. D. Claussen and S. R. Cherry, Performance test of an LSO-APD detector in a 7-T MRI scanner for simultaneous PET/MRI, *J Nucl Med*, 2006, **47**, 639-647.
- [27] S. Wachter, S. Tomek, A. Kurtaran, N. Wachter-Gerstner, B. Djavan, A. Becherer, M. Mitterhauser, G. Dobrozemsky, S. Li, R. Potter, R. Dudczak and K. Kletter, ¹¹C-acetate positron emission tomography imaging and image fusion with computed tomography and magnetic resonance imaging in patients with recurrent prostate cancer, *J Clin Oncol*, 2006, **24**, 2513-2519.
- [28] I. H. El-Sayed, X. H. Huang and M. A. El-Sayed, Surface plasmon resonance scattering and absorption of anti-EGFR antibody conjugated gold nanoparticles in cancer diagnostics: Applications in oral cancer, *Nano Lett.*, 2005, **5**, 829-834.

- [29] N. Nitin, D. J. Javier and R. Richards-Kortum, Oligonucleotide-Coated Metallic Nanoparticles as a Flexible Platform for Molecular Imaging Agents, *Bioconjugate Chem.*, 2007, **18**, 2090-2096.
- [30] K. Sokolov, M. Follen, J. Aaron, I. Pavlova, A. Malpica, R. Lotan and R. Richards-Kortum, Real-time vital optical imaging of precancer using anti-epidermal growth factor receptor antibodies conjugated to gold nanoparticles, *Cancer Res*, 2003, **63**, 1999-2004.
- [31] S. A. Corr, S. J. Byrne, R. Tekoriute, C. J. Meledandri, D. F. Brougham, M. Lynch, C. Kerskens, L. O'Dwyer and Y. K. Gun'ko, Linear Assemblies of Magnetic Nanoparticles as MRI Contrast Agents, *J. Am. Chem. Soc.*, 2008, **130**, 4214-4215.
- [32] Y.-C. Chung, I. H. Chen and C.-J. Chen, The surface modification of silver nanoparticles by phosphoryl disulfides for improved biocompatibility and intracellular uptake, *Biomaterials*, 2008, **29**, 1807-1816.
- [33] A. Khan, Preparation and characterization of magnetic nanoparticles embedded in microgels, *Mater. Lett.*, 2008, **62**, 898-902.
- [34] M. J. Serpe, C. D. Jones and L. A. Lyon, Layer-by-layer deposition of thermoresponsive microgel thin films, *Langmuir*, 2003, **19**, 8759-8764.
- [35] W. H. Blackburn and L. A. Lyon, Size-controlled synthesis of monodisperse core/shell nanogels, *Colloid and Polymer Science*, 2008, **286**, 563-569.

CHAPTER 7

FUTURE OUTLOOK

For some of the projects listed in previous chapters, a great deal could still be learned by continuing on the work. We will now look at the directions these projects could be taken.

- In Chapter 2, the many uses of AFFF-MALLS was discussed. One can envision a wide array of characterizations that could be done on the microgels synthesized in the Lyon group. One simple use that has not been explored yet is to measure the mass of the nanogels used in the targeted delivery projects discussed in this thesis. This could be helpful in many ways, such as determining the amount of encapsulated materials in the particles. Changes in mass after encapsulation could show how much material is in the particles, and then as the material is released, the mass should change again, giving an idea of release rate.

Another future use of the AFFF-MALLS could be to study degradable microgels. Degradable microgels could be very useful for drug delivery. By making particles biodegradable, a drug could be delivered to its target site, then the particles degraded for easy removal from the body. The use of AFFF-MALLS could allow for the study of degradation by determining shape and mass of the particles. It would be interesting to watch the changes in shape as particles are degrading. Also, one can envision a decrease in mass as determined by AFFF-MALLS as particles degrade.

- In Chapters 4 and 5, we looked at siRNA encapsulation in nanogels, as well as the targeted delivery of the siRNA to cancer cells. This work has moved past its early stages, but there are still many more experiments that can be done. While we have shown significant protein knockdown of EGF receptor, it would appear that other proteins could also be silenced. The knockdown of certain proteins can be beneficial as therapeutic agents, so it could be interesting to see if nanogel delivery of siRNA could be as effective with some of these proteins.

Another important experiment would be to determine if protein knockdown could be achieved *in vivo* by siRNA-loaded nanogels. While we have seen results that suggest nanogels can be targeted *in vivo* with no immediately obvious toxic effects (Chapter 6), the delivery of siRNA in mice has not been attempted. The concerns with *in vivo* delivery of siRNA would be if the particles hold onto the siRNA long enough for it to be delivered to its target, and if the particles would hinder nuclease degradation of the siRNA in the body.

Perhaps the most important experiment left to be done in this project is to do the chemotherapeutic studies once more to correct for the experimental error that occurred previously. Delivering siRNA via nanogels to cancer cells and following with Taxol treatment seems very promising so far as a chemotherapeutic technique. Correcting the error will give a clearer picture for how the cells respond at each concentration of siRNA delivered.

- Chapter 6 dealt with silver nanodot-encapsulated nanogel delivery *in vivo*. The work in this chapter is in its infancy. The results shown were with one set of Ag nanodots

that emit at ~ 600 nm. Our results suggest that nanogel efficiently hold onto the Ag nanodots, and can be targeted in mice. The next step in this project is to increase the concentration of Ag nanodots in the nanogels. This should be accomplished by simply increasing the Ag nanodots in solution before encapsulation in the nanogels.

The Dickson group at Georgia Tech has developed many different wavelength emitting Ag nanodots between 600-900 nm. Future studies should be done to show that Ag nanodots throughout this region can be efficiently encapsulated and retain their optical properties. If the Ag nanodot optical properties are not affected, more *in vivo* targeting studies should be done. Other future studies will be to continue to optimize both Ag nanodot encapsulation and *in vivo* imaging of the nanogels and nanodots.

VITA

William H. (Bart) Blackburn

Bart Blackburn was born in Montgomery, Alabama. He attended high school in Daphne, AL. He received a B.S. in Microbiology from Louisiana State University in 2001 and a M.N.S. from Louisiana State University in 2003 before coming to Georgia Tech to pursue a doctorate in Chemistry. Bart was the recipient of a Molecular Biophysics Traineeship for the 2005-2006 school year. Apart from research, he enjoys sports and spending time with his family.